Institute of
Oceanographic Sciences
Deacon Laboratory

Migration of uranium daughter radionuclides in natural sediments

S Colley & J Thomson

Report No 276 1990

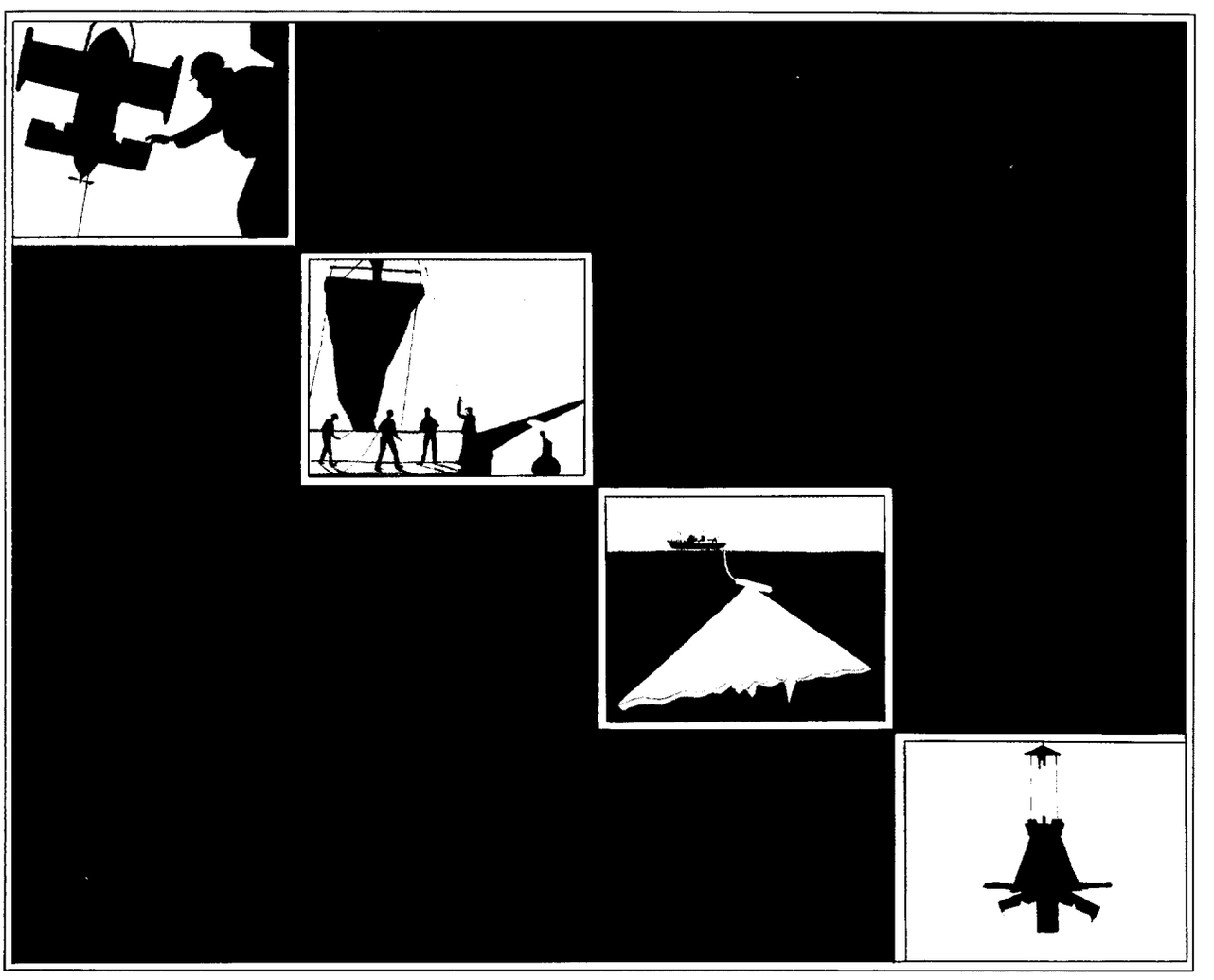

INSTITUTE OF OCEANOGRAPHIC SCIENCES

DEACON LABORATORY

Wormley, Godalming,
Surrey, GU8 5UB, U.K.

Telephone: 0428 79 4141
Telex: 858833 OCEANS G
Telefax: 0428 79 3066

Director: Dr. C.P. Summerhayes

INSTITUTE OF OCEANOGRAPHIC SCIENCES
DEACON LABORATORY
Report No. 276

Migration of uranium daughter radionuclides in natural sediments

S. Colley and J. Thomson

1990

DOCUMENT DATA SHEET

AUTHOR	PUBLICATION DATE
COLLEY, S. & THOMSON, J.	1990

TITLE

Migration of uranium daughter radionuclides in natural sediments.

REFERENCE

Institute of Oceanographic Sciences Deacon Laboratory, Report, No. 276, 89pp. & appendix.

(Also issued as: DoE Report No: DOE/RW/90.017*)*

ABSTRACT

The observation of U relocations in deep-sea sediments, with preservation of the resulting U profile shapes in single turbidite units for at least 750 kyr, has provided an opportunity to study diffusion of U decay series radionuclides at depth in the sediment column. Although the concentrations of radionuclides are present at natural levels of radioactivity, the study of diffusion in a natural geochemical 'analogue' situation provides useful *in-situ* data for processes active over relatively long time periods for comparison with predictive models. Comparison of parent-daughter pairs of the ^{238}U natural series (^{238}U-^{234}U; ^{234}U-^{230}Th; ^{230}Th-^{226}Ra; ^{226}Ra-^{210}Po) in GME turbidites shows that the only nuclide to exhibit evidence of diffusion is ^{226}Ra. Effective diffusion coefficients (D_{eff}) in the range 6×10^{-9} - 1×10^{-9} cm^2 s^{-1} have been calculated for ^{226}Ra in these sediments with between 35% and 70% of total ^{226}Ra available for pore water diffusion. The symmetrical distribution of ^{226}Ra around the ^{230}Th peaks indicates that pore water advection is absent. Other nuclides which might be expected to show evidence of migration are ^{234}U and ^{222}Rn. Although leaching experiments demonstrate that ^{234}U is potentially preferentially mobile, this is not seen in the core, suggesting that the geochemical environment of the sediments acts to immobilise ^{234}U as soon as it is liberated to pore waters. A maximum possible D_{eff} of 10^{-15} - 10^{-14} cm^2 s^{-1} for ^{234}U can be derived. ^{230}Th would not be expected to diffuse in the pore waters, and this is confirmed by the maximum D_{eff} of 10^{-14} - 5×10^{-13} cm^2 s^{-1} found for this nuclide. The profiles of ^{226}Ra and ^{210}Po show good agreement, which indicates that ^{222}Rn, an intermediate daughter in this part of the decay series does not migrate. ^{222}Rn has no interaction with the solid phase but the extent of its diffusion is limited by its relatively short half-life. A maximum possible D_{eff} of 10^{-7} - 10^{-5} cm^2 s^{-1} for ^{222}Rn can be derived for these sediments.

ISSUING ORGANISATION

Institute of Oceanographic Sciences
Deacon Laboratory
Wormley, Godalming
Surrey GU8 5UB. UK.

TELEPHONE 0428 79 4141

TELEX 858833 OCEANS G

TELEFAX 0428 79 3066

KEYWORDS

DIFFUSION
POLONIUM
PORE WATER
RADIOACTIVE WASTE DISPOSAL
RADIONUCLIDE MIGRATIONS
RADIUM
SEDIMENTS
THORIUM
URANIUM

CONTRACT

PROJECT

PRICE £26.00

Copies of this report are available from:
The Library, Institute of Oceanographic Sciences Deacon Laboratory.

CONTENTS

1. INTRODUCTION

1.1 Background and project objectives

In evaluation of any HLRW disposal option, the requirement is to demonstrate that waste radionuclides remain isolated from the biosphere and are contained locally. The longevity of some waste radioisotopes means that isolation times on the order of hundreds of thousands of years are desired. Predictions over such time scales are obtained from mathematical models incorporating thermodynamic principles, tuned as appropriate to local field conditions. Studies of natural geochemical "analogue" situations are attractive to gain actual field data for comparison with model predictions over such long periods. This report investigates aberrantly high U contents occasionally developed in deep-sea sediments over the past 750 kyr. The systematics of radioactive ingrowth and decay on a known time-scale allow a prediction of expected uranium daughter activities for comparison with those observed. Such information is relevant to other actinides besides uranium, since all actinides decay through chains of the same radio-elements before achieving stability. For example. the nuclear waste actinides ^{242}Cm, ^{242}Am and ^{238}Pu and the natural actinide ^{238}U all decay identically through ^{234}U until stable ^{206}Pb is produced.

The project arises from work conducted at IOSDL as part of the UK Department of the Environment's radioactive waste management and research programme. Between 1984 and 1987 an area of the Madeira Abyssal Plain was examined in detail. The sediments of the area were found to be dominated by turbidites, large volumes of sediment transported from depositional areas in relatively shallow water and rapidly re-deposited in deeper water as single units. Many of these turbidites are fine grained and relatively ungraded, so that the turbidite units are homogeneous in the horizontal and vertical (JARVIS & HIGGS, 1987; THOMSON *et al.*, 1988). The different units in the GME area are designated by an alphabetical sequence, with the most recent designated *a* (WEAVER & KUIJPERS, 1983; WEAVER & ROTHWELL, 1987).

A new phenomenon of uranium marine geochemistry was observed and elucidated in those turbidites which were organic-rich (COLLEY *et al.*, 1984; COLLEY & THOMSON, 1985; WILSON *et al.*, 1985, 1986; THOMSON *et al.*, 1987). The sequence of events is that organic-rich sediment, with an enhanced U content, is emplaced by a turbidity current into deep-sea pelagic conditions. Bottom water oxygen penetrates into the surficial layers of this new turbidite unit, oxidises the labile organic carbon, and releases the authigenic U fraction to solution in oxic pore water conditions. A marked redox contrast is set up in the sediment at the level of zero oxygen, and this contrast progresses downwards as the oxidation front diffuses deeper into the turbidite with time. Uranium is progressively relocated to the weakly reducing conditions immediately below the active front and a U peak develops. This front remains active only as long as the upper reaches of the turbidite are in

diffusive contact with bottom water oxygen; thus it ceases on emplacement of the next turbidite. Figure 1 illustrates the development of the resulting U concentration/depth profile characteristic of the process. Colley and Thomson (1985) found that this profile shape was preserved in buried turbidites where the oxidation fronts responsible were no longer active for up to 250 kyr, and that the U peaks were located just below the colour changes in the turbidites, which marked the extents of penetration of the fronts when active.

The above work used conventional piston cores, < 20 m long. In the study area, such lengths correspond to sediments up to the age of turbidite *k*, about 300 kyr old. The appreciation that the sediments down to 40 or 50 m were of interest for waste disposal caused the Nuclear Energy Agency's Sea-bed Working Group to organise a dedicated cruise to retrieve cores which were as long as achievable. That work was undertaken on the 1985 ESOPE (Étude des Sédiments Océaniques par Pénétration) cruise of MS *Marion Dufresne*, using the 30 m STACOR piston coring device. Samples from two cores from that cruise, MD10 and MD24, have been used in this work. The multi-disciplinary nature of the ESOPE cruise has resulted in good stratigraphic, geochemical and geotechnical data being available for these cores (NOZAKI *et al.*, 1987; DE LANGE *et al.*, 1987; SANTSCHI *et al.*, 1988; BUCKLEY & CRANSTON, 1989; SCHUTTENHELM *et al.*, 1989). These long cores contain turbidites up to *y*, around 750 kyr in age.

A U profile for MD24 (Figure 2), obtained by a reconnaissance delayed neutron technique, demonstrated that the characteristic U profile shape seen in younger turbidites is obviously preserved in turbidites up to 750 kyr old (COLLEY *et al.*, 1989). Figure 2 omits the younger turbidites previously investigated on other cores, and therefore commences at turbidite *g*. It is such old turbidites which have been selected for this project.

The work summarised above has concentrated on U geochemistry, but the older units in cores MD10 and 24 suggest that an investigation of the radioactive daughters is also warranted. With time, the primordial U isotopes ^{238}U and ^{235}U decay through a succession of daughter radionuclides (Figures 3 & 4). Given sufficient time, the condition of *secular equilibrium* is achieved, in which the activity of each radionuclide in each chain is identical with that of the chain parent. Clearly, this can only occur if there is no loss of daughter radionuclides from the decay chain, *i.e.* in a closed system. The time at which secular equilibrium is achieved is governed by the daughter half-life, and as a rule of thumb corresponds to $6 \times t_{\frac{1}{2}\,daughter}$. The objectives of the project are therefore:

(a) to determine U and its long-lived daughter radionuclides (specifically the isotopes ^{234}U, ^{230}Th, ^{226}Ra, ^{210}Po and ^{231}Pa) in selected turbidites with ages between 250 kyr and 750 kyr. The observed profiles will be compared with those predicted by radioactive

ingrowth systematics to determine whether diffusion of U-daughter nuclides away from the peak areas has occurred; and

(b) to utilise the experimental data to estimate effective diffusion coefficients of the different nuclides for modelling purposes. Such data will be relevant to the *in-situ* geochemical conditions of the sediments over the long time scales indicated.

2. ANALYTICAL DEVELOPMENT AND METHODS

2.1 Introduction

Uranium profiles for cores MD24 and MD10 were obtained by a reconnaissance technique using a delayed neutron method. In order to carry out more detailed investigations, the essential early component of the contract was to develop and verify a radiochemical analytical scheme for determination of ^{238}U, ^{234}U, ^{232}Th, ^{230}Th, ^{231}Pa, ^{226}Ra and ^{210}Po. Initially, it was hoped that determinations of all isotopes (except ^{231}Pa) could be carried out using a single sample aliquot, with ^{226}Ra being determined (via ^{222}Rn separation) from the combined solutions produced and conserved during the chemical separations for the U, Th and Po isotopes. In practice, this approach proved unreliable because the high acid strengths and the presence of ammonia in the solutions made evaporation to a reasonable volume without precipitation almost impossible (Table 1). The acid strengths of the samples also caused corrosion within the metal components of the radon separation line. ^{226}Ra is therefore routinely determined using a separate sediment subsample dissolution.

What follows in Sections 2.2 and 2.3 are descriptions of the two methods finally chosen for the radiochemical analysis, together with an intercalibration of the methods to allow direct comparison of the ^{226}Ra values with the isotopes determined separately (Section 2.4). Subsequent sections describe the method used to determine ^{231}Pa (Section 2.5), and other experiments addressing specific problems which arose during the project (Sections 2.6-2.7).

2.2 Radiochemical separations of U and Th isotopes and ^{210}Po

The method employed for determination of U and Th isotopes and ^{210}Po is a modified version of that described by Thomson (1982) for α-emitting isotopes of U and Th in deep-sea sediments. A 1.5-2 g sample of dried and powdered sediment is weighed accurately into a 40 ml platinum crucible and is moistened with water, followed by 10 ml 7M nitric acid to decompose calcium carbonate. After effervescence has ceased, accurately measured aliquots of calibrated $^{232}U/^{228}Th$

and ^{208}Po spikes are added, and the mixture is heated to dryness. Potassium fluoride (7.5 g) is added and mixed with the dried sample, and the crucible is covered and heated with a high-temperature air-blast burner to fuse silicates, with occasional swirling of the contents to incorporate all the sediment into the fusion flux. After fusion, the cooled cake is converted to a sulphate system by addition of 10 ml concentrated sulphuric acid and, after completion of the vigorous reaction of fluoride evolution, 7.5 g of sodium sulphate is added to the crucible. The temperature is gradually increased over an air-blast burner until a pyrosulphate fusion is achieved. The cooled cake from the second fusion is dissolved in 6M HCl with 5 ml 40% w/v hydrogen peroxide, heated, and the hydrated oxides are precipitated when the solution has become clear by addition of concentrated ammonia liquor to a final pH of 7-8. After cooling, the precipitate is centrifuged down and the supernatant liquid decanted off. In the present study, a second dissolution of the precipitate followed by a repeat precipitation was often found to be necessary to achieve dissolution of calcium sulphate, formed from the large amounts of calcium carbonate present in most samples.

The precipitate is then re-dissolved in 1M hydrochloric acid for plating of Po isotopes, a procedure which has been incorporated into the analytical scheme of Thomson (1982) at this point. Po is plated spontaneously from a solution in a PTFE plating cell on to a silver disc at elevated temperature (FLYNN, 1968). Initially, the solution was modified using the method of Smith and Hamilton (1984): 2 ml of citrate solution was added and the pH was adjusted to 1.5-1.6 using ammonia solution. After heating to 80°C, 1 g of ascorbic acid was added to complex iron, and the holder containing the silver disc was added to the solution. The sample was stirred rapidly and heated for 1.5-2 hours. The complete oxidation of this relatively large amount of ascorbic and citric acids later in the separation procedure proved time consuming, and consequently a simpler procedure has been adopted. Po is now plated from a heated solution in 1M HCl to which 100 mg of ascorbic acid has been added (sufficient to cause the solution to be colourless). The plating is carried out at a lower temperature (approximately 50°C) for a longer time (up to five hours). The discs are removed before they become dull to avoid loss of peak resolution during α-spectrometry.

The remaining sample solution is then evaporated to dryness and an aliquot of hydrogen peroxide is added to destroy the ascorbic acid. This solution is evaporated to dryness and an aliquot of concentrated nitric acid is added and again evaporated. The precipitate is then re-dissolved in dilute hydrochloric acid, heated, and the hydrated oxides are again precipitated by addition of concentrated ammonia liquor to a pH of 7-8. Subsequent processing follows the scheme of Thomson (1982). After centrifugation and decanting off the supernatant, the precipitate is re-dissolved in 25 ml of 6M hydrochloric acid, in readiness for the first column. This initial column separates Th isotopes and aluminium (present in the eluate) from U isotopes and iron (which are retained on the column to be eluted later). After removal of the bulk of the Fe from the U solution using di-isopropyl ether, both the U and Th splits are converted to the nitrate system and two further

ion-exchange columns purify the U- and Th-containing solutions. Total dissolution of the Th subsamples prior to the Th purification column was not achieved for most samples used in the study and it was necessary to filter these solutions through 0.4 μm Nuclepore filters before their addition on to the columns. Electroplating of sources for α-spectrometry is achieved using the method of Thomson (1982) based on that of Talvitie (1972). U, Th and Po sources are counted on two Canberra spectrometers, each receiving the outputs of four detectors. The sources are generally counted for 2-3 days to collect at least 1000 counts in each peak of interest. It occasionally takes longer to achieve 1000 counts for ^{232}Th because of the low-to-moderate concentration of this isotope in the calcareous samples encountered here.

2.3 Analysis of ^{226}Ra

Considerable effort was expended early in this study to establish a reliable method for the analysis of ^{226}Ra. A separate sub-sample is used for this analysis for the reasons set out in Section 2.1.

Three methods for sample dissolution were investigated. Three samples were dissolved using a separate fluoride/pyrosulphate fusion as described in Section 2.2. However, a white crystalline precipitate formed in the 1M HCl solutions during storage in all three cases. This was thought to be a sulphate compound formed as a result of the pyrosulphate fusion. Repeat analyses of ^{226}Ra showed a gradual decrease in apparent concentration with increasing time from the initial dissolution of the sample (Figure 5; Table 2). It appeared that ^{226}Ra was progressively being incorporated into some crystal lattice, and that its daughter ^{222}Rn was no longer available for outgassing, being trapped within the crystals. This method is therefore unsatisfactory for ^{226}Ra analysis. The other two methods assessed were a lithium metaborate fusion and a hydrofluoric acid/perchloric acid dissolution. A large homogenised sediment sample (10323 bulk) was prepared and was used extensively as a laboratory standard to test the reproducibility of these methods. Four subsamples were fused with lithium metaborate, sealed and analysed repeatedly over periods of up to 107 days to ensure that the decrease in ^{226}Ra concentration seen when the pyrosulphate fusion was used did not recur. A further two subsamples were dissolved using HF/$HClO_4$ and made up in a dilute nitric acid solution, and repeat determinations of ^{226}Ra were again made over a long time-period to assess solution stability. Table 3 shows means of repeat analyses of the six subsamples. Figures 6 and 7 show ^{226}Ra determinations for two of the subsamples *versus* elapsed time since sample fusion, confirming solution stability. The results show that both methods produce comparable ^{226}Ra values but, because the lithium metaborate fusion is easier in terms of time and effort, it was adopted as the standard dissolution technique for ^{226}Ra in this study. The method is adapted from that of Ingamells (1964), substituting 1M hydrochloric acid for the dilute nitric acid used by that

author. A powdered sediment sample (0.75 g) is heated in a 25 ml platinum crucible for ten minutes in a furnace at 500°C, to destroy organic material. When cool, lithium metaborate is added in a flux-to-sample ratio of 5:1 and the mixture is fused at 900°C for approximately one hour. The molten fusion is then poured into 150 ml cold 1M hydrochloric acid and the crucible is immersed in the liquid, the whole being stirred vigorously overnight to aid dissolution. The resulting solution is transferred to a clean 500 ml Dreschel bottle modified with high performance vacuum taps to seal the inlet and outlet tubes. The solution is then purged with helium and sealed, at which time ^{222}Rn ingrowth commences. After a period of storage to allow ingrowth of ^{222}Rn ($t_{\frac{1}{2}}$ = 3.824 days), the sample is stripped of ^{222}Rn for thirty minutes using re-circulated helium, and ^{222}Rn is adsorbed on to a charcoal column held at - 70°C in a cold bath (Lucas, 1957). Two samples may be run simultaneously using parallel systems. The adsorbed ^{222}Rn is subsequently transferred to a scintillation counting cell by heating the charcoal column to 470°C in a tube furnace and flushing the desorbed gas into the cell with helium. After a period of three hours has elapsed, allowing radioactive equilibrium to be established between ^{222}Rn and its daughters ^{218}Po and ^{214}Po, the samples are counted on an Applied Techniques Company dual-counting system. Four samples may be processed and counted within each twenty-four hour period by this method.

After each analysis, the Dreschel bottles are re-sealed using the vacuum taps and ^{222}Rn ingrowth again commences. The samples may thus be repeatedly stripped for ^{222}Rn measurement, although routinely only duplicate analyses are carried out. The precision of the analysis has improved with practice and with a rigorous adherence to a standard procedure for processing each sample.

It was necessary to determine counting efficiencies individually for each scintillation cell. These were determined using two standards calibrated for ^{226}Ra; a uraninite solution supplied by Dr. M. Ivanovich (UKAERE, Harwell) and known to be in radioactive equilibrium, and DL1a, a Canadian CANMET Standard, also at secular equilibrium. A weighed aliquot of the uraninite solution was sealed in a Dreschel bottle, and a lithium metaborate fusion was used to dissolve a sample of DL1a, which was also sealed in a Dreschel bottle. Repeat determinations of efficiencies were carried out for each detector in use and these range from 87.7% to 95.7% (Table 4). Detector backgrounds are determined by filling the counting cells with helium and counting the activities. System blanks are determined by using Dreschel bottles filled with 1M HCl and carrying out separations in the same way as for samples. Detector backgrounds range from 0.06-0.22 dpm/min, and system blanks are < 0.2 dpm/min.

2.4 Intercalibration of the overall analytical method

It was necessary to carry out an intercalibration exercise to allow direct comparison of the results obtained for U, Th and Po isotopes with those obtained by the separate ^{226}Ra method. This involved a re-calibration of the $^{232}U/^{228}Th$ and ^{208}Po spikes, using a reference material with known activity values for U, Th, Ra and Po isotopes. The calibrated standard used for this purpose was a uraninite supplied by Dr. M. Ivanovich (UKAERE, Harwell). Subsequently, two samples of DL1a (the CANMET standard) were analysed using the new spike calibration values and the results were compared with the recommended values for this reference material. The recommended values for the uraninite and for DL1a are shown in Table 5. The uraninite was supplied in acid solution and radiochemical separation commenced at the Po-plating stage. Subsamples of DL1a were prepared in the same way as for sediment samples (following the method outlined in Section 2.2). Prepared U, Th and Po discs were counted using an α-spectrometer for a few days, to minimise counting uncertainties. Different standard-to-spike ratios were used in each analysis. For each of four uraninite samples processed, a spike activity was calculated from the peak integrals using the recommended values for ^{238}U, ^{234}U and ^{230}Th in turn. In this way, twelve measurements of the $^{232}U/^{228}Th$ spike activity were produced and the mean of these measurements (corrected for radioactive decay of the spike since calibration) is now used to calculate sediment U and Th concentrations. Back-calculation of the ^{208}Po spike is similarly achieved by using the recommended value for ^{210}Po in the uraninite and calculating ^{208}Po values from the peak integrals and volumes of spike and standard used. A mean of these four determinations of ^{208}Po spike activity is used, taking spike radioactive decay since calibration into account, to calculate sample ^{210}Po contents.

The activities of the radionuclides in two subsamples of DL1a were then determined using the new spike calibration, and were compared with the recommended values for this standard. The results are shown in Table 6. In general, good agreement is achieved between recommended values for DL1a and those calculated using the new spike calibration.

The precision of the analytical method is further indicated by the activities determined in two subsamples of the laboratory sediment standard 10323 bulk shown in Table 6.

The use of the recommended values for ^{226}Ra for the uraninite and DL1a when calculating the efficiencies of the counting cells used in the ^{226}Ra determinations (Section 2.3) achieves the necessary intercalibration of the methods and thus the profiles for ^{238}U, ^{234}U, ^{230}Th and ^{210}Po can be compared directly with those for ^{226}Ra.

2.5 Determination of ^{231}Pa

^{231}Pa was determined indirectly *via* its daughter nuclide ^{227}Th, with which it is assumed to be in secular equilibrium. The dominant interference in the determination of ^{227}Th by α–spectrometry is the overlap of ^{224}Ra and ^{212}Bi, radioactive daughters of ^{228}Th. The contribution of ^{224}Ra and ^{212}Bi can be estimated accurately using the intensities of the ^{220}Rn and ^{216}Po peaks (each of 100% abundance at equilibrium relative to ^{228}Th) and is usually of the same magnitude as the count rate in the ^{227}Th peak, thus contributing considerably to the ^{231}Pa error (MANGINI & SONNTAG, 1977). In addition, ^{223}Ra grows in during counting, with an energy which overlaps the ^{227}Th peak. This ingrowth is balanced (to within 1%) by the decay of ^{227}Th during the first thirty hours after plating (MOORE & SOMAYAJULU, 1974), so there is a requirement to count the sample as soon after plating as possible, and then only for a limited length of time.

Five samples were chosen from the U peak region of turbidite *s*, where high concentrations of ^{231}Pa (and hence ^{227}Th) occur. The method of fusion and dissolution is the same as for the analysis of U, Th and Po isotopes, except that sample sizes of 2 g are used, and no spikes are added prior to fusion. After the second precipitation, the hydrated oxide precipitates are re-dissolved in 50 ml 7N HNO_3 and loaded on to anion exchange columns conditioned with 50 ml 7N HNO_3. Following washing with 7N HNO_3, the columns are eluted with 70 ml 6M HCl. TTA extractions are carried out on the samples prior to plating to remove ^{231}Pa which might interfere in the spectra. Electroplating is carried out as described in Section 2.2 and the samples are counted immediately. The $^{227}Th/^{230}Th$ ratio is calculated as follows:

$$\frac{^{227}Th}{^{230}Th} = \frac{\Sigma^{227}Th \text{ area} - 1.3\,[(\Sigma^{220}Rn + \Sigma^{216}Po)/2]}{\Sigma^{230}Th \times {}^{227}Th \text{ decay correction} \times 0.988}$$

The time for the ^{227}Th decay correction is taken from the midpoint of the anion exchange column to the midpoint of the electroplating. The results of the analyses of the samples from turbidite *s* will be discussed in a later section (Section 3.4).

2.6 Determination of ^{226}Ra potentially available for diffusion in pore water solution

Comparisons of ^{230}Th and ^{226}Ra profiles through the turbidite sections analysed in core MD24 indicated that a limited amount of diffusion of ^{226}Ra had taken place. Initial attempts to model the data assumed that all the ^{226}Ra was available for diffusion in pore water solution, but a case must be considered where only a proportion of the total ^{226}Ra, with a larger diffusion coefficient, is mobile. An experiment was designed to estimate this proportion.

Nine samples from core MD24 were chosen for this study. They have a range of ^{226}Ra contents and are from both turbidite and pelagic sections. Weighed quantities (1 g) of the sediment samples were slurried with distilled water (100 ml) and sealed to develop ^{222}Rn by ingrowth from ^{226}Ra. After sufficient time for ^{222}Rn ingrowth, the ^{222}Rn was separated and counted in the usual way. Following duplicate determinations, the samples were opened and the sediment was removed by filtration through 0.4 μm Nuclepore filters. The filtrates were re-sealed and ^{226}Ra was again measured in duplicate (*via* ^{222}Rn) for each sample.

The results obtained from the sediment slurries indicate the gross amount of ^{222}Rn released into the water during the initial storage period, whether by direct production of ^{222}Rn from ^{226}Ra bound within the surfaces of sediment particles, or by production from ^{226}Ra which has been released into the solution phase. (^{222}Rn produced from decay of ^{226}Ra within sediment particles and unable to move into the surrounding water will not contribute to this gross result.) The analysis of the filtrate indicates the amount of ^{226}Ra removed from the sediment to solution during the slurrying procedure. The results from these determinations will be discussed in a later section (Section 4.6).

2.7 Determination of the authigenic U component

Previous work on the most recent turbidite (*a*) in the GME area, demonstrated that it is possible to leach the authigenic U component preferentially from sediment samples (COLLEY & THOMSON, 1985). This is the fraction of the total U content in a U-rich turbidite which is remobilised to form the U peak during the downward progress of the oxidation front. The residue following leaching contains U representing the detrital U component. Good agreement was found between predicted detrital U content and residual U contents after leaching for the most recent turbidite.

Leaching experiments were carried out on three samples from turbidite *s*, to determine whether the authigenic U component remains extractable in this much older turbidite. Samples (2 g) were stirred with 100 ml acetic acid buffered to pH 5 with sodium acetate for thirty minutes at room temperature, following the procedure of Grossman and Miller (1961). After centrifugation and washing of the residue with distilled water, the leachate and leachate residue were spiked individually and analysed separately by α-spectrometry (COLLEY & THOMSON, 1985). Calcium carbonate concentrations were determined for each of the three samples using a Coulometrics coulometer, in order to predict the detrital U values by an alternative method. This method and the results from the leaching experiment will be discussed in Section 4.4.

3. RESULTS

3.1 Introduction

Following the completion of method development, a full set of radiochemical analyses (excepting ^{231}Pa) was obtained for turbidite *t* from MD24. This turbidite was treated first because the reconnaissance U profile had indicated that the lower turbidites in MD24 (particularly *u*, *v* and *w*) had uneven U distributions, whereas that for turbidite *t* was comparatively smooth (Figure 2). Subsequently, samples from turbidite *w* and surrounding units in core MD24 were analysed because this section represents the oldest sediment in the two cores available for study. A smooth U profile was obtained for the lower part of turbidite *v* and turbidite *w* using α-spectrometry, much more like the expected idealised profile of Figure 1, indicating the limited precision of the reconnaissance technique. At a later stage, analyses were obtained from turbidite *s* in MD24. This turbidite was of particular interest because it has the largest maximum/minimum U contrast in core MD24 (see Figure 2). Results from this turbidite were therefore expected to show a well-developed radiochemical disequilibrium near the U peak maximum if diffusion was active.

A U profile was obtained, using the reconnaissance method, for the lower section of core MD10. This core has several extra turbidite units which are not present in core MD24, and the effects of the presence of these on the U profile could be deduced by comparison with the U profile for core MD24.

3.2 Analytical results for core MD24

The results of analyses for ^{238}U, ^{234}U, ^{230}Th, ^{226}Ra, ^{210}Po and ^{232}Th are tabulated in Tables 7-10 for the two continuous sections of core MD24 which have been investigated (turbidites *s* and *t*, and turbidite *w* and surrounding units). The quoted uncertainties are derived from one-sigma counting statistics only. Table 11 shows summations of individual nuclide values for the various turbidite units analysed. There is good agreement between totals for ^{238}U, ^{234}U, ^{230}Th and ^{226}Ra, but ^{210}Po values are consistently low, and $^{210}Po/^{226}Ra$ activity ratios within the units are all lower than unity (Table 12). This suggests that there has been a loss of ^{210}Po (or a precursor) during storage or during the chemical separation stage. (The loss of *all* ^{222}Rn from the powdered samples over two years of storage would result in the decay of ^{210}Pb to 0.934 of its initial value. In this case, the ^{210}Po measurements would also require to be multiplied by $\frac{1}{0.934} = 1.07$ to adjust them to the initial value.) Operationally, the ^{210}Po results have all been multiplied by a correction factor of 1.057, *i.e.* $[(\Sigma^{238}U + \Sigma^{234}U + \Sigma^{230}Th + \Sigma^{226}Ra)/4\Sigma^{210}Po]$ and it is these corrected ^{210}Po results

which will be used in subsequent discussions. The column headed $^{210}Po^{*}/^{226}Ra$ in Table 12 uses corrected ^{210}Po data in the calculation of the activity ratios.

Figures 8 to 15 show profiles of parent and daughter nuclide pairs *versus* depth within the two sections analysed. The parent data points are joined through individual turbidite units *only* in each case, to indicate the profile shapes. Figures 16 and 17 show $^{226}Ra/^{230}Th$ activity ratios *versus* depth for the same two sections, together with traces of the corresponding U profiles to indicate the positions of the U peaks.

3.3 Uranium profile for core MD10

Figure 18 shows a stratigraphic log and U concentration/depth profile for the lower part of core MD10 (on the right), together with the log and U profile for MD24 already available. Equivalent units may be correlated between the two cores using the dashed lines as guides. Table 13 lists the U concentration data for MD10 obtained using the reconnaissance method.

3.4 Analyses of ^{231}Pa from turbidite *s*

Table 14 shows the $^{227}Th/^{230}Th$ activity ratios and ^{231}Pa values for the five samples analysed from turbidite *s* in MD24. In spite of choosing samples with high U values from the region of the U peak, the peak integrals in the ^{227}Th energy region, after correction for ^{212}Bi and ^{224}Ra overlap, ranged from 27 to 193. No further work on the distribution of ^{231}Pa was carried out because it is not present in sufficient concentrations to give analyses of acceptable precision with this method.

4. DISCUSSION

4.1 Comparison of U profiles from cores MD10 and MD24

It is evident from a comparison of the stratigraphic logs of MD10 and MD24 (Figure 18) that MD10 contains additional turbidite units (*l2*, *l3*, *s1* and an un-named unit below *s1*, denoted as *s2* in this text) which are not represented in MD24. The thin units *l2* and *l3* are U-poor and will not be considered further. Turbidite *s1* is classified as an organic-rich turbidite (DE LANGE *et al.*, 1987) and there is a colour change within the turbidite marking the position of a relict oxidation front. There is a small U peak below this colour change, with maximum U concentrations reaching 3.4 ppm. Turbidite *s2* has a high $CaCO_3$ content (> 75% $CaCO_3$) and is not enriched in U.

The presence of *s1* and *s2* has caused different U redistribution patterns in turbidite *t* in MD10 and MD24. These extra units were laid down in MD10 within the continuous period of pelagic sedimentation between turbidites *t* and *s* seen in MD24. In the latter case, where there was no interruption to pelagic sedimentation, dissolved O_2 was able to diffuse into the top of turbidite *t* throughout the whole time period, and a colour change and U peak typical of organic-rich turbidites were developed.

Where the extra turbidite units are present in MD10, bottom-water 0_2 diffusion into turbidite *t* was terminated relatively quickly by the arrival of turbidite *s2,* and a colour change and U peak have not been developed in *t* in the succession sampled by MD10 (Figure 18). Further, the deposition of turbidite *s1* must also have followed relatively quickly after *s2* because a U peak and C_{org} step are present in *s1*, implying that the surface of this turbidite was exposed to bottom water influence for a significant time period, contemporaneous with the active front in turbidite *t* in MD24. The oxidation of *s1* in MD10, and of *t* in MD24 was then terminated by the incursion and emplacement of turbidite *s* throughout the area.

Other differences in U distribution between the two cores can be seen when turbidites *o* and *p* are compared. In MD24, turbidite *p* exhibits a U peak, although this is not associated with a colour change in the sediment. A similar development is not seen in MD10. The lower part of turbidite *o* in MD10 shows a regular increase in U content with depth, which may result from a grain size or compositional change, and is not seen in MD24 (Figure 18).

Core MD10 did not penetrate far enough to sample turbidites *v*, *w*, *x* and *y* which are represented in MD24. Apart from the presence of the additional turbidites *s1* and *s2* in MD10 among the old turbidites of most importance in this work, most other features of the cores are comparable. Less work has therefore been expended on core MD10, because MD24 provides examples of turbidites which are stratigraphically older, and more appropriate for the present study.

4.2 Radionuclide profiles in core MD24

A qualitative inspection of Figures 8 to 11 shows that there is a remarkable agreement between the parent and daughter nuclide profiles for ^{238}U, ^{234}U and ^{230}Th in the two sections analysed from MD24. This indicates that there is good radiochemical closure for the decay sequence $^{238}U \rightarrow {}^{234}U \rightarrow {}^{230}Th$ in both of the sections (turbidites *s* and *t*, and turbidite *w* and surrounding units). This is confirmed by the weighted means of $^{234}U/^{238}U$ and $^{230}Th/^{234}U$ activity ratios within the thick turbidite units analysed (Table 12). Most of the average activity ratios are near unity, the secular equilibrium values expected for these nuclide pairs. Therefore, there does not appear to

have been any preferential migration of ^{234}U away from the U peak maxima in any of the turbidite units analysed, although this might have been expected. Such a mechanism has been invoked in other situations to explain anomalous $^{234}U/^{238}U$ activity ratios, and will be discussed more fully later (Section 4.4).

It has been shown in this work (COLLEY *et al.*, 1989) that it is possible to construct quasi-isochrons for certain turbidites present in the GME area (turbidites *a, d, e, f, h* and *t*). The assumption is made that for each turbidite the homogeneity of the unit on emplacement provides a constant ($^{230}Th/^{232}Th$) and ($^{238}U/^{232}Th$) throughout the turbidite thickness. Variation in ($^{238}U/^{232}Th$) from this constant input value is provided as a result of the downward relocation of the authigenic U component. This violates the closed system formality of the isochron model (ALLEGRE, 1968), because the U redistribution takes place over some tens of thousands of years, and homogeneity of ($^{238}U/^{232}Th$) since emplacement has therefore not been conserved. A precise chronological significance is not, therefore, expected from the slope of the line constructed for each turbidite, and these are therefore termed 'quasi-isochrons'. Colley *et al.* (1989) showed that quasi-isochrons constructed for progressively older turbidites rotated from the horizontal (for the most recent turbidite *a*) towards the line for turbidite *t*, which is indistinguishable from the equiline. This line, with slope 1 and intercept zero, is attained after six ^{230}Th half-lives (450,000 years) have elapsed, but *only if* no loss of intermediate members of the decay sequence occurs.

Isochrons have now been constructed for turbidites *s* and *w* (Figures 19 and 20), and these are also indistinguishable from the equiline. The data from turbidites *s, t* and *w* are noteworthy, since the equiline can only be maintained in a situation where the system is chemically closed between ^{238}U and ^{230}Th, *i.e.* no migration of ^{234}Th, ^{234}Pa or ^{234}U can be active.

Inspection of Figures 14 and 15 also indicates that there has been no significant migration within the decay chain between ^{226}Ra and ^{210}Po, because of the coincidence of the profile shapes. The average activity ratios within the large turbidite units confirm this (Table 12: $^{210}Po^{*}/^{226}Ra$). A poorer agreement between the profiles had been anticipated because of the presence of ^{222}Rn in the decay chain between ^{226}Ra and ^{210}Po. This nuclide, although having a short half life (3.824 days), has no interaction with the solid phase, and might be expected to show significant diffusion. Further discussion of this parent-daughter pair will be included in Section 4.7.

The only radionuclide to show clear evidence of migration in the two sections analysed is ^{226}Ra. Figures 12 and 13 show that ^{226}Ra is deficient where ^{230}Th is at maximum values in turbidites *s, t* and *w*. Depth profiles of $^{226}Ra/^{230}Th$ (Figures 16 and 17) show that ^{226}Ra is also in excess where ^{230}Th has its lowest values. A comparison of $^{226}Ra/^{230}Th$ activity ratios with the trace of the U distribution through the turbidite emphasises the ^{226}Ra deficits at the U peak maxima

(Figures 16 and 17). In general, ^{226}Ra does not appear to have been lost from the two sections sampled to any great extent because the averages of $^{226}Ra/^{230}Th$ activity ratios within the thick units *s*, *t* and *w* are near unity (Table 12), and the summations of ^{226}Ra and ^{230}Th analyses through the major units agree well (Table 11). The high $^{226}Ra/^{230}Th$ and low $^{210}Po/^{226}Ra$ activity ratios found in the units below turbidite *w* suggest that there may be a problem with the analysis of ^{226}Ra at low concentrations, giving rise to elevated ^{226}Ra values.

4.3 A mathematical model to quantify diffusion

A standard model which has been used in previous work to evaluate an effective diffusion coefficient (D) for radionuclides in near-surface sediments is:

$$\frac{\delta R}{\delta t} = D\frac{\delta^2 R}{\delta Z^2} - S\frac{\delta R}{\delta Z} - \lambda R + P = 0 \qquad (1)$$

where R is the concentration of the nuclide, S is the sedimentation rate, λ is the decay constant for the nuclide and P is the production term for the nuclide, all in consistent units (GOLDBERG & KOIDE, 1962; SARMA, 1964; GUINASSO & SCHINK, 1975; KADKO, 1980a). Where pore water data are available, the equation can be modified to take account of the presence of both solid phase and dissolved species (KADKO, 1980a; COCHRAN & KRISHNASWAMI, 1980; KADKO & HEATH, 1984; KADKO *et al.*, 1987).

This model is unsuitable for the present study for a number of reasons:

1. The model assumes a constant production (P) of the radionuclide at all depths in the sediment. This condition is not satisfied in the sections studied in core MD24, where the development of U peaks has led to an irregular production of daughter radionuclides with depth, even in a single turbidite unit.

2. The model is defined for a steady state situation near the sediment-water interface, and includes a term S, for the constant accumulation of new sediment. In the case of MD24, the sections are all at > 22 m in the sediment column, and were deposited at least 600 kyr b.p. Present day sediment accumulation can, therefore, be ignored. In the absence of diffusion, secular equilibrium should have been reached in the ^{238}U decay chain at and below ^{230}Th over this time period. The $^{226}Ra/^{230}Th$ activity ratio-versus-depth profiles indicate, however, that diffusion of ^{226}Ra ($t_{\frac{1}{2}}$ = 1622 years) away from the peak maxima is occurring. The time period of 600 kyr is much greater than the 10 kyr required for the development of a steady state ^{226}Ra diffusion profile in equilibrium with production from ^{230}Th.

An alternative model has been developed to satisfy the conditions in the buried turbidites sampled by core MD24. The new model treats each data set as a series of strips defined by the positions of the data points.

Considering the diffusing substance in an element of width $\delta\beta$, with strength $C_o\delta\beta$, then the concentration at a point P, distance β from the element at time t is:

$$\frac{C_o}{2}\frac{\delta\beta}{\sqrt{(\pi Dt)}}\exp\left[-\beta^2/4Dt\right] \tag{2}$$

(CRANK, 1956). This is shown in Figure 21a. The complete solution for a strip of width 2h is given by summing successive elements $\delta\beta$ in the strip thus:

$$C(z,t) = \frac{C_o}{2\sqrt{(\pi Dt)}}\int_{z-h}^{z+h}\exp\left[-\beta^2/4Dt\right]\delta\beta \tag{3}$$

Substituting $\alpha = \frac{\beta}{2\sqrt{(Dt)}}$, $d\alpha = \frac{\delta\beta}{2\sqrt{(Dt)}}$, $\beta^2 = \frac{z^2}{4Dt}$ and $\beta = \frac{z}{2\sqrt{Dt}}$, equation (3) becomes

$$C(z,t) = \frac{C_o}{\sqrt{\pi}}\int_{A}^{B}\exp(-\alpha^2)\,d\alpha, \tag{4}$$

where $A = \frac{z-h}{2\sqrt{(Dt)}}$ and $B = \frac{z+h}{2\sqrt{(Dt)}}$

Equation (4) can be written as

$$C(z,t) = \frac{C_o}{\sqrt{\pi}}\left\{\int_{A}^{o}\exp\left[-\alpha^2\right]d\alpha + \int_{o}^{B}\exp\left[-\alpha^2\right]d\alpha\right\} \tag{5}$$

or equivalently

$$C(z,t) = \frac{C_o}{\sqrt{\pi}}\left\{\int_{o}^{-A}\exp\left[-\alpha^2\right]d\alpha + \int_{o}^{B}\exp\left[-\alpha^2\right]d\alpha\right\} \tag{6}$$

The error function (written erf y) is a standard mathematical function where

$$\text{erf}\,y = \frac{2}{\sqrt{\pi}}\int_{o}^{y}\exp\left(-\alpha^2\right)d\alpha \tag{7}$$

so considering (7), equation (6) may be rewritten as

$$C(z,t) = \frac{C_o}{2}\left\{\text{erf}\,[(h-z)/2\sqrt{(Dt)}] + \text{erf}\,[(h+z)/2\sqrt{(Dt)}]\right\} \quad (8)$$

This is the equation describing diffusion of a single strip of width 2h with its centre at the origin (Figure 21b).

The model is used for parent/daughter pairs, where the parent produces a daughter at a known rate, free to diffuse for the time period of the daughter mean life. The input to the model is the parent profile, approximated as a series of strips (Figure 22a). Using equation (8) the concentration of the daughter at any point on the z axis due to diffusion of one strip can be found. The total concentration at a point is given by the sum of the contributions made by each of the strips at that point, and a model profile for the daughter nuclide is produced by such a summation at all the input depths.

Several errors are introduced during the assimilation of the experimental parent data into the model, because of the approximation of the profile into strips.

(i) Consider three data points with concentrations of 3, 3.5 and 4.5 units (Figure 22b). The model constructs strips with heights 3.25 and 4 units between these points. If t tends to zero in equation (8), $\frac{h+z}{2\sqrt{(Dt)}} \rightarrow \infty$, and erf $(\infty) = 1$ so $C \approx C_o$, and at $z = \pm h$, $C \approx \frac{C_o}{2}$. The value at $z = (-h_2, +h_1)$ would therefore be $0.5 \times 3.25 + 0.5 \times 4 = 3.625$, according to the model. The true data point at that depth is 3.5, so a 3.5% error is introduced for this example. This suggests that the model behaves better for large values of Dt. Figure 23 shows the results of allowing a single strip to diffuse for a fixed time with different values of D. At lower values of D (7×10^{-12} and 7×10^{-11} $cm^2\ s^{-1}$) the profiles are constrained by the model to pass through 2.5 dpm/g at $\pm$ 5 cm, whereas at a higher value of D (and therefore of Dt), the profile is no longer sufficiently pronounced to pass through 2.5 dpm/g and the resulting errors will be smaller. For this reason, when experimental data are assimilated into the model and then retrieved, the values may change slightly.

(ii) Errors can be introduced where the strip width is large. In Figure 24, the area labelled B and omitted from strip II, is smaller than the area labelled A, which is included in strip II. It is therefore important to minimise strip width where possible, particularly in the regions of the profile where the greatest changes in concentration with depth occur.

(iii) Another source of error results from the loss of material at the end points of the profiles. This effect can be minimised by inserting dummy data points at some distance above and below

the profile ends with the same concentrations as the true end points. The diffusion profiles produced for the dummy points usually compensate for losses incurred at the end points but, in most instances, one or more end points are omitted when goodness of fit between model and experimental data is tested.

A further small error is introduced during the computational stage due to approximation of the error function. The error only appears beyond the fifth decimal place, however, and can therefore be ignored.

By choosing realistic values of D, model profiles of the daughter can be constructed and compared with the experimental profiles obtained using radiochemical analysis. Goodness of fit is assessed by minimising the sums of the squares of the differences (SSD) between the modelled and experimental data points. As an example, Figure 25 shows the sums of squares of differences (SSD) versus D, with a minimum SSD occurring for an optimum D of 4×10^{-8} cm^2 s^{-1}.

Various computer programmes were written using this model for application to specific parent-daughter pairs. The results for ^{238}U-^{234}U, ^{234}U-^{230}Th, ^{230}Th-^{226}Ra and ^{226}Ra-^{210}Po will be described in the following sections.

4.4 Geochemical behaviour of ^{234}U

An inspection of Figures 8 and 9 shows that there is good agreement between the concentration-depth profiles for the ^{238}U-^{234}U parent-daughter pair in the two sections analysed in MD24. Table 12 also indicates that there is no evidence for preferential ^{234}U migration within individual turbidite units. This is unexpected, because previous studies of ^{238}U and ^{234}U have shown that ^{234}U is able to migrate preferentially in pore-water solution in certain circumstances. Ku (1965) invoked migration of 30% of the total ^{234}U in slowly accumulated red clays to explain $^{234}U/^{238}U$ activity ratios at depth in the sediment lower than the expected secular equilibrium value of 1.00. Preferential mobility of ^{234}U also results in lower than expected $^{234}U/^{238}U$ activity ratios in sapropel layers which have enhanced U contents (MANGINI & DOMINIK, 1979). Marked $^{234}U/^{238}U$ disequilibrium resulting from upward migration of ^{234}U has also been found above a U peak in a single turbidite where an oxidation front was still active after 330,000 years (COLLEY *et al.*, 1984). Values up to 1.5 for the $^{234}U/^{238}U$ activity ratio were found above the U peak. The mechanism for ^{234}U migration requires mobilisation of ^{234}U in the (VI) oxidation state following *in-situ* production from ^{238}U in the (IV) oxidation state. Damage to the mineral lattice as a result of recoil during the α-decay of ^{238}U enhances the preferential leaching of ^{234}U (FLEISCHER & RAABE, 1978). Kolodny and Kaplan (1970) showed that approximately 30% of ^{234}U is susceptible to such leaching.

The model developed in Section 4.3 has been applied to the ^{238}U-^{234}U parent-daughter profiles to test the observations of lack of ^{234}U mobility. The mean life of ^{234}U was used in the calculations ($t_{mean} = 1.1 \times 10^{13}$ s). It was not possible, however, to produce any model ^{234}U profiles showing improved agreement with the experimental ^{234}U profiles over the agreements between the ^{234}U experimental data sets and ^{238}U data assimilated into the model assuming no diffusion. (The sum of the squares of the differences between the profiles omitting the topmost point (SSD_{-1}) for the section containing turbidites *s* and *t* = 2.68, and for turbidite *w* and surrounding units $SSD_{-3} = 1.00$). It is possible, however, to calculate an upper limit for D, above which the SSDs show a worsening of agreement between the parent-daughter profiles. Figures 26 and 27 show SSD_{-1} and SSD_{-3} *versus* varying D for the two sections studied, and Table 15 summarises the values obtained. A maximum D of 10^{-15} - 10^{-14} cm^2 s^{-1} can be deduced for ^{234}U in these two sections.

Colley and Thomson (1985) showed that it is possible to leach the authigenic U from samples from the most recent turbidite *a* of the Madeira Abyssal Plain, to leave a refractory level representing the detrital U component. The authigenic U component is that fraction of the total U content in a U-rich turbidite which is remobilised to form the U peak during the downward progress of the oxidation front. An operational U *versus* $CaCO_3$ plot was established for Atlantic sediments with negligible authigenic U (COLLEY & THOMSON, 1985). This relationship allows an independent estimation of detrital U content from the corresponding sediment $CaCO_3$ value only. Good agreement was found between the predicted detrital U content and residual U contents after leaching for this recent turbidite (COLLEY & THOMSON, 1985).

Leaching experiments were carried out on three samples from turbidite *s* in order to determine whether the authigenic U component is similarly still extractable in this older turbidite example by the method described in Section 2.7. Table 16 shows the experimentally-derived results for the three samples from turbidite *s*, together with the values predicted from the U/$CaCO_3$ relationship.

There is broad agreement between the predicted and measured detrital U contents except for the sample from the U peak in turbidite *s*, where the leach has not removed all of the predicted authigenic U component. The $^{234}U/^{238}U$ activity ratios of the detrital fraction are all well below the secular equilibrium value of 1.00. The leach has therefore removed some ^{234}U preferentially from the detrital U fraction. As a consequence, the activity ratios of the leached U fractions are all greater than unity (1.08-1.84). Authigenic U incorporated into sediments at the present time would be expected to have a $^{234}U/^{238}U$ activity ratio of sea water (1.14), and this ratio decays towards unity with a half-life of approximately 250 kyrs. Turbidite *s* was emplaced 600-700 kyrs ago, so the activity ratio of the authigenic U fraction would be expected to be between 1.018 and 1.035. However, the high values found for sample 312, and especially for sample 284 (which is above the relict oxidation front where

authigenic U is absent) also indicate that some ^{234}U has been leached from the detrital phase. The results indicate that U has not been incorporated into a more leach-resistant phase since turbidite *s* was buried. As a corollary, it appears that, since ^{234}U is potentially more mobile than ^{238}U but has not in fact migrated, then the geochemical conditions are acting to immobilise ^{234}U in these sediments.

Extremely low pore water U concentrations (0.1-0.5 ppb) have been measured in samples from core MD24 (SANTSCHI *et al.*, 1988). These values are lower by orders of magnitude than the predicted solubility of UO_2 or U_4O_9, and these authors suggested that solubility of U(IV) was controlled by an adsorbed phase. Both the pore water data (SANTSCHI *et al.*, 1988) and solid phase data here therefore indicate uranium immobility.

4.5 Geochemical behaviour of ^{230}Th

^{230}Th is not expected to diffuse in sediment pore waters because of its strong reactivity with particle surfaces. The immobility of this isotope in the sediment column is used as the basis for determining sediment accumulation rates over time scales of 450 kyr or $6 \times t_{\frac{1}{2}}$ (GOLDBERG & BRULAND, 1974; KU, 1976).

An inspection of Figures 10 and 11 shows that there is good agreement between the concentration-depth profiles for the ^{234}U-^{230}Th parent-daughter pair in the two sections analysed in core MD24. The isochron plots for turbidites *s* and *w* (Figures 19 & 20) and turbidite *t* (COLLEY *et al.*, 1989) confirm that the system is chemically closed between ^{238}U and ^{230}Th, because the equiline is maintained in these units.

It is possible to calculate an upper limit for D, above which the SSDs show a worsening of agreement between the ^{230}Th experimental data and the ^{234}U data assimilated into the model (SSD_{-1} = 3.16 for turbidites *s* and *t* and SSD_{-3} = 0.87 for turbidite *w* and surrounding units). Figures 26 and 27 show SSD_{-1} and SSD_{-3} *versus* varying D for the two sections studied, and Table 15 summarises the values obtained. A maximum D of 10^{-14} - 5×10^{-13} cm^2 s^{-1} can be deduced for ^{230}Th in these two sections.

4.6 Geochemical Behaviour of ^{226}Ra

A computer programme encoding the model developed in Section 4.3 was used to calculate model ^{226}Ra profiles from the parent ^{230}Th data. The mean life of ^{226}Ra ($t_{mean} = 7.3 \times 10^{10}$ s) was used throughout as the diffusion period, and suitable values for D were substituted to optimise

the fit between the experimental ^{226}Ra and model ^{226}Ra data. In the absence of pore water data for dissolved ^{226}Ra, it was initially assumed that 100% ^{226}Ra was mobile.

Figures 28 and 29 show the best fit model ^{226}Ra profiles, together with the data obtained by radiochemical analysis, for the two sections in core MD24. The value for D giving the best fit for the section containing turbidites *s* and *t* is 7×10^{-10} cm^2 s^{-1} and the sum of the squares of the differences between the two profiles, omitting the top sample, (SSD_{-1}), is 6.04. A value for D of 1×10^{-10} cm^2 s^{-1} is obtained for the section containing turbidite *w* and surrounding units (SSD_{-1} = 3.99), but there is poor agreement between modelled and real data near the top of the profile. If the top three points are omitted during the calculation of SSD, the best fit is obtained when D = 7×10^{-10} cm^2 s^{-1} (SSD_{-3} = 2.80). The results are summarised in Table 17, which also shows SSD values obtained when the ^{226}Ra data profiles are compared with ^{230}Th data incorporated into the model assuming no diffusion. The agreement between the model and experimental ^{226}Ra profiles shows a marked improvement on the agreement between the ^{226}Ra experimental data and ^{230}Th profiles constructed by assimilating the ^{230}Th data into the model assuming no diffusion. It is encouraging to note that similar values for D give best fits for both of the sections studied in MD24.

It is possible to refine the diffusion model for ^{226}Ra by considering a situation where only a proportion of ^{226}Ra is mobile. Numerous authors have shown that ^{226}Ra and ^{222}Rn may diffuse in sediment pore waters, and may be released into the overlying water column from near-surface sediments in certain circumstances (KU, 1965; BROECKER, 1965; KEY *et al.*, 1979; KADKO, 1980a & b; COCHRAN & KRISHNASWAMI, 1980; BERELSON *et al.*, 1987). Characteristic concentration *versus* depth profiles are developed for these nuclides, with excess concentrations in bottom waters and consequent deficiencies near the top of the sediment column. Investigations of such near-surface sediments have shown that only a proportion of ^{226}Ra is released to pore water solution by recoil following the α-decay of ^{230}Th adsorbed on particle surfaces. Some ^{226}Ra may be recoiled into the interiors of mineral grains, however, and is not available for diffusion. Surface adsorption (assumed reversible) may also act to remove some ^{226}Ra from solution, so that only a proportion is free to diffuse in pore waters and out into the water column. The fraction of total ^{222}Rn released to pore water may be greater than for ^{226}Ra, because of further weakening of mineral lattice positions as a result of an additional α-decay (KADKO, 1980a). ^{222}Rn has no interaction with the solid phase, and a greater proportion of this nuclide is available for diffusion into the water column to supply the observed ^{222}Rn excess in bottom waters. Estimates of ^{222}Rn emissivity (^{222}Rn supplied to pore waters from the α-decay of ^{226}Ra in pore water and in the solid phase) range from 30% to 75% depending on sediment type and depth in the sediment column (KU, 1965; KEY *et al.*, 1979; KADKO, 1980a; COCHRAN & KRISHNASWAMI, 1980). Values at the lower end of this range tend to be found from carbonate-rich sediments (KEY *et al.*, 1979). Cochran and Krishnaswami (1980) suggested that the ^{226}Ra-^{222}Rn decay could be used as an analogue of the ^{230}Th-^{226}Ra decay to

estimate the fraction of ^{230}Th decays which would recoil ^{226}Ra atoms to pore water, and found by experiment that 61-75% of ^{226}Ra decays produced ^{222}Rn in the fluid phase.

The study undertaken on MD24 allows investigation of radionuclide diffusion at depth in the sediment column. Due to the lack of pore water ^{226}Ra data, the initial treatment of the data assumed that there was 100% mobility of ^{226}Ra. By analogy with the near-surface work previously reported by other authors, the case is considered where only a proportion of the total ^{226}Ra, with a larger diffusion coefficient, is mobile in pore water solution. Experiments have been designed to estimate this proportion (see Section 2.6), for use in refining the modelling of ^{226}Ra diffusion.

Table 18 shows the results of ^{226}Ra determinations on the sediment slurries prior to filtration, and Figure 30 shows a plot of slurry ^{226}Ra *versus* total ^{226}Ra. The gradient of the best fit line is 0.35, suggesting that 35% of total ^{226}Ra is potentially free to diffuse in pore water solution. This value is within the range quoted above for ^{222}Rn emissivity (considered analogous to ^{226}Ra release to pore waters). Results of analysis of the filtrates after filtration through 0.4 μm Nuclepore filters were more equivocal. Repeated analyses with increasing storage time yielded generally decreasing concentrations of ^{226}Ra. This suggested that ^{226}Ra was being progressively removed from solution into a newly-forming solid phase, rather similar to the phenomenon described in Section 2.3. It is the values from the slurry determinations which will be used to refine the diffusion model.

Further evidence for the value of 35% for the proportion of ^{226}Ra free to diffuse in pore water solution was provided using the mathematical model applied to the section containing turbidites *s* and *t* in MD24. Only a constant proportion of the parent ^{230}Th data was allowed to diffuse using the model, and the resulting profile was summed with the immobile ^{230}Th proportion to produce a composite daughter ^{226}Ra profile. The mobile proportion and values for D were varied until an optimum fit was obtained between the model and experimental ^{226}Ra profiles. Table 19 shows the values of SSD_{-1} (omitting the uppermost sample in each case) for varying proportions of mobile ^{226}Ra, and the values of D required to produce the best fit profiles. A minimum SSD_{-1} of 2.14 is found when 35% of the ^{226}Ra production profile is allowed to diffuse with an effective diffusion coefficient of 6×10^{-9} cm^2 s^{-1}. The agreement between the modelled profile and the experimental data is much better than for the simple case where 100% ^{226}Ra was assumed to be mobile. Figure 31 shows the modelled profile (with 35% ^{226}Ra mobile) together with the experimental ^{226}Ra data. A comparison with Figure 28 shows that the goodness of fit has improved particularly in the lower part of turbidite *s* and near the peak in turbidite *t*. The persistent divergence between the profiles in the lower part of *s* suggests that there may be a porosity change resulting from grain size variation, or a change in chemical composition of the solid phase. A more sophisticated model, applying different values for D through the section would be needed to treat this situation.

Table 20 shows the results of a similar treatment for the core section containing turbidite *w* and surrounding units. In this case, the best fit (SSD_{-3}) is obtained for a mobile proportion of between 50 and 80%, giving values for D of between 2×10^{-9} and $1 \times 10^{-9} cm^2 s^{-1}$. Figure 32 shows an illustration for the case where 70% of the profile has been allowed to diffuse with a value for D of $1 \times 10^{-9} cm^2 s^{-1}$. The discrepancy in the mobile proportions required to produce an optimum fit between model and experimental ^{226}Ra data for the two sections analysed may be due to the inclusion of data from turbidites *x* and *y*. It has already been suggested (Section 4.2) that the ^{226}Ra analyses in these units may be elevated due to a problem with analysis of ^{226}Ra at low concentrations. Good agreement between model and ^{226}Ra data which are elevated by an analytical difficulty would require mobilisation of a greater proportion of the ^{230}Th profile into this part of the section. Turbidite *w* also has a slightly greater porosity (0.74) as compared with turbidites *s* and *t* (0.72 and 0.71 respectively) (SCHULTHEISS, ESOPE results; pers. comm.). This difference may be sufficient to allow a greater proportion of ^{226}Ra to diffuse in turbidite *w*.

The values for D found for the two core sections are similar ($6 \times 10^{-9} cm^2 s^{-1}$ and $1 \times 10^{-9} cm^2 s^{-1}$), considering the different proportions of mobile ^{226}Ra required to give agreement between the model and experimental ^{226}Ra data. They are between two and nine times higher than the values for D obtained when 100% ^{226}Ra was considered to be mobile.

The diffusion coefficient used in the models is an effective diffusion coefficient (D_{eff}). As such, the D_{eff} values include all modifications to the free solution coefficient or molecular diffusion coefficient (D_m). These modifications include tortuosity, reversible absorption from solution to the solid phase, and any chemical reaction which irreversibly removes the migrating species from solution to the solid phase. The formulations required to include such effects have been considered by Berner (1976) and Lever (1986). While the proper elucidation of these effects would require modelling of collateral pore water and solid phase data, an evaluation of the validity of the D_{eff} values found for ^{226}Ra can be made from published work.

With the assumption that ^{226}Ra adsorption is related to the dissolved concentration of ^{226}Ra by a constant K (a special case of the Langmuir isotherm theory), and that no irreversible chemical reactions are involved, then (BERNER, 1976):

$$D_{eff} = \frac{D_m}{1 + K}$$

Cochran and Krishnaswami (1980) and Kadko *et al.* (1987) have modelled pore water and solid phase ^{226}Ra data in a set of Pacific cores. In order to fit the data, they found that it was necessary to vary K in proportion to the amount of Mn in the solid phase (the absorptive capacity of manganese oxyhydroxide towards various cations is well known). In the case of oxic sediments with relatively low

(< 0.5%) Mn contents, values of K in the range 1 - 5 x 10^3 were necessary. If Mn is the single controlling factor, such values would be expected to be higher than applicable to core MD24, because manganese oxyhydroxides are expected to be absent in the reducing environment of this core. Nevertheless, since D_m for a sediment porosity of 0.7-0.87 is 2 - 3 x 10^{-6} cm^2 s^{-1} (COCHRAN & KRISHNASWAMI, 1980), D_{eff} values in the range 2 x 10^{-9} - 6 x 10^{-10} may be directly calculated from previous findings. As explained, these are lower limits on the D_{eff} values expected on geochemical grounds. The values found of D_{eff} = 7 x 10^{-10} cm^2 s^{-1} (for 100% mobility) - 6 x 10^{-9} cm^2 s^{-1} (with 35% mobility) in core MD24 are therefore considered to agree well with the values found in previous investigations.

4.7 Geochemical behaviour of ^{210}Po

The radionuclide ^{222}Rn is the most likely member in the decay sequence between ^{226}Ra and ^{210}Po to be mobile. As an inert gas, ^{222}Rn has no interaction with the solid phase, and may be expected to have a more rapid solution diffusion coefficient than an ion. There is good agreement between the concentration-depth profiles for ^{226}Ra and ^{210}Po in core MD24, suggesting little movement of ^{222}Rn (Figures 14 & 15). Attempts were made to use the model developed in Section 4.3 to produce daughter ^{210}Po profiles from the parent ^{226}Ra data using the mean life of ^{222}Rn (4.77 x 10^5 s); this is equivalent to assuming that the ^{210}Po profile is identical with that of ^{222}Rn, and that all ^{222}Rn produced is free to diffuse. Figure 33 and Table 21 show SSDs for varying values of D for the two sections analysed in core MD24. The model produces upper limits for D above which the goodness of fit progressively worsens. Maximum values for D of 10^{-5} cm^2 s^{-1} and 10^{-7} cm^2 s^{-1} are found for the sections containing turbidites *s* and *t*, and *w* and surrounding units respectively. The slight minimum in SSD for turbidites *s* and *t* at a D of 10^{-6} cm^2 s^{-1} was considered too small to be significant.

5. CONCLUSIONS

This investigation of U-series decay systematics in the deep-water distal turbidite sequence of the GME area has shown that:

1. Solid phase U profiles are laterally consistent relative to the associated colour change in transects up to 110 km long in the GME area (COLLEY *et al.*, 1989). The characteristic U profile shape is evident in organic-rich turbidites which are up to 750 kyr old in cores MD10 and MD24, whereas previous work had established this back only to 250 kyr. Apart from the

presence and effects of a few extra, thin turbidites in MD10, most features of the two cores investigated can be correlated and are similar.

2. There is a remarkable degree of chemical closure in the $^{238}U \rightarrow {}^{230}Th$ decay sequence. This can be demonstrated by the construction of quasi-isochrons from ($^{230}Th/^{232}Th$) *versus* ($^{238}U/^{232}Th$) plots for individual turbidites in core MD24. Data from three turbidites with ages between 600 and 750 kyr conform to the equiline, which can only be maintained in a situation where there is no migration in the intermediate members of the decay sequence $^{238}U \rightarrow {}^{230}Th$. As a corollary, the values of the $^{234}U/^{238}U$ activity ratios through the turbidites investigated in this study do not deviate from the secular equilibrium value of 1.00, despite the potential for ^{234}U migration demonstrated by chemical leaching experiments. Any ^{234}U produced in the (VI) oxidation state by recoil must be reduced and/or immobilised in the immediate locality of its production. This conclusion is consistent with pore water U investigations conducted elsewhere on core MD24, where pore water U concentrations much lower than predicted values from thermodynamic considerations were found (SANTSCHI *et al.*, 1988). Application of a mathematical model, designed to determine the effective diffusion coefficient D, cannot improve on the fit between the ^{238}U and ^{234}U data profiles, but a maximum possible value for the ^{234}U effective diffusion coefficient of 10^{-15} - 10^{-14} $cm^2\ s^{-1}$ can be derived by consideration of the goodness of fit between the parent and model daughter profiles. A maximum possible value of D_{eff} for ^{230}Th of 10^{-14} - 5×10^{-13} $cm^2\ s^{-1}$ can be calculated in a similar manner using the ^{234}U-^{230}Th parent-daughter profiles.

3. There is no measurable migration in intermediate members of the decay sequence $^{226}Ra \rightarrow {}^{210}Po$. This is demonstrated by the coincidence of the radionuclide-versus-depth profiles, and by the conformity of the $^{210}Po/^{226}Ra$ activity ratios with the secular equilibrium value of 1.00 through the turbidites investigated, although the analytical uncertainties are somewhat greater for this parent-daughter pair. Application of a mathematical model designed to determine the effective diffusion coefficient D, cannot improve on the fit between the experimental ^{226}Ra and ^{210}Po data profiles. A maximum possible effective diffusion coefficient of between 10^{-7} and 10^{-5} $cm^2\ s^{-1}$ can be derived for ^{222}Rn, an intermediate radionuclide in the decay sequence $^{226}Ra \rightarrow {}^{210}Po$ by consideration of the goodness of fit of the profiles.

4. The only radionuclide showing clear evidence of migration in the turbidites analysed in core MD24 is ^{226}Ra. In the absence of pore water ^{226}Ra data, an effective diffusion coefficient of 7×10^{-10} $cm^2\ s^{-1}$ can be calculated using a mathematical model, and with the assumption that 100% of ^{226}Ra is free to move. The fit between model and experimental

^{226}Ra data can be improved by allowing only a proportion of total ^{226}Ra to be mobile. Optimum proportions were found to be 35% (a value showing good agreement with experimental work) for the section containing turbidites *s* and *t* and 70% for the section containing turbidite *w*, producing values for D of 6×10^{-9} - $1 \times 10^{-9} cm^2 s^{-1}$. The values found for D take into account effects such as tortuosity and sorption (if present) and, as such, represent effective diffusion coefficients in this sedimentary environment. The values for D, and for the proportion of mobile ^{226}Ra, show good agreement with previous work concerned with near surface sediments rather than deep in the sediments as here.

5. The presence of pore water advection does not need to be invoked to explain the ^{226}Ra profiles found in MD24. The daughter nuclide profiles are disposed symmetrically with respect to the parent profiles, indicating that migration of the daughter in pore water solution in this core results from diffusive processes alone. Advection upwards or downwards would be expected to displace a mobile daughter away from an immobile parent in the same sense.

ACKNOWLEDGEMENTS

The authors would like to thank Mark Talbot for his work on the development and application of the mathematical model used to determine the effective diffusion coefficients. They are grateful for the assistance given by the participants on the ESOPE cruise of the MS *Marion Dufresne*.

REFERENCES

ALLEGRE, C.J. 1968 ^{230}Th dating of volcanic rocks: A comment.
Earth & Planetary Science Letters, 5, 209-210.

BERELSON, W.M., BUCHHOLTZ, M.R., HAMMOND, D.E. & SANTSCHI, P.H. 1987 Radon fluxes measured with the MANOP Bottom Lander.
Deep-Sea Research, 34, 1209-1228.

BERNER, R.A. 1976 Inclusion of adsorption in the modelling of early diagenesis.
Earth & Planetary Science Letters, 29, 333-340.

BROECKER, W.S. 1965 An application of natural radon to problems in oceanic circulations.
pp. 116-145 in Proceedings of the Symposium on Diffusion in the Oceans and Freshwaters.
New York: Lamont Geological Observatory.

BUCKLEY, D.E. & CRANSTON, R.E. 1988 Early diagenesis in deep sea turbidites: the imprint of paleo-oxidation zones.
Geochimica et Cosmochimica Acta, 52, 2925-2939.

COCHRAN, J.K. & KRISHNASWAMI, S. 1970 Radium, uranium and ^{210}Pb in deep-sea sediments and sediment pore waters from the north equatorial Pacific.
American Journal of Science, 280, 849-889.

COLLEY, S. & THOMSON, J. 1985 Recurrent uranium relocations in distal turbidites emplaced in pelagic conditions.
Geochimica et Cosmochimica Acta, 49, 2339-2348.

COLLEY, S., THOMSON, J., WILSON, T.R.S. & HIGGS, N.C. 1984 Post-depositional migration of elements during diagenesis in brown clay and turbidite sequences in the North East Atlantic.
Geochimica et Cosmochimica Acta, 48, 1223-1235.

COLLEY, S., THOMSON, J. & TOOLE, J. 1989 Uranium relocations and derivation of quasi-isochrons for a turbidite/pelagic sequence in the Northeast Atlantic.
Geochimica et Cosmochimica Acta, 53, 1223-1234.

CRANK, J. 1956 The Mathematics of Diffusion.
Oxford: Clarendon Press, Oxford, 347 pp.

DE LANGE, G.J., JARVIS, I. & KUIJPERS, A. 1987 Geochemical characteristics and provenance of late Quaternary sediments from the Madeira Abyssal Plain, N. Atlantic.
pp. 147-165 in Geology and Geochemistry of Abyssal Plains (eds. Weaver, P.P.E. and Thomson, J.).
Oxford: Blackwells, 246 pp.
(Geological Society of London Special Publication 31.)

FLEISCHER, R.L. & RAABE, O.G. 1978 Recoiling alpha-emitting nuclei. Mechanism for uranium series disequilibrium.
Geochimica et Cosmochimica Acta, 42, 973-978.

FLYNN, W.W. 1968 The determination of low levels of polonium-210 in environmental materials.
Analytica Chimica Acta, 43, 221-227.

GOLDBERG, E.D. & BRULAND, K.W. 1974 Radioactive chronologies.
pp. 451-489 in The Sea, Vol. 5 (ed. Goldberg, E.D.).
New York: John Wiley & Sons, 895 pp.

GROSSMAN, R.B. & MILLER, J.C. 1961 Carbonate removal from soils by a modification of the acetate buffer method.
Soil Science of America Proceedings, 25, 325-236.

GUINASSO, N.L., Jr. & SCHINK, D.R. 1975 Quantitative estimates of biological mixing rates in abyssal sediments.
Journal of Geophysical Research, 80, 3032-3043.

INGAMELLS, C.O. 1964 Rapid chemical analysis of silicate rocks.
Talanta, 11, 665-666.

JARVIS, I. & HIGGS, N.C. 1987 Trace element mobility during early diagenesis in distal turbidites: late Quaternary of the Madeira Abyssal Plain, N. Atlantic.
pp. 179-213 in Geology and Geochemistry of Abyssal Plains (eds. Weaver, P.P.E. & Thomson, J.).
Oxford: Blackwells, 246 pp.
(Geological Society of London Special Publication 31.)

KADKO, D. 1980a ^{230}Th, ^{226}Ra and ^{222}Rn in abyssal sediment.
Earth & Planetary Science Letters, 49, 360-380.

KADKO, D. 1980b A detailed study of some uranium series nuclides at an abyssal hill area near the East Pacific Rise at 8°45'N.
Earth & Planetary Science Letters, 51, 115-131.

KADKO, D. & HEATH, G.R. 1984 Models of depth-dependent bioturbation at MANOP site H and the Eastern Equatorial Pacific.
Journal of Geophysical Research, 89, 6567-6574.

KADKO, D., COCHRAN, J.K. & LYLE, M. 1987 The effect of bioturbation and adsorption gradients on solid and dissolved radium profiles in sediments from the eastern equatorial Pacific.
Geochimica et Cosmochimica Acta, 51, 1613-1623.

KEY, R.M., GUINASSO, N.L., Jr. & SCHINK, D.R. 1979 Emanation of radon-222 from marine sediments.
Marine Chemistry, 7, 221-250.

KOLODNY, Y. & KAPLAN, I.R. 1970 Uranium isotopes in sea-floor phosphorites.
Geochimica et Cosmochimica Acta, 34, 3-24.

KU, T-L. 1965 An evaluation of the ^{234}U/^{238}U method as a tool for dating pelagic sediments.
Journal of Geophysical Research, 70, 3457-3474.

KU, T-L. 1976 The uranium-series methods of age determination.
Annual Review of Earth and Planetary Sciences, 4, 347-379.

LEVER, D.A. 1986 Some notes on experiments measuring diffusion of sorbed nuclides through porous media.
Atomic Energy Research Establishment Harwell, AERE R 12321, Harwell, 24 pp.

LUCAS, H.F. 1957 Improved low-level alpha-scintillation counter for radon.
Review of Scientific Instruments, 28, 680-683.

MANGINI, A. & DOMINIK, J. 1979 Late Quaternary sapropel on the Mediterranean Ridge: U-budget and evidence for low sedimentation rates.
Sedimentary Geology, 23, 113-125.

MANGINI, A. & SONNTAG, C. 1977 ^{231}Pa dating of deep-sea cores *via* ^{227}Th counting.
Earth & Planetary Science Letters, 37, 251-256.

MOORE, W.S. & SOMAYAJULU, B.L.K. 1974 Age determinations of fossil corals using ^{230}Th/^{234}Th and ^{230}Th/^{227}Th.
Journal of Geophysical Research, 79, 5065-5068.

NOZAKI, Y., SATO, M. & SHIMOOKA, K. 1987 Th-230 dating of ~ 30 m long piston cores taken from two North Atlantic abyssal plains during the ESOPE cruise.
Geochemical Journal, 21, 125-131.

SANTSCHI, P.H., BAJO, C., MANTOVANI, M., ORCIUOLO, D., CRANSTON, R.E. & BRUNO, J. 1988 Uranium in pore waters from North Atlantic (GME and Nares Abyssal Plain) sediments.
Nature, 331, 155-157.

SARMA, T.P. 1964 Dating of marine sediments by ionium and protactinium methods.
Carnegie Institute of Technology. Ph.D. Thesis.

SCHUTTENHELM, R.E. *et al.* 1989 Geoscience Investigations of Two North Atlantic Abyssal Plains, the ESOPE International Exped.
Luxemburg: Commission of European Communities, 1293 pp. (in 2 vols) (EUR 12330, 12331)

SMITH, J.D. & HAMILTON, T.F. 1984 Improved technique for recovery and measurement of polonium-210 from environmental materials.
Analytica Chimica Acta, 160, 69-77.

TALVITIE, N.A. 1972 Electrodeposition of actinides for alpha spectrometric determination.
Analytical Chemistry, 44, 280-283.

THOMSON, J. 1982 A total dissolution method for determination of the α-emitting isotopes of uranium and thorium in deep-sea sediments.
Analytica Chimica Acta, 142, 259-268.

THOMSON, J., COLLEY, S., HIGGS, N.C., HYDES, D.J., WILSON, T.R.S. & SØRENSEN, J. 1987 Geochemical oxidation fronts in North East Atlantic distal turbidites and their effects in the sedimentary records.
pp. 167-177 in Geology and Geochemistry of Abyssal Plains (eds. Weaver, P.P.E. and Thomson, J.).
Oxford: Blackwells, 246 pp.
(Geological Society of London Special Publication 31.)

THOMSON, J., COLLEY, S. & WEAVER, P.P.E. 1988 Bioturbation into a recently emplaced deep-sea turbidite surface as revealed by $^{210}Pb_{excess}$, $^{230}Th_{excess}$ and planktonic foraminifera distributions.
Earth & Planetary Science Letters, 90, 157-173.

WEAVER, P.P.E. & KUIJPERS, A. 1983 Climatic control of turbidite deposition on the Madeira Abyssal Plain.
Nature, 306, 360-363.

WEAVER, P.P.E. & ROTHWELL, R.G. 1987 Sedimentation on the Madeira Abyssal Plain over the last 300,000 years.
pp. 71-86 in Geology and Geochemistry of Abyssal Plains (eds. Weaver, P.P.E. and Thomson, J.).
Oxford: Blackwell, 246 pp.
(Geological Society of London Special Publication 31.)

WILSON, T.R.S., THOMSON, J., COLLEY, S., HYDES, D.J., HIGGS, N.C. & SØRENSEN, J. 1985 Early organic diagenesis: the significance of progressive subsurface oxidation fronts in pelagic sediments.
Geochimica et Cosmochimica Acta, 49, 811-822.

WILSON, T.R.S., THOMSON, J., HYDES, D.J., COLLEY, S., CULKIN F. & SØRENSEN, J. 1986 Oxidation fronts in pelagic sediments: diagenetic formation of metal-rich layers.
Science, 232, 972-975.

TABLE 1 - Comparison of results obtained using combined solutions from the separation steps of U/Th/Po analyses, with those obtained using a lithium metaborate fusion on a separate subsample.

Sample No.	Mean of ^{226}Ra values obtained using combined solutions from U/Th/Po separation	Mean of ^{226}Ra values obtained using separate lithium metaborate fusion
MD 24 318	1.66 ± 0.03	2.65 ± 0.04
MD 24 321 (a)	2.33 ± 0.03	5.69 ± 0.07
MD 24 321 (b)	4.06 ± 0.04	

Table 2 - Repeat determinations of ^{226}Ra for three samples dissolved using the fluoride/pyrosulphate fusion method. The values in brackets are the accepted concentrations for the samples determined by other methods.

SD N 1/2 (8.3 dpm.g)		MD 24 322 (6.3 dpm/g)		MD 24 335 (5.2 dpm/g)	
Days elapsed since dissolution	^{226}Ra dpm/g	Days elapsed since dissolution	^{226}Ra dpm/g	Days elapsed since dissolution	^{226}Ra dpm/g
18	5.8 ± 0.1	10	3.52 ± 0.06	10	2.81 ± 0.06
25	4.38 ± 0.06	13	2.95 ± 0.07	13	2.46 ± 0.07
33	2.93 ± 0.05	18	2.82 ± 0.06	18	2.15 ± 0.06
53	2.11 ± 0.04	32	2.37 ± 0.04	32	1.93 ± 0.04
56	2.01 ± 0.05	39	2.11 ± 0.04	39	1.34 ± 0.04
60	2.00 ± 0.05	62	2.05 ± 0.06	60	1.35 ± 0.05

SDN 1/2 is an IAEA sediment standard.

TABLE 3 - Means of replicate ^{226}Ra determinations of six subsamples of the laboratory standard 10323 bulk.

Subsample No.	No. of analyses	^{226}Ra dpm/g
1	13	3.43 ± 0.03*
2	6	3.55 ± 0.04
3	6	3.59 ± 0.04
4	7	3.54 ± 0.03
5	11	3.51 ± 0.02
6	11	3.54 ± 0.02

* The initial determination of ^{226}Ra is low for this sample If this value is omitted, the mean for twelve analyses is 3.48 ± 0.02 dpm/g.

Note: Subsamples 1-4 were dissolved using lithium metaborate fusion: subsamples 5 and 6 were dissolved using hydrofluoric acid and perchloric acid.

TABLE 4 - Means of repeat determinations of counting efficiencies for the scintillation cells used in this study.

Detector No.	349	350	351	354	355	356	358
Repeat determinations of efficiency	94.8 ± 1.2 90.9 ± 0.7 95.0 ± 0.3 98.1 ± 0.9 90.7 ± 0.7 93.7 ± 1.2 95.2 ± 0.8 96.7 ± 0.7 94.0 ± 0.8 93.9 ± 0.7 94.5 ± 0.6 92.8 ± 0.7	95.2 ± 1.2 97.6 ± 0.9 93.6 ± 0.7 95.9 ± 0.3	86.4 ± 0.7 89.3 ± 0.8 89.0 ± 1.2 87.5 ± 0.5 92.8 ± 1.6 87.1 ± 0.8 86.8 ± 0.8	94.4 ± 0.7 94.0 ± 0.8 94.4 ± 0.9 93.3 ± 0.8 97.0 ± 1.2 94.3 ± 0.5	90.7 ± 0.8 90.1 ± 0.8 90.5 ± 1.5 90.9 ± 0.4 92.5 ± 1.1 90.8 ± 0.8 96.2 ± 0.5	91.8 ± 0.5 95.8 ± 1.2 94.1 ± 0.8 94.9 ± 0.6 93.6 ± 0.7 94.7 ± 0.8	93.9 ± 0.6 94.8 ± 0.9 94.2 ± 0.6 93.5 ± 0.6
Mean	94.3 ± 0.2	95.7 ± 0.3	87.7 ± 0.3	94.3 ± 0.3	92.2 ± 0.2	93.6 ± 0.3	94.0 ± 0.3

TABLE 5 - Recommended values for the standards used in the intercalibration of the overall method. Both standards are in secular equilibrium.

Standard	Activity
Harwell uraninite	14.976 dpm/g ^{238}U
DL1a	0.0116 ± 0.0003% U
	0.0076 ± 0.0004% Th
	1.40 ± 0.04 Bq/g ^{226}Ra
	1.40 ± 0.04 Bq/g ^{210}Po

TABLE 6 - (a) Comparison of results for DL1a calculated using the new spike calibration with recommended values for this standard.

(b) Results for two analyses of the laboratory standard 10323 bulk showing the precision of the method.

Sample	U ppm	^{238}U dpm/g	Th ppm	$^{230}Th/^{232}Th$ activity ratio	$^{234}U/^{238}U$ activity ratio	^{230}Th dpm/g	^{234}U dpm/g	^{210}Po dpm/g
(a) DL1a (mean of two samples analysed)	115 ± 1	86 ± 1	83 ± 1	4.28 ± 0.05	1.00 ± 0.01	86 ± 1	85 ± 1	87 ± 2
Recommended values	116 ± 3	85 ± 2	76 ± 1	4.59 ± 0.27	1.00 ± 0.03	85 ± 2	85 ± 2	84 ± 2
(b) 10323 bulk								
(i)	3.44 ± 0.05	2.57 ± 0.03	7.4 ± 0.1	1.80 ± 0.02	1.00 ± 0.01	3.24 ± 0.04	2.58 ± 0.03	3.29 ± 0.09
(ii)	3.45 ± 0.05	2.58 ± 0.03	7.2 ± 0.1	1.84 ± 0.03	1.01 ± 0.02	3.22 ± 0.05	2.61 ± 0.03	3.57 ± 0.10

TABLE 7 - Radionuclide data for the section of core MD24 containing turbidites s and t

Sample No.	Depth m	^{238}U dpm/g	^{234}U dpm/g	^{230}Th dpm/g	^{226}Ra dpm/g	^{210}Po dpm/g	$^{234}U/^{238}U$ activity ratio	$^{230}Th/^{234}U$ activity ratio	$^{226}Ra/^{230}Th$ activity ratio	$^{210}Po/^{226}Ra$ activity ratio
Turbidite s										
282	22.17	1.56 ± 0.05	1.36 ± 0.05	1.40 ± 0.05	1.77 ± 0.05	1.45 ± 0.06	0.87 ± 0.04	1.03 ± 0.05	1.26 ± 0.06	0.82 ± 0.04
283	22.22	1.21 ± 0.03	1.14 ± 0.03	1.25 ± 0.04	1.35 ± 0.05	1.26 ± 0.05	0.95 ± 0.03	1.10 ± 0.05	1.08 ± 0.05	0.93 ± 0.05
284	22.28	1.21 ± 0.03	1.19 ± 0.03	1.11 ± 0.04	1.55 ± 0.03	1.38 ± 0.05	0.98 ± 0.03	0.93 ± 0.04	1.40 ± 0.06	0.89 ± 0.04
285	22.38	1.93 ± 0.04	2.07 ± 0.04	1.64 ± 0.04	2.09 ± 0.03	1.93 ± 0.07	1.07 ± 0.03	0.79 ± 0.02	1.27 ± 0.04	0.92 ± 0.04
286	22.47	2.27 ± 0.06	2.30 ± 0.06	2.47 ± 0.07	2.73 ± 0.05	2.85 ± 0.07	1.02 ± 0.03	1.07 ± 0.04	1.11 ± 0.04	1.04 ± 0.03
287	22.56	3.66 ± 0.08	3.97 ± 0.09	3.69 ± 0.09	3.47 ± 0.08	3.49 ± 0.06	1.08 ± 0.03	0.93 ± 0.03	0.94 ± 0.03	1.01 ± 0.03
288	22.61	6.3 ± 0.1	6.3 ± 0.1	6.3 ± 0.1	5.7 ± 0.1	5.1 ± 0.2	0.99 ± 0.02	1.01 ± 0.03	0.90 ± 0.02	0.89 ± 0.04
289	22.66	5.8 ± 0.1	5.7 ± 0.1	6.7 ± 0.1	5.9 ± 0.1	5.3 ± 0.1	0.98 ± 0.01	1.17 ± 0.03	0 88 ± 0.02	0.90 ± 0.02
290	22.71	6.6 ± 0.1	6.7 ± 0.1	7.0 ± 0.1	5.6 ± 0.1	5.7 ± 0.2	1.02 ± 0.02	1.05 ± 0.03	0.80 ± 0.02	1.02 ± 0.04
291	22.76	6.3 ± 0.1	6.4 ± 0.1	6.3 ± 0.1	5.5 ± 0.1	5.3 ± 0.1	1.01 ± 0.02	0.98 ± 0.03	0.87 ± 0.02	0.96 ± 0.03
293	22.78	6.2 ± 0.2	6.3 ± 0.2	6.2 ± 0.1	5.2 ± 0.1	4.89 ± 0.19	1.02 ± 0.03	0.98 ± 0.04	0.84 ± 0.02	0.94 ± 0.04
294	22.79	6.3 ± 0.2	6.1 ± 0.2	6.0 ± 0.1	5.3 ± 0.1	5.3 ± 0.1	0.97 ± 0.02	1.00 ± 0.03	0.88 ± 0.02	1.00 ± 0.03
296	22.81	5.7 ± 0.1	5.7 ± 0.1	5.9 ± 0.2	4.99 ± 0.06	4.89 ± 0.11	1.01 ± 0.01	1.04 ± 0.04	0.85 ± 0.03	0.98 ± 0.02
297	22.83	5.2 ± 0.1	5.3 ± 0.1	4.92 ± 0.12	4.69 ± 0.07	4.79 ± 0.19	1.02 ± 0.02	0.92 ± 0.03	0.95 ± 0.03	1.02 ± 0.04
299	22.85	4.67 ± 0.10	4.69 ± 0.10	4.56 ± 0.10	4.46 ± 0.07	4.42 ± 0.14	1.00 ± 0.02	0.97 ± 0.03	0.98 ± 0.03	0.99 ± 0.04
301	22.88	4.67 ± 0.09	4.67 ± 0.09	4.22 ± 0.09	4.45 ± 0.05	3.93 ± 0.13	0.98 ± 0.02	0.90 ± 0.03	1.05 ± 0.03	0.88 ± 0.03
303	22.92	3.88 ± 0.12	3.74 ± 0.12	3.89 ± 0.14	3.95 ± 0.05	3.13 ± 0.13	0.96 ± 0.03	1.04 ± 0.05	1.02 ± 0.04	0.79 ± 0.03
305	22.97	3.36 ± 0.07	3.33 ± 0.07	3.42 ± 0.10	3.52 ± 0.05	3.13 ± 0.09	0.99 ± 0.02	1.03 ± 0.04	1.03 ± 0.03	0.89 ± 0.03
307	23.01	3.07 ± 0.07	3.11 ± 0.07	3.15 ± 0.08	3.35 ± 0.06	2.91 ± 0.12	1.01 ± 0.03	1.01 ± 0.03	1.06 ± 0.03	0.87 ± 0.04
309	23.05	2.98 ± 0.05	3.06 ± 0.05	2.96 ± 0.08	3.33 ± 0.04	3.01 ± 0.06	1.03 ± 0.02	0.97 ± 0.03	1.13 ± 0.03	0.90 ± 0.02
310	23.10	2.81 ± 0.07	2.67 ± 0.06	2.54 ± 0.08	3.08 ± 0.04	3.16 ± 0.10	0.95 ± 0.03	0.95 ± 0.04	1.21 ± 0.04	1.03 ± 0.04
311	23.15	2.84 ± 0.11	2.72 ± 0.11	3.00 ± 0.08	3.14 ± 0.06	2.63 ± 0.08	0.96 ± 0.04	1.10 ± 0.05	1.05 ± 0.03	0.84 ± 0.03
312	23.20	2.55 ± 0.05	2.55 ± 0.05	2.72 ± 0.06	2.86 ± 0.05	2.71 ± 0.07	0.98 ± 0.02	1.07 ± 0.03	1.05 ± 0.03	0.95 ± 0.03
313	23.25	2.50 ± 0.06	2.55 ± 0.06	2.34 ± 0.07	2.84 ± 0.05	2.81 ± 0.12	1.02 ± 0.03	0.92 ± 0.03	1.21 ± 0.04	0.99 ± 0.05
314	23.25	2.17 ± 0.07	2.31 ± 0.08	2.22 ± 0.06	2.81 ± 0.05	2.55 ± 0.09	1.07 ± 0.04	0.96 ± 0.04	1.27 ± 0.04	0.91 ± 0.04
315	23.48	1.88 ± 0.04	1.84 ± 0.03	1.80 ± 0.04	2.62 ± 0.05	2.48 ± 0.08	0.98 ± 0.02	0.98 ± 0.03	1.46 ± 0.04	0.95 ± 0.04
Pelagic										
316	23.51	1.05 ± 0.03	1.28 ± 0.03	1.37 ± 0.02	1.65 ± 0.03	1.14 ± 0.04	1.22 ± 0.04	1.08 ± 0.03	1.20 ± 0.03	0.69 ± 0.03
Turbidite t										
317	23.60	1.71 ± 0.05	1.81 ± 0.06	1.71 ± 0.06	2.48 ± 0.05	2.13 ± 0.08	1.06 ± 0.04	0.94 ± 0.05	1.45 ± 0.06	0.86 ± 0.04
318	23.67	1.70 ± 0.06	1.73 ± 0.06	1.84 ± 0.05	2.49 ± 0.05	2.60 ± 0.06	1.02 ± 0.04	1.06 ± 0.05	1.35 ± 0.05	1.04 ± 0.03
319	23.76	2.99 ± 0.09	3.02 ± 0.09	3.34 ± 0.07	4.04 ± 0.05	3.55 ± 0.15	1.01 ± 0.03	1.11 ± 0.04	1.21 ± 0.03	0.88 ± 0.04
320	23.80	3.92 ± 0.13	4.05 ± 0.13	3.90 ± 0.17	4.09 ± 0.04	3.72 ± 0.12	1.03 ± 0.03	0.96 ± 0.05	1.05 ± 0.05	0.91 ± 0.03
321	23.85	6.2 ± 0.2	6.0 ± 0.2	5.9 ± 0.2	5.7 ± 0.1	4.96 ± 0.11	0.95 ± 0.02	0.99 ± 0.04	0.97 ± 0.04	0.87 ± 0.02
322	23.90	7.3 ± 0.2	7.1 ± 0.2	7.0 ± 0.2	6.3 ± 0.1	5.5 ± 0.1	0.98 ± 0.02	0.98 ± 0.04	0.90 ± 0.03	0.87 ± 0.02
323	23.95	6.8 ± 0.2	6.8 ± 0.2	6.6 ± 0.1	6.1 ± 0.1	5.4 ± 0.1	1.00 ± 0.02	0.97 ± 0.03	0.92 ± 0.02	0.89 ± 0.02
324	24.00	6.7 ± 0.1	6.8 ± 0.1	6.8 ± 0.1	5.9 ± 0.1	5.6 ± 0.2	1.01 ± 0.01	0.99 ± 0.02	0.87 ± 0.02	0.95 ± 0.04
329	24.05	5.6 ± 0.1	5.5 ± 0.1	5.5 ± 0.1	5.6 ± 0.1	4.88 ± 0.14	0.98 ± 0.02	1.01 ± 0.03	1.02 ± 0.03	0.87 ± 0.03
331	24.07	4.51 ± 0.26	4.37 ± 0.26	5.2 ± 0.1	5.0 ± 0.1	5.3 ± 0.2	0.95 ± 0.05	1.18 ± 0.08	0.96 ± 0.03	1.06 ± 0.05
333	24.09	5.3 ± 0.2	5.6 ± 0.2	5.3 ± 0.1	5.3 ± 0.1	5.2 ± 0.2	1.05 ± 0.04	0.95 ± 0.04	1.00 ± 0.03	0.98 ± 0.04
335	24.12	5.3 ± 0.1	5.4 ± 0.1	5.7 ± 0.1	5.2 ± 0.1	4.74 ± 0.08	1.01 ± 0.02	1.05 ± 0.03	0.91 ± 0.02	0.91 ± 0.02
336	24.14	5.5 ± 0.3	5.3 ± 0.2	5.6 ± 0.2	5.3 ± 0.1	4.94 ± 0.17	0.97 ± 0.04	1.05 ± 0.04	0.95 ± 0.04	0.93 ± 0.04
339	24.20	5.4 ± 0.2	5.4 ± 0.2	5.2 ± 0.1	5.3 ± 0.1	4.51 ± 0.13	1.00 ± 0.03	0.97 ± 0.04	1.02 ± 0.03	0.85 ± 0.03
340	24.25	4.7 ± 0.2	5.0 ± 0.2	5.0 ± 0.1	5.1 ± 0.1	5.0 ± 0.2	1.06 ± 0.05	1.01 ± 0.05	1.02 ± 0.03	0.98 ± 0.04
342	24.35	4.84 ± 0.15	4.90 ± 0.15	4.80 ± 0.14	5.1 ± 0.1	4.38 ± 0.12	1.01 ± 0.03	0.98 ± 0.04	1.06 ± 0.04	0.86 ± 0.03
343	24.54	4.68 ± 0.08	4.49 ± 0.08	4.61 ± 0.13	4.88 ± 0.07	4.56 ± 0.14	0.96 ± 0.02	1.03 ± 0.03	1.06 ± 0.03	0.93 ± 0.03
344	24.77	4.31 ± 0.23	4.04 ± 0.22	4.57 ± 0.09	4.45 ± 0.07	4.34 ± 0.12	0.94 ± 0.05	1.13 ± 0.07	0.97 ± 0.02	0.98 ± 0.03
345	24.97	4.59 ± 0.11	4.69 ± 0.11	4.34 ± 0.17	4.55 ± 0.07	5.0 ± 0.1	1.02 ± 0.02	0.93 ± 0.04	1.05 ± 0.04	1.10 ± 0.03

TABLE 8 Radionuclide data for the section of core MD24 containing turbidites v, w, x and y

Sample No.	Depth m	^{238}U dpm/g	^{234}U dpm/g	^{230}Th dpm/g	^{226}Ra dpm/g	^{210}Po dpm/g	$^{234}U/^{238}U$ activity ratio	$^{230}Th/^{234}U$ activity ratio	$^{226}Ra/^{230}Th$ activity ratio	$^{210}Po/^{226}Ra$ activity ratio
Turbidite v										
395	26.95	3.37 ± 0.06	3.42 ± 0.06	3.44 ± 0.07	3.46 ± 0.05	3.25 ± 0.14	1.01 ± 0.02	1.01 ± 0.03	1.01 ± 0.03	0.94 ± 0.04
397	26.99	3.22 ± 0.06	3.17 ± 0.06	3.14 ± 0.06	3.18 ± 0.05	3.01 ± 0.10	0.99 ± 0.02	0.99 ± 0.03	1.01 ± 0.03	0.95 ± 0.03
399	27.03	3.24 ± 0.07	3.14 ± 0.07	3.25 ± 0.07	3.25 ± 0.06	3.02 ± 0.09	0.97 ± 0.02	1.04 ± 0.03	1.00 ± 0.03	0.93 ± 0.03
401	27.10	3.13 ± 0.07	3.12 ± 0.07	3.04 ± 0.07	2.92 ± 0.08	2.95 ± 0.09	1.00 ± 0.03	0.97 ± 0.03	0.96 ± 0.03	1.01 ± 0.04
403	27.19	2.48 ± 0.04	2.51 ± 0.05	2.53 ± 0.07	2.94 ± 0.06	2.85 ± 0.09	1.01 ± 0.02	1.01 ± 0.03	1.16 ± 0.04	0.97 ± 0.04
Pelagic										
404	27.28	2.18 ± 0.04	2.15 ± 0.04	2.19 ± 0.06	2.78 ± 0.06	2.37 ± 0.08	0.98 ± 0.02	1.02 ± 0.03	1.27 ± 0.04	0.85 ± 0.03
405	27.31	2.01 ± 0.05	1.87 ± 0.04	1.94 ± 0.05	2.73 ± 0.03	2.63 ± 0.07	0.93 ± 0.03	1.04 ± 0.03	1.41 ± 0.04	0.96 ± 0.03
Turbidite w										
406	27.35	1.82 ± 0.04	1.85 ± 0.04	1.69 ± 0.05	2.15 ± 0.03	2.23 ± 0.07	1.01 ± 0.03	0.91 ± 0.03	1.27 ± 0.04	1.04 ± 0.04
407	27.38	1.79 ± 0.07	1.91 ± 0.07	1.90 ± 0.06	2.37 ± 0.02	2.16 ± 0.08	1.06 ± 0.05	0.99 ± 0.05	1.25 ± 0.04	0.91 ± 0.03
408	27.46	1.94 ± 0.05	2.04 ± 0.05	2.07 ± 0.05	2.54 ± 0.05	2.43 ± 0.07	1.05 ± 0.03	1.01 ± 0.03	1.23 ± 0.04	0.96 ± 0.03
409	27.49	2.34 ± 0.06	2.34 ± 0.06	2.48 ± 0.07	2.87 ± 0.04	2.51 ± 0.06	1.00 ± 0.03	1.06 ± 0.04	1.16 ± 0.04	0.87 ± 0.02
410	27.54	3.31 ± 0.11	3.06 ± 0.10	3.23 ± 0.08	3.49 ± 0.06	3.18 ± 0.09	0.93 ± 0.03	1.06 ± 0.04	1.08 ± 0.03	0.91 ± 0.03
411	27.59	4.06 ± 0.08	4.09 ± 0.09	4.18 ± 0.08	4.06 ± 0.07	3.40 ± 0.09	1.01 ± 0.02	1.02 ± 0.03	0.97 ± 0.03	0.84 ± 0.03
412	27.64	4.30 ± 0.08	4.20 ± 0.08	4.36 ± 0.10	3.98 ± 0.06	3.63 ± 0.11	0.98 ± 0.02	1.04 ± 0.03	0.91 ± 0.03	0.91 ± 0.03
413	27.69	3.99 ± 0.09	4.09 ± 0.10	4.14 ± 0.13	3.73 ± 0.06	3.83 ± 0.10	1.02 ± 0.03	1.01 ± 0.04	0.90 ± 0.03	1.03 ± 0.03
415	27.71	4.04 ± 0.10	4.12 ± 0.10	4.05 ± 0.10	3.59 ± 0.05	3.61 ± 0.09	1.02 ± 0.03	0.98 ± 0.03	0.89 ± 0.03	1.01 ± 0.03
417	27.73	3.74 ± 0.08	3.86 ± 0.08	3.83 ± 0.09	3.78 ± 0.05	3.38 ± 0.07	1.03 ± 0.02	0.99 ± 0.03	0.99 ± 0.03	0.89 ± 0.02
419	27.75	3.48 ± 0.07	3.57 ± 0.08	3.52 ± 0.08	3.59 ± 0.04	3.56 ± 0.12	1.03 ± 0.02	0.99 ± 0.03	1.02 ± 0.03	0.99 ± 0.04
421	27.77	3.65 ± 0.08	3.69 ± 0.08	3.62 ± 0.08	3.56 ± 0.03	3.14 ± 0.12	1.01 ± 0.02	0.98 ± 0.03	0.98 ± 0.02	0.88 ± 0.03
423	27.79	3.59 ± 0.08	3.55 ± 0.08	3.34 ± 0.08	3.41 ± 0.04	3.16 ± 0.08	0.99 ± 0.02	0.94 ± 0.03	1.02 ± 0.03	0.93 ± 0.03
425	27.83	3.25 ± 0.07	3.26 ± 0.07	3.18 ± 0.07	3.31 ± 0.04	3.04 ± 0.09	1.00 ± 0.02	0.98 ± 0.03	1.04 ± 0.03	0.92 ± 0.03
427	27.87	3.13 ± 0.08	2.98 ± 0.07	3.03 ± 0.07	3.13 ± 0.04	3.12 ± 0.10	0.95 ± 0.03	1.02 ± 0.03	1.03 ± 0.03	1.00 ± 0.03
429	27.93	2.91 ± 0.05	2.92 ± 0.05	2.96 ± 0.05	3.07 ± 0.05	3.04 ± 0.06	1.00 ± 0.02	1.01 ± 0.02	1.04 ± 0.02	0.99 ± 0.03
430	27.97	3.19 ± 0.12	3.09 ± 0.12	3.06 ± 0.06	3.08 ± 0.05	2.99 ± 0.09	0.97 ± 0.04	0.99 ± 0.04	1.01 ± 0.03	0.97 ± 0.03
431	28.06	2.96 ± 0.06	2.99 ± 0.06	3.13 ± 0.07	3.39 ± 0.05	2.94 ± 0.09	1.01 ± 0.02	1.05 ± 0.03	1.08 ± 0.03	0.87 ± 0.03
432	28.14	2.71 ± 0.05	2.69 ± 0.05	2.80 ± 0.06	2.88 ± 0.05	2.69 ± 0.07	0.99 ± 0.02	1.04 ± 0.03	1.03 ± 0.03	0.93 ± 0.03
433	28.34	3.03 ± 0.06	3.07 ± 0.06	3.03 ± 0.06	2.91 ± 0.05	2.84 ± 0.08	1.01 ± 0.02	0.99 ± 0.03	0.96 ± 0.03	0.98 ± 0.03
434	28.54	3.30 ± 0.11	3.14 ± 0.10	3.19 ± 0.07	3.29 ± 0.05	3.07 ± 0.08	0.95 ± 0.03	1.02 ± 0.04	1.03 ± 0.03	0.93 ± 0.03
435	28.74	2.80 ± 0.06	2.85 ± 0.06	2.89 ± 0.05	2.89 ± 0.09	2.67 ± 0.09	1.02 ± 0.02	1.01 ± 0.03	1.00 ± 0.04	0.92 ± 0.04
436	28.92	3.03 ± 0.08	3.33 ± 0.08	3.45 ± 0.06	3.05 ± 0.06	2.93 ± 0.10	1.06 ± 0.03	1.04 ± 0.03	0.88 ± 0.02	0.96 ± 0.04
437	29.04	3.01 ± 0.07	3.23 ± 0.07	3.39 ± 0.08	2.83 ± 0.07	3.01 ± 0.10	1.08 ± 0.03	1.05 ± 0.03	0.83 ± 0.03	1.06 ± 0.04
Pelagic										
438	29.05	2.56 ± 0.08	2.82 ± 0.09	3.07 ± 0.07	2.69 ± 0.05	2.60 ± 0.10	1.10 ± 0.04	1.09 ± 0.04	0.88 ± 0.03	0.83 ± 0.03
439	29.06	1.70 ± 0.06	1.40 ± 0.05	1.49 ± 0.05	2.37 ± 0.04	2.07 ± 0.08	0.82 ± 0.04	1.06 ± 0.05	1.59 ± 0.06	0.87 ± 0.04
440	29.14	1.49 ± 0.04	1.33 ± 0.04	1.32 ± 0.04	2.29 ± 0.05	2.00 ± 0.07	0.89 ± 0.03	0.99 ± 0.04	1.73 ± 0.06	0.83 ± 0.03
Turbidite x										
441	29.24	1.22 ± 0.03	1.14 ± 0.03	1.23 ± 0.03	1.77 ± 0.04	1.45 ± 0.06	0.93 ± 0.03	1.08 ± 0.05	1.44 ± 0.07	0.82 ± 0.04
442	29.39	1.19 ± 0.04	1.02 ± 0.03	1.11 ± 0.03	1.43 ± 0.03	1.23 ± 0.03	0.86 ± 0.03	1.09 ± 0.04	1.29 ± 0.04	0.86 ± 0.03
Pelagic										
443	29.59	1.56 ± 0.04	1.25 ± 0.03	1.37 ± 0.05	1.57 ± 0.04	1.30 ± 0.04	0.80 ± 0.02	1.10 ± 0.05	1.15 ± 0.05	0.83 ± 0.03
Turbidite y										
444	29.70	1.14 ± 0.03	0.98 ± 0.02	1.02 ± 0.04	1.19 ± 0.04	1.05 ± 0.05	0.86 ± 0.03	1.04 ± 0.05	1.17 ± 0.06	0.88 ± 0.05
445	29.74	0.64 ± 0.02	0.62 ± 0.02	0.62 ± 0.02	0.94 ± 0.03	0.82 ± 0.06	0.97 ± 0.04	1.00 ± 0.05	1.52 ± 0.07	0.87 ± 0.07
446	29.93	0.25 ± 0.01	0.32 ± 0.01	0.29 ± 0.01	0.69 ± 0.03	0.37 ± 0.02	1.27 ± 0.07	0.91 ± 0.04	2.38 ± 0.13	0.54 ± 0.04

TABLE 9 - Further radionuclide data for the section of core MD24 containing turbidites *s* and *t*.

Sample No.	Depth m	U ppm	Th ppm	Th/U	$^{230}Th/^{232}Th$ activity ratio
Turbidite *s*					
282	22.17	2.09 ± 0.07	14.4 ± 0.4	6.9 ± 0.3	0.40 ± 0.01
283	22.22	1.61 ± 0.04	9.6 ± 0.3	6.0 ± 0.2	0.54 ± 0.02
284	22.28	1.62 ± 0.04	6.4 ± 0.2	3.95 ± 0.15	0.71 ± 0.03
285	22.38	2.58 ± 0.06	5.9 ± 0.2	2.30 ± 0.08	1.14 ± 0.03
286	22.47	3.03 ± 0.08	6.1 ± 0.2	2.01 ± 0.09	1.66 ± 0.06
287	22.56	4.90 ± 0.11	6.1 ± 0.2	1.23 ± 0.05	2.51 ± 0.08
288	22.61	8.5 ± 0.2	5.6 ± 0.2	0.67 ± 0.03	4.63 ± 0.14
289	22.66	7.8 ± 0.1	5.6 ± 0.2	0.72 ± 0.02	4.93 ± 0.13
290	22.71	8.8 ± 0.2	5.9 ± 0.2	0.67 ± 0.02	4.89 ± 0.14
291	22.76	8.5 ± 0.2	5.9 ± 0.2	0.69 ± 0.02	4.39 ± 0.12
293	22.78	8.3 ± 0.2	6.2 ± 0.2	0.75 ± 0.03	4.10 ± 0.11
294	22.79	8.4 ± 0.2	6.0 ± 0.2	0.72 ± 0.03	4.12 ± 0.11
296	22.81	7.6 ± 0.1	6.0 ± 0.3	0.79 ± 0.04	4.08 ± 0.18
297	22.83	7.0 ± 0.1	5.6 ± 0.2	0.80 ± 0.03	3.65 ± 0.11
299	22.85	6.3 ± 0.1	5.4 ± 0.2	0.86 ± 0.03	3.48 ± 0.10
301	22.88	6.4 ± 0.1	5.7 ± 0.2	0.89 ± 0.03	3.07 ± 0.09
303	22.92	5.2 ± 0.2	5.9 ± 0.3	1.13 ± 0.06	2.73 ± 0.12
305	22.97	4.50 ± 0.10	6.0 ± 0.2	1.33 ± 0.06	2.35 ± 0.09
307	23.01	4.11 ± 0.10	5.6 ± 0.2	1.37 ± 0.06	2.31 ± 0.08
309	23.05	3.99 ± 0.06	5.8 ± 0.1	1.45 ± 0.04	2.11 ± 0.05
310	23.10	3.76 ± 0.09	5.5 ± 0.2	1.47 ± 0.07	1.89 ± 0.07
311	23.15	3.80 ± 0.15	5.6 ± 0.2	1.48 ± 0.08	2.21 ± 0.08
312	23.20	3.46 ± 0.07	6.1 ± 0.2	1.77 ± 0.06	1.83 ± 0.05
313	23.25	3.34 ± 0.08	5.8 ± 0.2	1.74 ± 0.08	1.66 ± 0.07
314	23.35	2.90 ± 0.10	5.9 ± 0.2	2.04 ± 0.09	1.54 ± 0.05
315	23.48	2.52 ± 0.05	5.4 ± 0.1	2.14 ± 0.07	1.37 ± 0.04

TABLE 9 continued

Sample No.	Depth m	U ppm	Th ppm	Th/U	$^{230}Th/^{232}Th$ activity ratio
Pelagic					
316	23.51	1.41 ± 0.04	2.05 ± 0.06	1.45 ± 0.05	2.73 ± 0.08
Turbidite t					
317	23.60	2.29 ± 0.07	7.0 ± 0.3	3.06 ± 0.15	1.01 ± 0.04
318	23.67	2.27 ± 0.08	8.5 ± 0.2	3.75 ± 0.16	0.89 ± 0.02
319	23.76	4.00 ± 0.11	5.7 ± 0.2	1.42 ± 0.05	2.42 ± 0.06
320	23.80	5.2 ± 0.2	5.4 ± 0.3	1.03 ± 0.07	2.98 ± 0.16
321	23.85	8.4 ± 0.2	5.0 ± 0.2	0.63 ± 0.03	4.82 ± 0.14
322	23.90	9.7 ± 0.3	4.78 ± 0.20	0.49 ± 0.02	6.0 ± 0.2
323	23.95	9.1 ± 0.3	5.1 ± 0.2	0.56 ± 0.02	5.3 ± 0.1
324	23.00	9.0 ± 0.1	5.1 ± 0.1	0.57 ± 0.01	5.5 ± 0.1
329	24.05	7.5 ± 0.1	5.1 ± 0.2	0.69 ± 0.03	4.41 ± 0.12
331	24.07	6.0 ± 0.4	5.3 ± 0.2	0.87 ± 0.06	4.04 ± 0.11
333	24.09	7.1 ± 0.3	4.79 ± 0.15	0.67 ± 0.03	4.56 ± 0.13
335	24.12	7.1 ± 0.2	5.0 ± 0.2	0.70 ± 0.03	4.64 ± 0.12
336	24.14	7.3 ± 0.4	5.3 ± 0.2	0.73 ± 0.05	4.32 ± 0.17
339	24.20	7.3 ± 0.2	5.4 ± 0.2	0.75 ± 0.03	3.98 ± 0.09
340	24.25	6.3 ± 0.3	5.2 ± 0.2	0.82 ± 0.05	4.00 ± 0.10
342	24.35	6.5 ± 0.2	4.85 ± 0.20	0.75 ± 0.04	4.07 ± 0.15
343	24.54	6.3 ± 0.1	5.1 ± 0.2	0.82 ± 0.03	3.70 ± 0.13
344	24.77	5.8 ± 0.3	4.89 ± 0.14	0.85 ± 0.05	3.85 ± 0.09
345	24.97	6.2 ± 0.2	4.89 ± 0.27	0.80 ± 0.05	3.65 ± 0.19

TABLE 10 - Further radionuclide data for the section of core MD24 containing turbidites *v*, *w*, *x* and *y*.

Sample No.	Depth m	U ppm	Th ppm	Th/U	$^{230}Th/^{232}Th$ activity ratio
Turbidite *v*					
395	26.95	4.51 ± 0.08	5.2 ± 0.2	1.16 ± 0.04	2.72 ± 0.08
397	26.99	4.31 ± 0.08	4.81 ± 0.13	1.12 ± 0.04	2.69 ± 0.07
399	27.03	4.33 ± 0.10	5.0 ± 0.2	1.16 ± 0.05	2.65 ± 0.08
401	27.10	4.18 ± 0.10	5.1 ± 0.2	1.22 ± 0.05	2.54 ± 0.07
403	27.19	3.31 ± 0.06	6.9 ± 0.2	2.09 ± 0.07	1.51 ± 0.05
Pelagic					
404	27.28	2.92 ± 0.06	5.6 ± .2	1.92 ± 0.07	1.61 ± 0.05
405	27.31	2.69 ± 0.06	11.7 ± 0.3	4.34 ± 0.14	0.68 ± 0.02
Turbidite *w*					
406	27.35	2.43 ± 0.05	6.7 ± 0.2	2.77 ± 0.11	1.03 ± 0.04
407	27.38	2.40 ± 0.09	6.3 ± 0.2	2.61 ± 0.13	1.25 ± 0.05
408	27.46	2.60 ± 0.06	5.7 ± 0.2	2.19 ± 0.08	1.50 ± 0.05
409	27.49	3.13 ± 0.08	5.2 ± 0.2	1.67 ± 0.07	1.95 ± 0.07
410	27.54	4.43 ± 0.14	5.1 ± 0.2	1.14 ± 0.05	2.64 ± 0.09
411	27.59	5.4 ± 0.1	5.1 ± 0.1	0.94 ± 0.03	3.38 ± 0.09
412	27.64	5.8 ± 0.1	4.97 ± 0.16	0.86 ± 0.03	3.62 ± 0.12
413	27.69	5.3 ± 0.1	5.0 ± 0.2	0.94 ± 0.05	3.38 ± 0.14
415	27.71	5.4 ± 0.1	5.0 ± 0.2	0.93 ± 0.04	3.33 ± 0.12
417	27.73	5.0 ± 0.1	5.3 ± 0.2	1.07 ± 0.04	2.95 ± 0.09
419	27.75	4.65 ± 0.10	4.91 ± 0.16	1.06 ± 0.04	2.95 ± 0.09
421	27.77	4.88 ± 0.10	5.3 ± 0.2	1.09 ± 0.04	2.82 ± 0.09
423	27.79	4.81 ± 0.10	4.69 ± 0.16	0.98 ± 0.04	2.94 ± 0.10
425	27.83	4.35 ± 0.10	5.1 ± 0.2	1.16 ± 0.05	2.59 ± 0.08
427	27.87	4.19 ± 0.10	5.0 ± 0.2	1.20 ± 0.05	2.48 ± 0.08

TABLE 10 - continued

Sample No.	Depth m	U ppm	Th ppm	Th/U	$^{230}Th/^{232}Th$ activity ratio
429	27.93	3.90 ± 0.06	5.0 ± 0.1	1.28 ± 0.04	2.43 ± 0.06
430	27.97	4.26 ± 0.16	5.4 ± 0.1	1.26 ± 0.06	2.35 ± 0.06
431	28.06	3.96 ± 0.08	5.5 ± 0.2	1.39 ± 0.05	2.34 ± 0.07
432	28.14	3.62 ± 0.06	5.2 ± 0.2	1.45 ± 0.05	2.20 ± 0.06
433	28.34	4.06 ± 0.08	5.4 ± 0.1	1.33 ± 0.04	2.32 ± 0.06
434	28.54	4.42 ± 0.14	5.5 ± 0.2	1.24 ± 0.05	2.39 ± 0.07
435	28.74	3.74 ± 0.08	5.2 ± 0.1	1.39 ± 0.05	2.29 ± 0.06
436	28.92	4.19 ± 0.11	5.7 ± 0.1	1.35 ± 0.05	2.51 ± 0.06
437	29.04	4.02 ± 0.10	5.6 ± 0.2	1.39 ± 0.06	2.50 ± 0.08
Pelagic					
438	29.05	3.43 ± 0.11	6.6 ± 0.2	1.93 ± 0.08	1.91 ± 0.05
439	29.06	2.28 ± 0.08	17.0 ± 0.4	7.5 ± 0.03	0.36 ± 0.01
440	29.14	1.99 ± 0.06	14.0 ± 0.3	7.0 ± 0.3	0.39 ± 0.01
Turbidite x					
441	29.24	1.63 ± 0.04	10.1 ± 0.4	6.2 ± 0.3	0.50 ± 0.02
442	29.39	1.59 ± 0.05	6.8 ± 0.2	4.28 ± 0.18	0.67 ± 0.02
Pelagic					
443	29.59	2.09 ± 0.05	14.6 ± 0.4	7.0 ± 0.3	0.39 ± 0.01
Turbidite y					
444	29.70	1.53 ± 0.03	10.4 ± 0.3	6.8 ± 0.2	0.40 ± 0.02
445	29.74	0.86 ± 0.03	5.7 ± 0.2	6.7 ± 0.3	0.45 ± 0.02
446	29.93	0.34 ± 0.01	2.18 ± 0.06	6.4 ± 0.3	0.55 ± 0.03

TABLE 11 - Summations of nuclide values within individual units from MD24

Unit (no. of analyses)	^{238}U dpm/g	^{234}U dpm/g	^{230}Th dpm/g	^{226}Ra dpm/g	^{210}Po dpm/g
S (26)	97.66	97.77	97.70	96.25	90.50
pelagic (1)	1.05	1.28	1.37	1.65	1.14
T (19)	92.05	92.00	92.91	92.88	86.31
Y (5)	15.44	15.36	15.40	15.75	15.08
pelagic (2)	4.19	4.02	4.13	5.51	5.00
W (24)	75.37	75.92	76.52	76.95	72.56
pelagic (3)	5.75	5.55	5.88	7.35	6.56
X (2)	2.41	2.16	2.34	3.20	2.68
pelagic (1)	1.56	1.25	1.37	1.57	1.30
Y (3)	2.03	1.92	1.93	2.82	2.24
Total	297.51	297.23	299.55	303.93	283.37

TABLE 12 - Weighted means of activity ratios within individual units from MD24.

Unit (no. of analyses)	$^{234}U/^{238}U$ activity ratio	$^{230}Th/^{234}U$ activity ratio	$^{226}Ra/^{230}Th$ activity ratio	$^{210}Po/^{226}Ra$ activity ratio	$^{210}Po^{*}/^{226}Ra$ activity ratio
s (26)	0.997 ± 0.004	0.976 ± 0.006	0.975 ± 0.006	0.932 ± 0.006	0.988 ± 0.007
pelagic (1)	1.22 ± 0.04	1.08 ± 0.03	1.20 ± 0.03	0.69 ± 0.03	0.73 ± 0.03
t (19)	0.999 ± 0.005	1.004 ± 0.008	0.986 ± 0.007	0.918 ± 0.007	0.980 ± 0.007
v (5)	0.996 ± 0.009	1.004 ± 0.013	1.015 ± 0.014	0.955 ± 0.016	1.009 ± 0.017
pelagic (2)	0.965 ± 0.017	1.030 ± 0.021	1.340 ± 0.028	0.905 ± 0.021	0.977 ± 0.024
w (24)	1.007 ± 0.005	1.006 ± 0.006	1.003 ± 0.006	0.935 ± 0.006	0.993 ± 0.007
pelagic (3)	0.927 ± 0.021	1.045 ± 0.025	1.140 ± 0.024	0.878 ± 0.021	0.923 ± 0.021
x (2)	0.895 ± 0.021	1.086 ± 0.031	1.327 ± 0.035	0.846 ± 0.024	0.896 ± 0.024
pelagic (1)	0.80 ± 0.02	1.10 ± 0.05	1.15 ± 0.05	0.83 ± 0.03	0.88 ± 0.04
y (3)	0.939 ± 0.023	0.972 ± 0.026	1.434 ± 0.043	0.705 ± 0.029	0.764 ± 0.034

* Corrected ^{210}Po results.

TABLE 13 - Uranium analyses for core MD10 (obtained using a commercial delayed neutron method)

Sample depth m	U ppm	Sample depth m	U ppm	Sample depth m	U ppm	Sample depth m	U ppm	Sample depth m	U ppm	Sample depth m	U ppm
Turbidite l		Pelagic		25.50	1.5	28.79	0.2	30.66	2.8	31.71	6.8
				25.525	1.7	28.80	0.2			31.72	6.9
20.02	0.2	22.74	0.4	25.55	1.3	28.81	0.4	Pelagic		31.73	7.1
				25.56	1.4	28.82	0.3			31.74	6.8
Foram sand		Turbidite o		25.57	1.0	28.83	0.5	30.73	1.2	31.75	7.1
				25.58	1.5	28.84	0.2			31.76	6.9
20.12	0.3	23.03	1.0	25.59	0.9	28.85	0.2	Turbidite s1		31.77	6.4
20.22	0.3	23.28	0.2	25.60	0.7	28.86	0.5			31.78	6.3
20.32	0.3	23.53	0.5	25.61	0.9	28.87	0.2	30.83	1.5	31.80	6.6
		23.83	0.8	25.62	0.9	28.88	0.8	30.89	1.7	31.82	6.6
Pelagic		24.03	0.5	25.63	1.3	28.90	0.2	30.98	2.4	31.84	6.4
		24.055	0.8	25.64	0.6	28.92	0.2	31.03	2.8	31.86	6.4
20.39	2.4	24.08	0.4	25.65	0.8	28.94	0.2	31.055	3.3	31.92	6.2
		24.105	0.8	25.66	0.9	28.96	0.4	31.08	3.4	31.97	5.9
Turbidite 2		24.13	0.8	25.69	1.0	28.98	0.5	31.105	3.4	32.02	6.6
		24.155	0.8	25.71	0.8	29.03	0.2			32.12	6.6
20.43	0.4	24.18	0.8	25.73	1.1	29.08	0.2	Pelagic		32.27	6.3
		24.205	1.2	25.75	0.8	29.18	0.2			32.47	5.8
Pelagic		24.23	1.1	25.79	0.8	29.30	0.5	31.13	2.5	32.67	5.3
		24.255	0.9	25.90	0.7	29.32	2.5	31.15	2.3	32.88	5.9
20.49	0.7	24.28	1.1	25.98	0.7						
		24.29	1.0	26.28	0.6	Pelagic		Turbidite s2		Pelagic	
Turbidite 11		24.30	1.1	26.48	0.8						
		24.31	1.6	26.74	0.5	29.38	2.7	31.18	2.2	33.05	1.5
20.53	1.5	24.32	1.5	27.08	1.2			31.19	1.9		
20.58	1.6	24.33	1.0			Turbidite s		31.20	1.8	Turbidite u	
20.64	1.0	24.34	1.2	Pelagic				31.21	2.0		
20.69	1.1	24.35	1.6			29.43	2.2	31.22	1.9	33.18	2.4
20.74	1.2	24.36	1.3	27.26	0.5	29.53	1.6	31.23	1.4	33.28	2.6
20.83	1.2	24.37	1.4			29.60	1.7	31.24	1.6	33.305	4.3
		24.38	1.2	Turbidite q		29.71	7.2	31.25	1.2	33.33	6.0
Pelagic		24.39	1.2			29.735	7.3	31.26	1.1	33.355	5.4
		24.40	1.5	27.48	1.1	29.76	7.3	31.27	1.4	33.38	6.0
20.98	2.1	24.41	1.2	27.73	0.2	29.79	7.1	31.28	1.3	33.405	5.4
		24.42	1.5	27.98	0.5	29.81	7.6	31.30	1.1	33.43	6.0
Turbidite 12		24.43	1.4	28.14	0.2	29.83	7.2	31.32	1.7	33.455	5.0
		24.48	1.7			29.84	7.0	31.34	1.5	33.48	5.2
21.13	1.6	24.53	1.8	Pelagic		29.85	6.6	31.36	1.5	33.50	5.4
		24.63	1.7			29.86	6.7	31.38	1.0	33.51	4.4
Pelagic		24.74	2.2	28.17	1.1	29.87	6.6	31.41	1.4	33.52	4.5
		24.93	2.4			29.88	5.9			33.53	4.9
21.28	2.0	25.03	2.8	Turbidite r		29.89	6.4	Pelagic?		33.54	4.5
		25.13	1.9			29.90	6.2			33.55	4.6
Turbidite 13		25.23	2.4	28.33	0.7	29.91	5.0	31.46	2.0	33.56	4.9
				28.43	0.5	29.92	6.5			33.57	4.2
21.43	1.4	Pelagic		28.53	0.3	29.93	6.0	Turbidite t		33.58	4.2
				28.555	0.4	29.95	5.2			33.59	4.9
Pelagic		25.35	3.1	28.58	0.5	29.97	5.0	31.50	3.2	33.60	4.4
		25.375	4.5	28.605	0.2	29.99	4.5	31.525	5.7	33.62	4.9
21.62	2.1			28.63	0.4	30.01	4.7	31.55	6.0	33.64	4.9
		Turbidite p		28.655	0.6	30.03	4.1	31.575	6.2	33.66	4.4
Turbidite n				28.68	0.2	30.08	3.5	31.625	6.2	33.68	4.1
		25.40	2.9	28.71	0.5	30.13	3.0	31.65	6.5	33.70	4.9
21.90	0.6	25.425	3.1	28.74	0.4	30.18	3.2	31.68	7.2	33.73	3.9
22.10	0.4	25.45	2.2	28.755	0.7	30.32	3.2	31.69	5.8	33.76	3.8
22.40	0.7	25.475	1.8	28.77	0.2	30.48	3.0	31.70	6.6		

Table 14 - ^{231}Pa results for the five samples analysed from turbidite *s*.

Sample No.	$^{227}Th/^{230}Th$ activity ratio	^{230}Th dpm/g	^{231}Pa dpm/g
286	0.050 ± 0.012	3.69 ± 0.09	0.18 ± 0.04
291	0.050 ± 0.006	6.3 ± 0.1	0.32 ± 0.04
293	0.058 ± 0.006	6.2 ± 0.1	0.36 ± 0.04
294	0.036 ± 0.015	6.0 ± 0.1	0.22 ± 0.09
296	0.064 ± 0.006	5.9 ± 0.2	0.38 ± 0.04

TABLE 15 - Values of the sums of the squares of the differences between parent experimental data after assimilation into the model assuming no diffusion and daughter experimental data, with varying D for ^{238}U - ^{234}U and ^{234}U - ^{230}Th in the two sections analysed in core MD24.

D	^{238}U - ^{234}U		^{234}U - ^{230}Th	
	s, t	*v, w, x, y*	*s, t*	*v, w, x, y*
$cm^2\ s^{-1}$	SSD_{-1}	SSD_{-3}	SSD_{-1}	SSD_{-3}
10^{-16}	2.68	1.00	3.16	0.87
10^{-15}	2.68	1.00	3.16	0.87
10^{-14}	2.68	1.03	3.16	0.87
5×10^{-14}	2.73	1.26	3.16	1.05
10^{-13}	2.85	1.45	3.16	1.05
5×10^{-13}	3.69	2.00	3.14	1.62
10^{-12}	4.82	2.28	3.35	1.94
5×10^{-12}	14.31	4.70	5.99	2.98
10^{-11}	25.76	7.54	9.67	4.02
5×10^{-11}	87.43	14.48	37.63	10.55
10^{-10}	126.79	17.42	64.19	16.00
10^{-9}	211.95	70.35	169.48	33.58
10^{-8}	519.34	185.89	342.06	132.65

TABLE 16 - Comparison of predicted and observed (HOAc/NaOAc leach at pH 5) U fractions in samples from turbidite *s* in core MD24.

			TOTAL			DETRITAL		AUTHIGENIC	
Sample No.	Depth cm	$CaCO_3$ (%)	U ppm	$^{234}U/^{238}U$ activity ratio		U ppm	$^{234}U/^{238}U$ activity ratio	U ppm	$^{234}U/^{238}U$ activity ratio
284	2228	45.1	1.62 ± 0.04	0.98 ± 0.03	Predicted*	1.46	1.0	0.16	1.02
			(1.51 ± 0.04	0.96 ± 0.03)	Observed	1.22 ± 0.04	0.76 ± 0.03	0.29 ± 0.01	1.83 ± 0.09
290	2271	51.3	8.80 ±0.2	1.02 ±0.02	Predicted*	1.29	1.0	7.5	1.02
			(8.80 ± 0.1	1.02 ± 0.02)	Observed	2.58 ± 0.08	0.84 ± 0.03	6.2 ± 0.1	1.08 ± 0.02
312	2320	52.0	3.46 ± 0.07	0.98 ± 0.02	Predicted*	1.27	1.0	2.19	1.02
			(3.35 ± 0.06	0.98 ± 0.02)	Observed	1.46 ± 0.05	0.82 ± 0.03	1.89 ± 0.04	1.18 ± 0.03

* Predictions based on (i) detrital U = 2.7 x (1 - $\%CaCO_3/100$, (ii) ^{234}U at secular equilibrium with ^{238}U in detrital component, (iii) authigenic U with maximum possible $^{234}U/^{238}U$ activity ratios of 1.02 (seawater value of 1.14 decayed for 650 kyr). The total U contents and $^{234}U/^{238}U$ activity ratios quoted are from (i) a single analysis of whole sediment and (ii) in parenthesis the sum of the observed detrital and authigenic fractions.

TABLE 17 - A summary of the optimum values obtained for the effective diffusion coefficient for the two sections in MD24. 100% ^{226}Ra mobility is assumed.

	D cm^2s^{-1}	SSD $^{226}Ra_{data}:^{226}Ra_{model}$
s and *t*	7×10^{-10}	SSD_{-1}: 6.04 (10.28)
v, *w*, *x* and *y*		
a	1×10^{-10}	SSD_{-1}: 3.99 (4.67)
b	7×10^{-10}	SSD_{-3}: 2.80 (4.66)

SSD: Sum of the squares of the differences between data sets. The values in parentheses are SSDs calculated for $^{226}Ra_{data}$ relative to ^{230}Th data incorporated into the model assuming no diffusion.

TABLE 18 - Results of ^{226}Ra determinations on sediment slurries together with total ^{226}Ra analyses for the nine samples investigated.

Sample	$^{226}Ra_{total}$ dpm/g	$^{226}Ra_{slurry}$ dpm/g
322	6.3 ± 0.1	2.30 ± 0.05
329	5.6 ± 0.1	2.15 ± 0.04
344	4.45 ± 0.07	1.90 ± 0.03
405	2.73 ± 0.03	1.46 ± 0.03
432	2.88 ± 0.05	1.47 ± 0.03
436	3.05 ± 0.06	1.16 ± 0.04
442	1.43 ± 0.03	0.64 ± 0.02
445	0.94 ± 0.03	0.54 ± 0.02
446	0.69 ± 0.03	0.32 ± 0.02

TABLE 19 - Values for the effective diffusion coefficient D obtained for varying proportions of mobile ^{226}Ra for the section containing turbidites *s* and *t*.

% mobile ^{226}Ra	D (cm^2s^{-1})	SSD_{-1}
25	1×10^{-8}	2.68
30	9×10^{-9}	2.33
35	6×10^{-9}	2.14
40	5×10^{-9}	2.23
50	3×10^{-9}	2.62
100	7×10^{-10}	6.04

TABLE 20 - Values for the effective diffusion coefficient D obtained for varying proportions of mobile ^{226}Ra for the section containing turbidites *v*, *w*, *x* and *y*.

% mobile ^{226}Ra	D cm^2s^{-1}	SSD_{-3}
25	3×10^{-9}	3.52
30	4×10^{-9}	3.22
35	3×10^{-9}	3.01
40	3×10^{-9}	2.84
50	2×10^{-9}	2.64
60	2×10^{-9}	2.60
70	1×10^{-9}	2.57
80	1×10^{-9}	2.59
100	7×10^{-10}	2.80

Table 21 - Values of the sums of the squares of the differences between ^{226}Ra experimental data assimilated into the model assuming no diffusion and ^{210}Po experimental data with varying D for the two sections analysed in core MD24.

D $cm^2\ s^{-1}$	*s* and *t* SSD_{-1}	*v*, *w*, *x*, *y* SSD_{-3}
10^{-8}	4.40	1.22
10^{-7}	4.40	1.22
10^{-6}	4.38	1.27
10^{-5}	4.41	1.34
5×10^{-5}	5.63	1.56
10^{-4}	7.73	2.06
10^{-3}	43.07	6.60

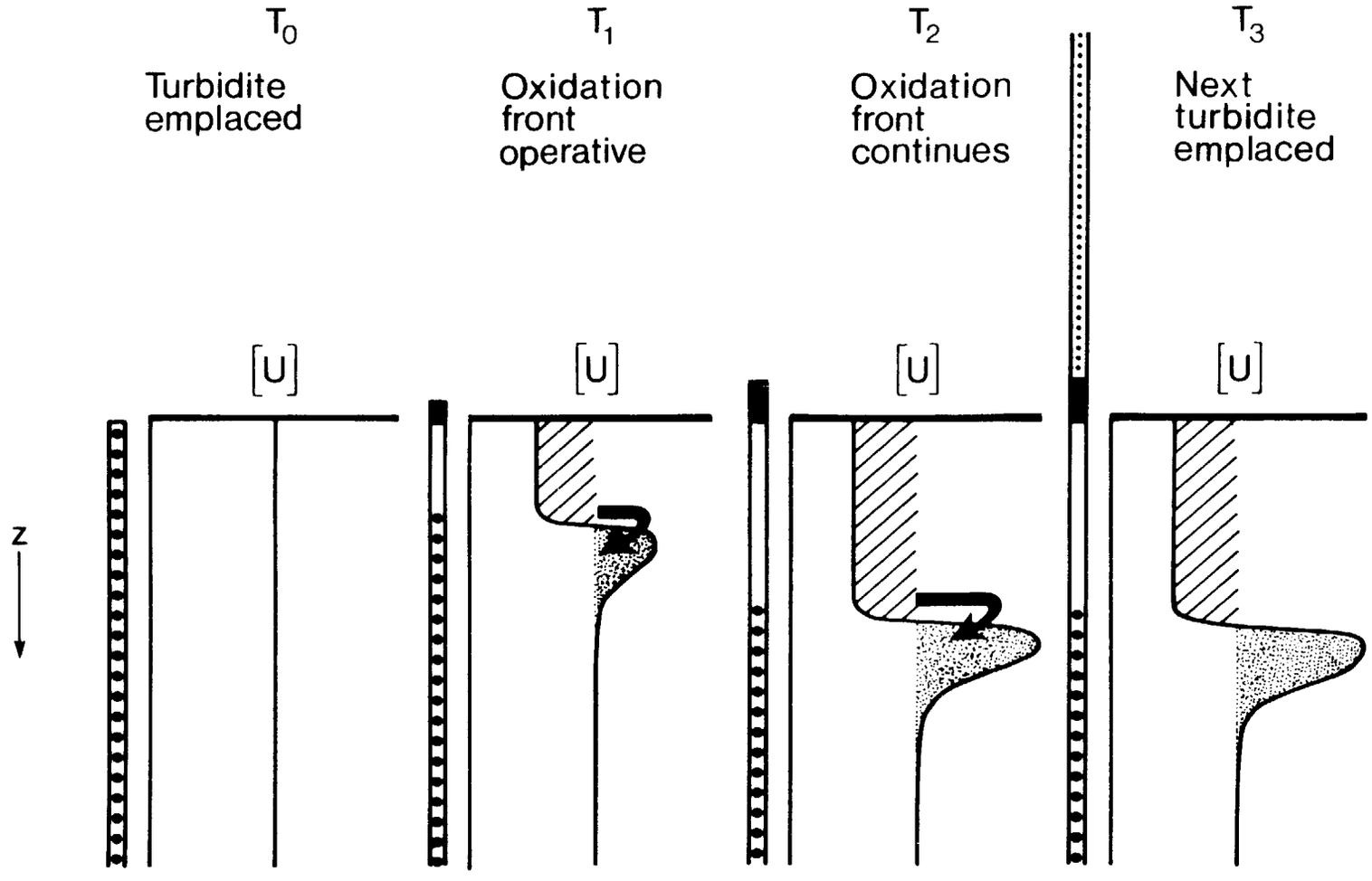

Figure 1 Representation of the formation of diagenetic U profiles in organic-rich GME distal turbidites. At T_o the turbidite is newly emplaced with a homogeneous content: both detrital and authigenic U forms are present. At T_1, bottom water oxygen has diffused into the turbidite surface, oxidising organic carbon and mobilising authigenic U only. A small quantity of pelagic sediment (represented by the solid black area in sediment column) has accumulated, and a fraction of the remobilised U has formed a peak below the progressive oxidation front. At T_2 the progressive oxidation front has moved further into the sediment and the U peak has been augmented and has migrated with the front. At T_3 another turbidite has been emplaced, the progressive oxidation front has been terminated because diffusive contact with bottom water has been blocked, and the U peak remains as a relict indicator of the process.

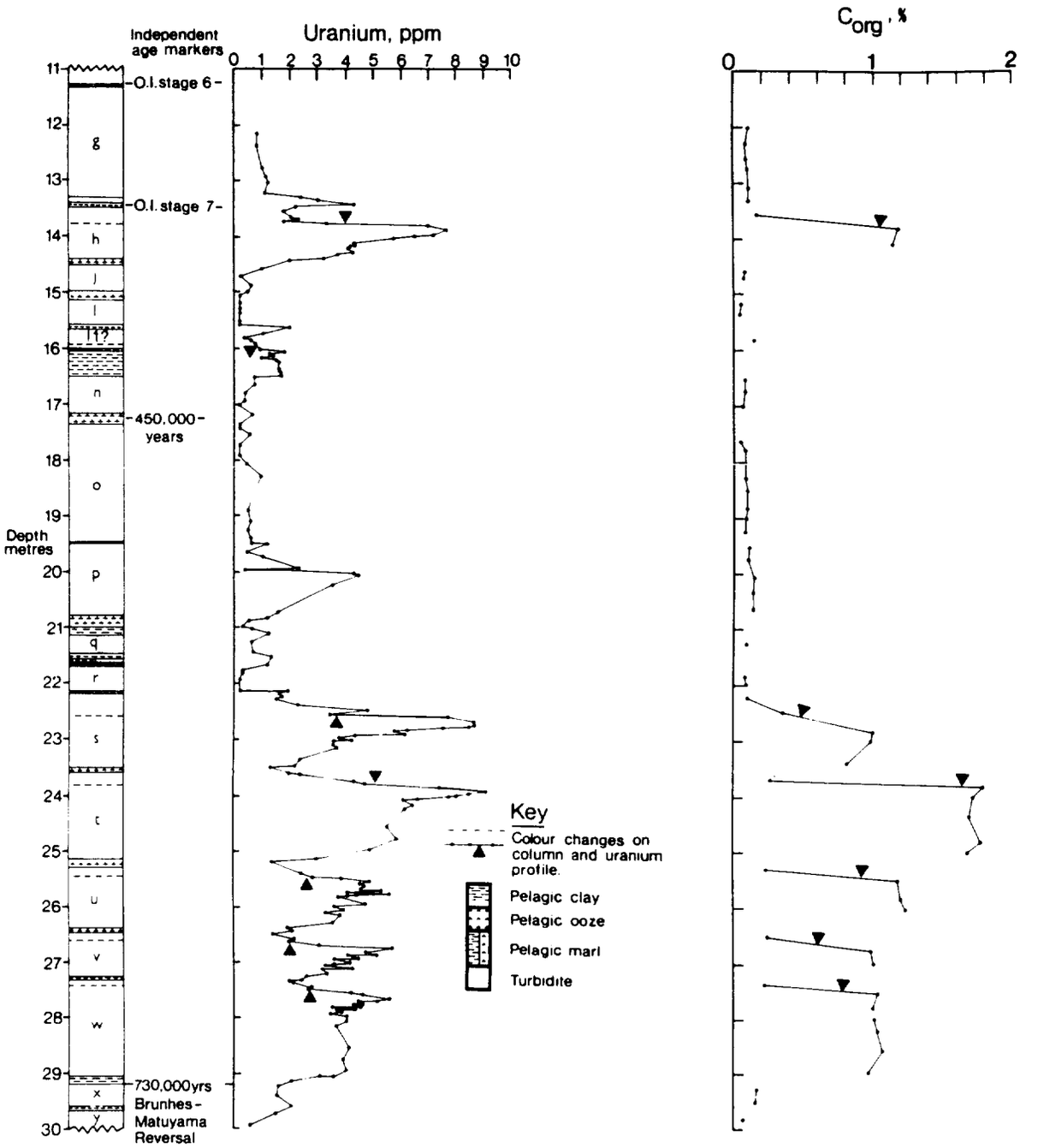

Figure 2 Stratigraphic log, solid phase U profile and organic C profiles of core MD24 (Colley *et al.*, 1989, Appendix 1). The organic C data are from the turbidite units only. This core overlaps with core 10688 reported by Colley and Thomson (1985) and has the same alphabetical nomenclature for the turbidite succession. All data from Schuttenhelm *et al.* (1989).

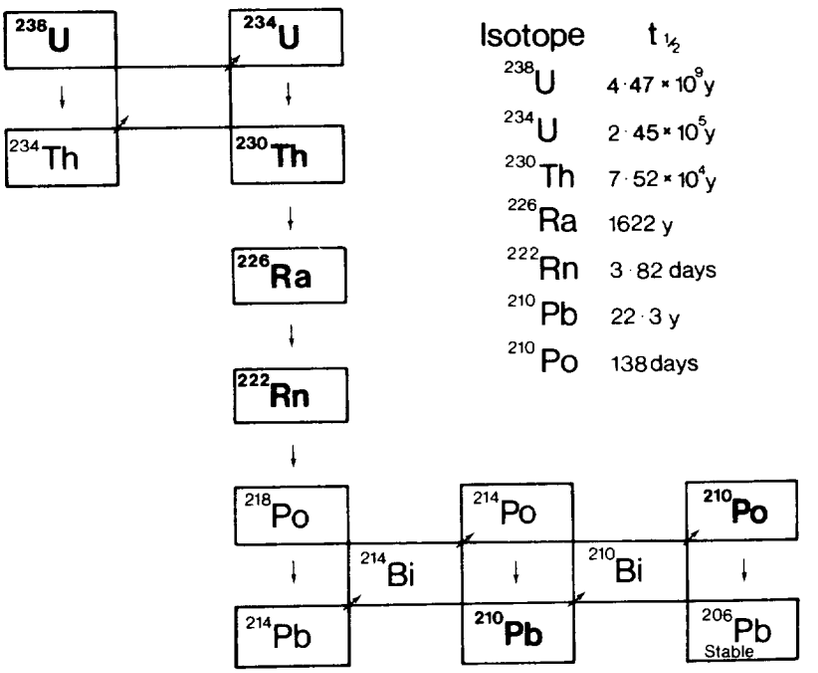

Figure 3 The uranium ($4n$ + 2) decay series. Radionuclides of interest to this study are highlighted.

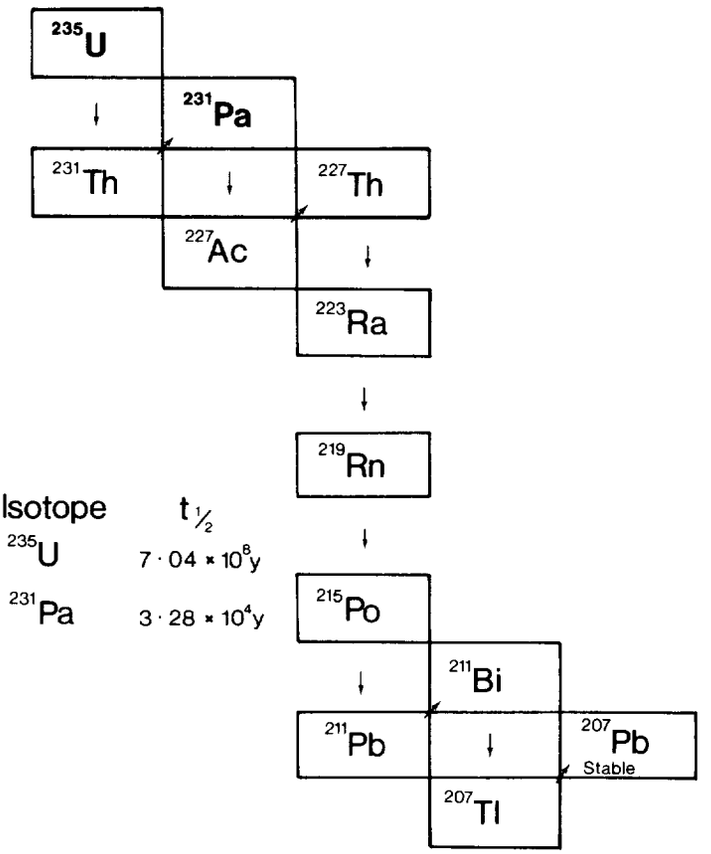

Figure 4 The actinium ($4n$ + 3) decay series. Radionuclides of interest to this study are highlighted.

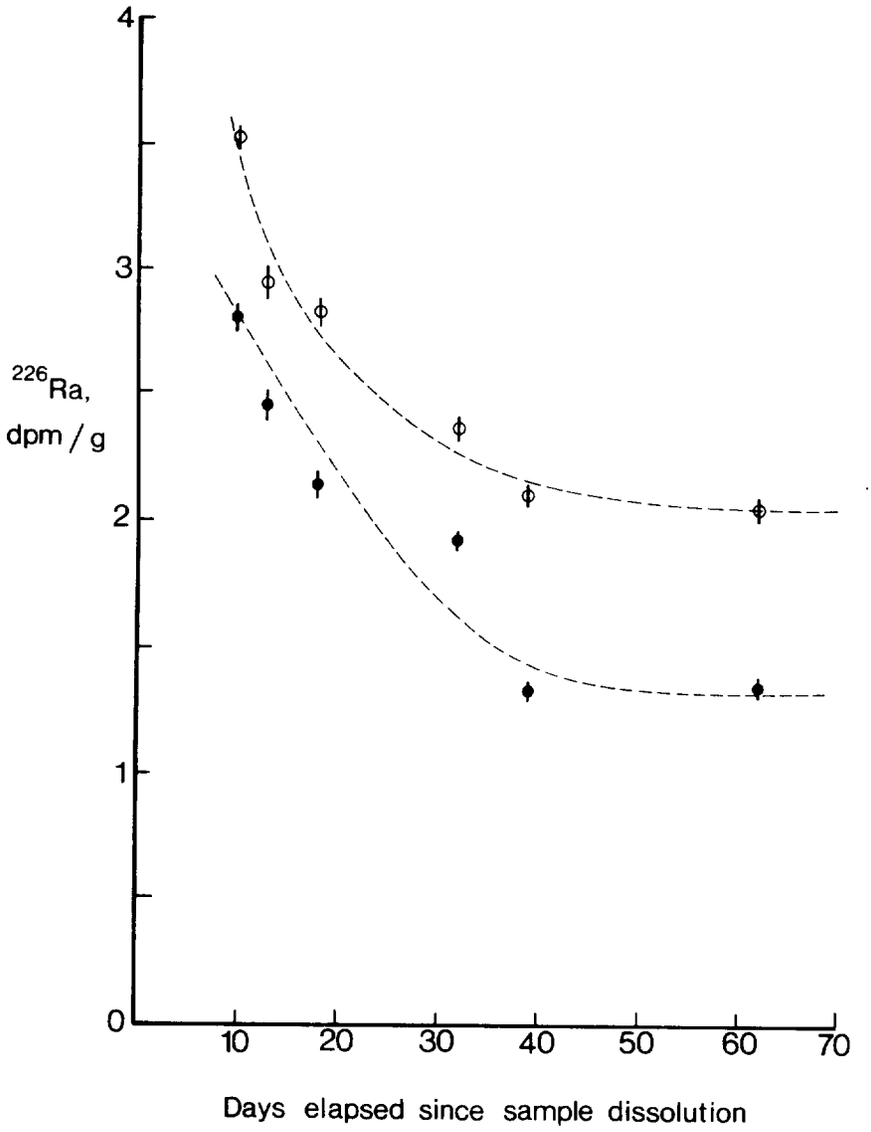

Figure 5 Repeat determinations of ^{226}Ra with increasing time elapsed since sample dissolution using a fluoride/pyrosulphate fusion for MD24 322 (circles) and MD24 335 (dots).

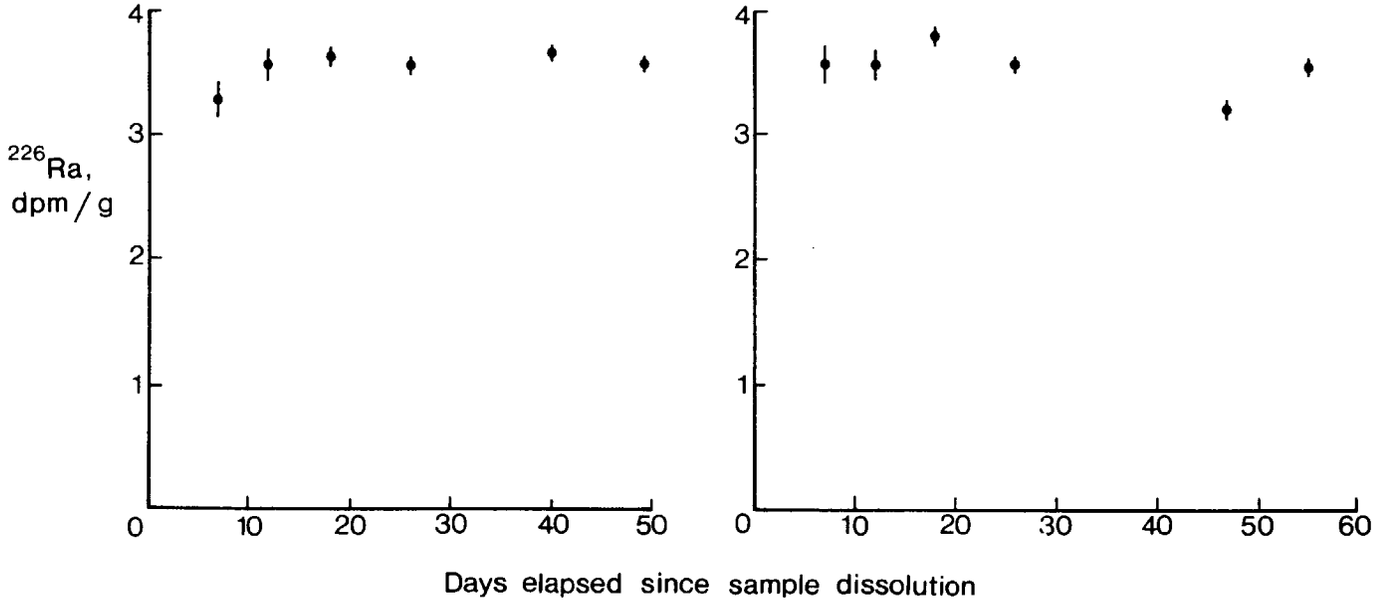

Figures 6 & 7 Repeat determinations of ^{226}Ra with increasing time elapsed since sample dissolution using a lithium metaborate fusion, for two subsamples of 10323 bulk.

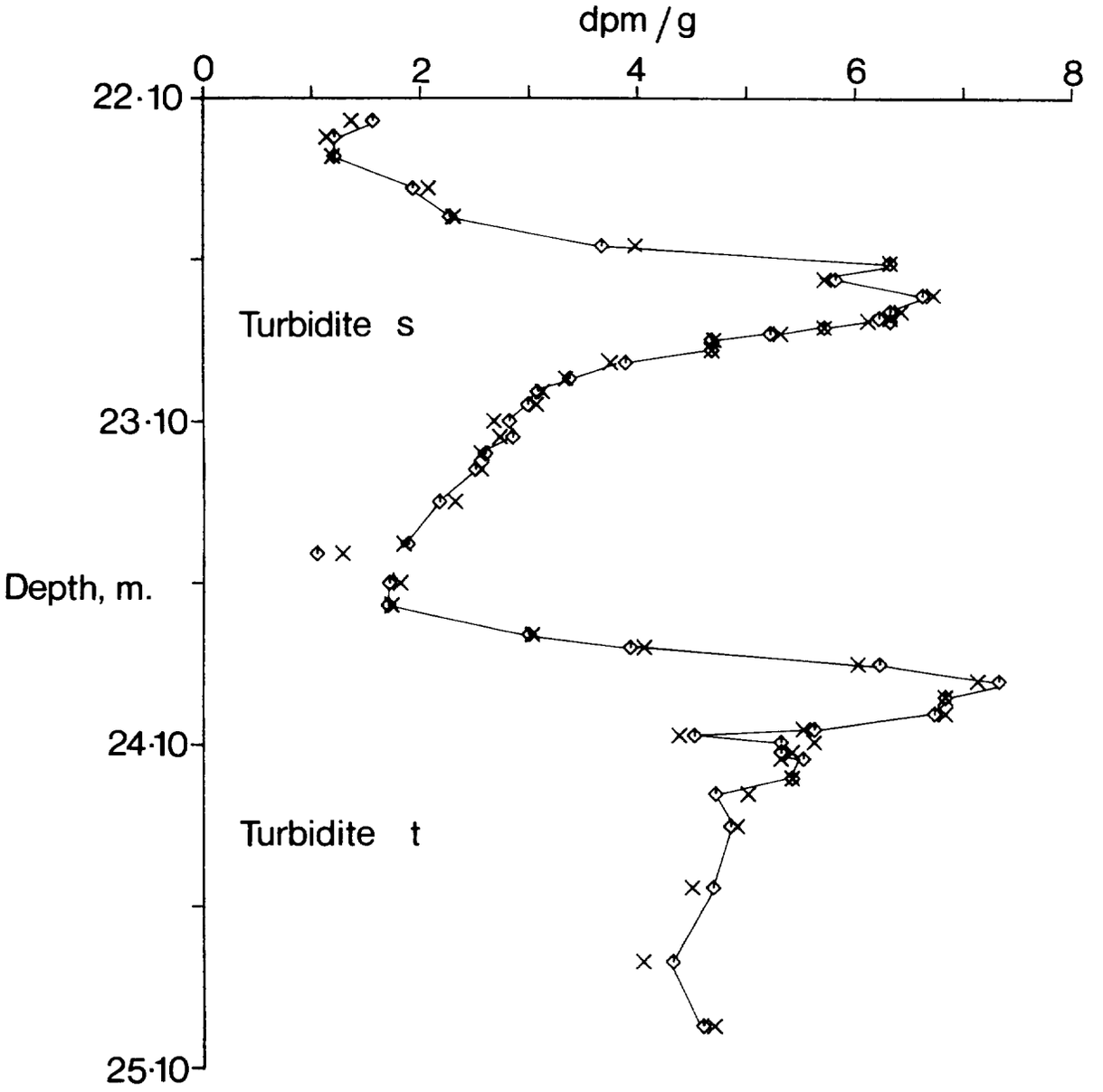

Figure 8 ^{238}U (diamonds) and ^{234}U (crosses) profiles *versus* depth for turbidites *s* and *t* from core MD24. The ^{238}U data points are joined together within the turbidite units to illustrate the profile shape.

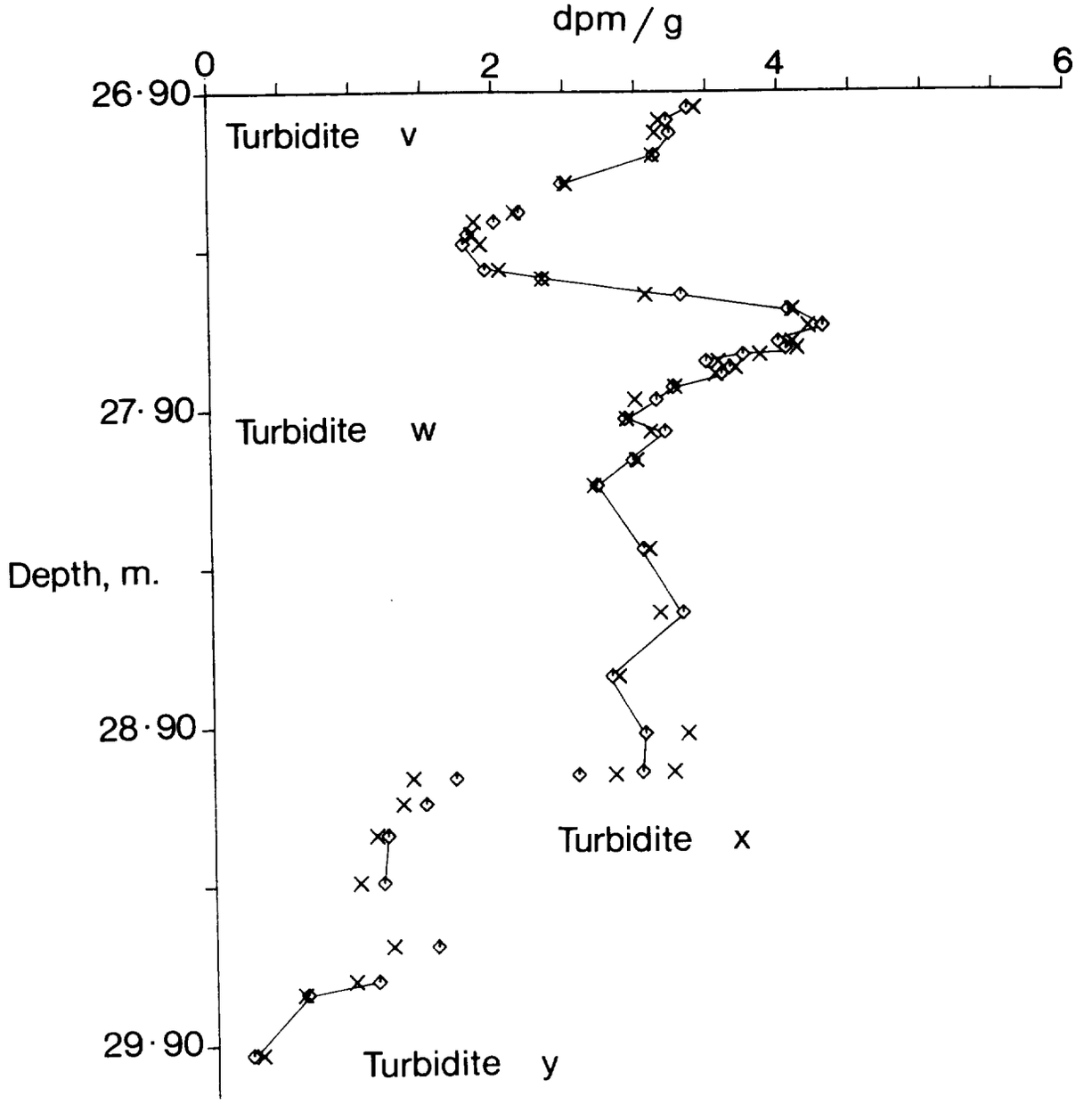

Figure 9 ^{238}U (diamonds) and ^{234}U (crosses) profiles *versus* depth for the lower part of turbidite *v* and for turbidites *w*, *x* and *y* from core MD24. The ^{238}U data points are joined together within the turbidite units to illustrate the profile shape.

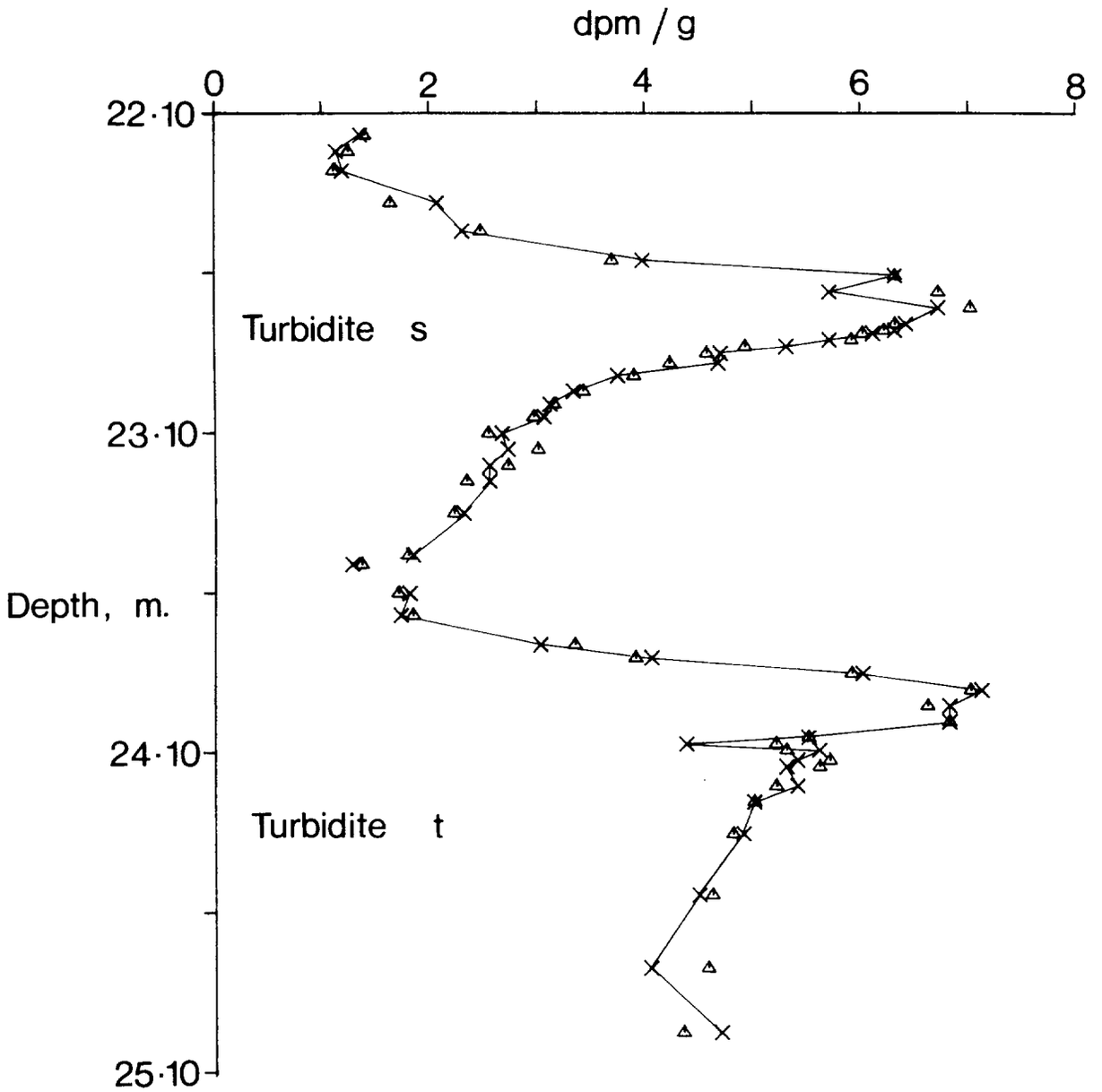

Figure 10 ^{234}U (crosses) and ^{230}Th (triangles) profiles *versus* depth for turbidites *s* and *t* from core MD24. The ^{234}U data points are joined together within the turbidite units to illlustrate the profile shape.

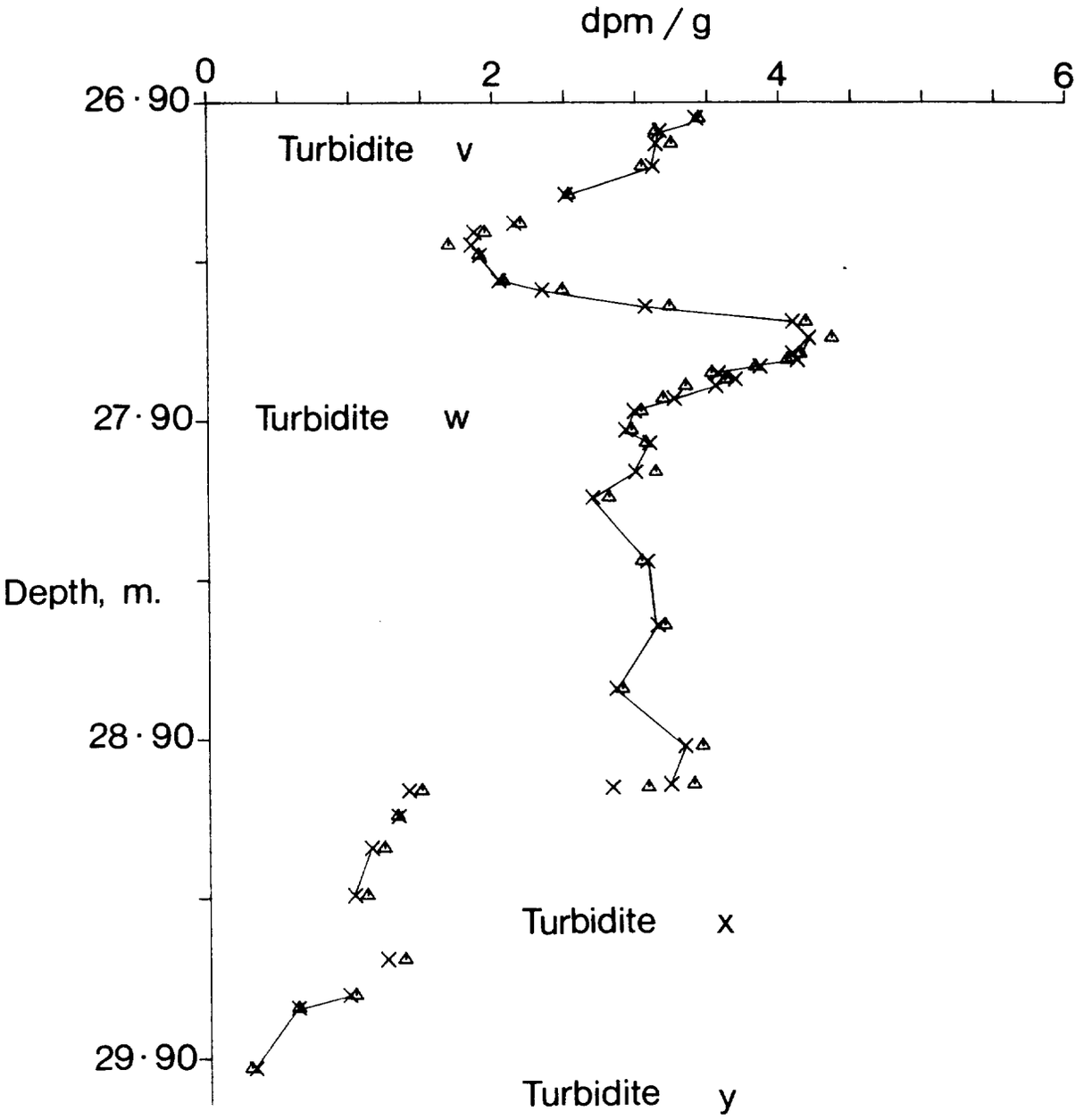

Figure 11 ^{234}U (crosses) and ^{230}Th (triangles) profiles *versus* depth for the lower part of turbidite *v*, and for turbidites w, *x* and *y* from core MD24. The ^{234}U data points are joined together within the turbidite units to illustrate the profile shape.

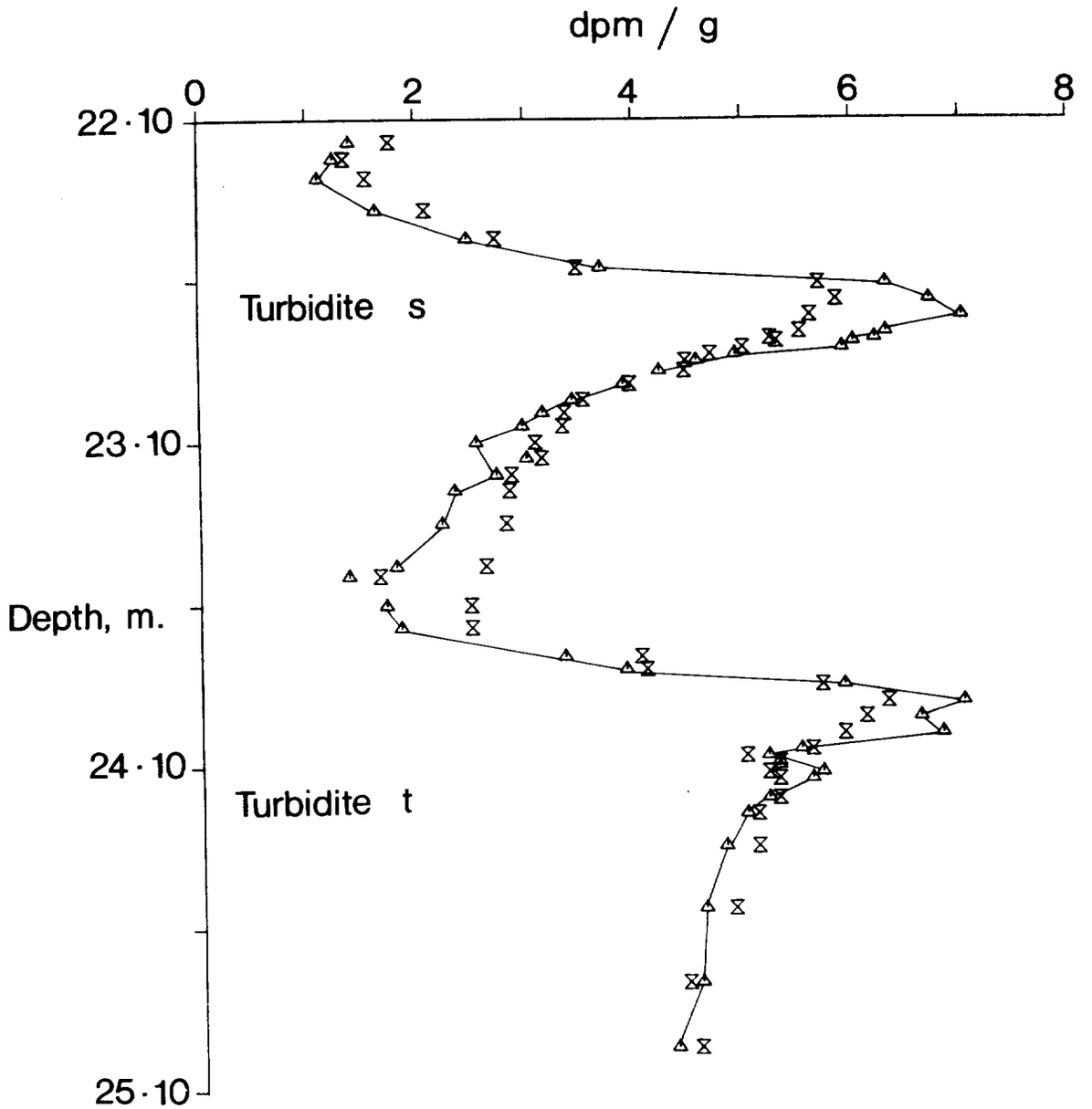

Figure 12 ^{230}Th (triangles) and ^{226}Ra (bow-ties) profiles *versus* depth for turbidites *s* and *t* from core MD24. The ^{230}Th data points are joined together within the turbidite units to illustrate the profile shape.

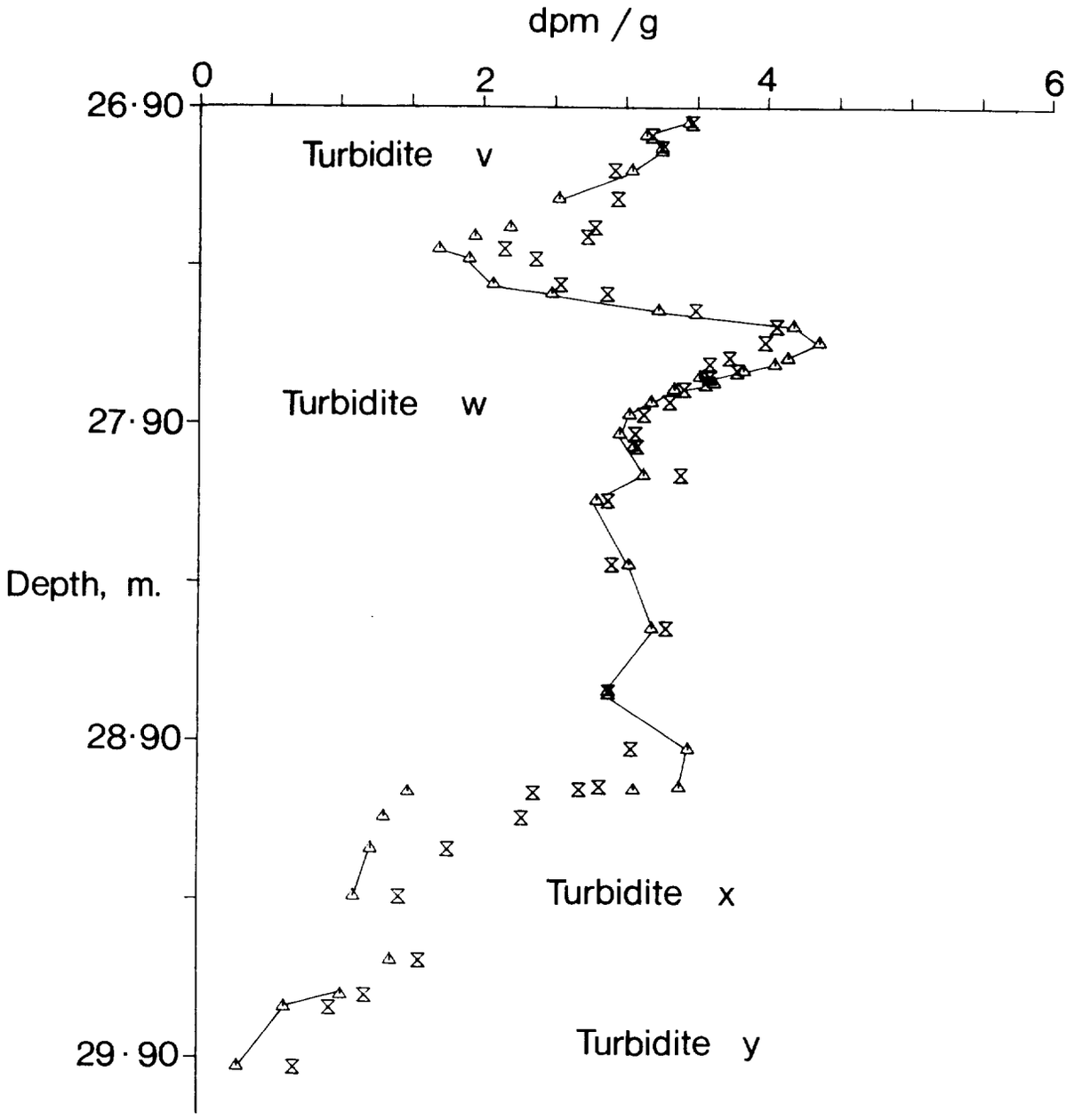

Figure 13 ^{230}Th (triangles) and ^{226}Ra (bow-ties) profiles *versus* depth for the lower part of turbidite *v*, and for turbidites *w*, *x* and *y* from core MD24. The ^{230}Th data points are joined together within the turbidite units to illustrate the profile shape.

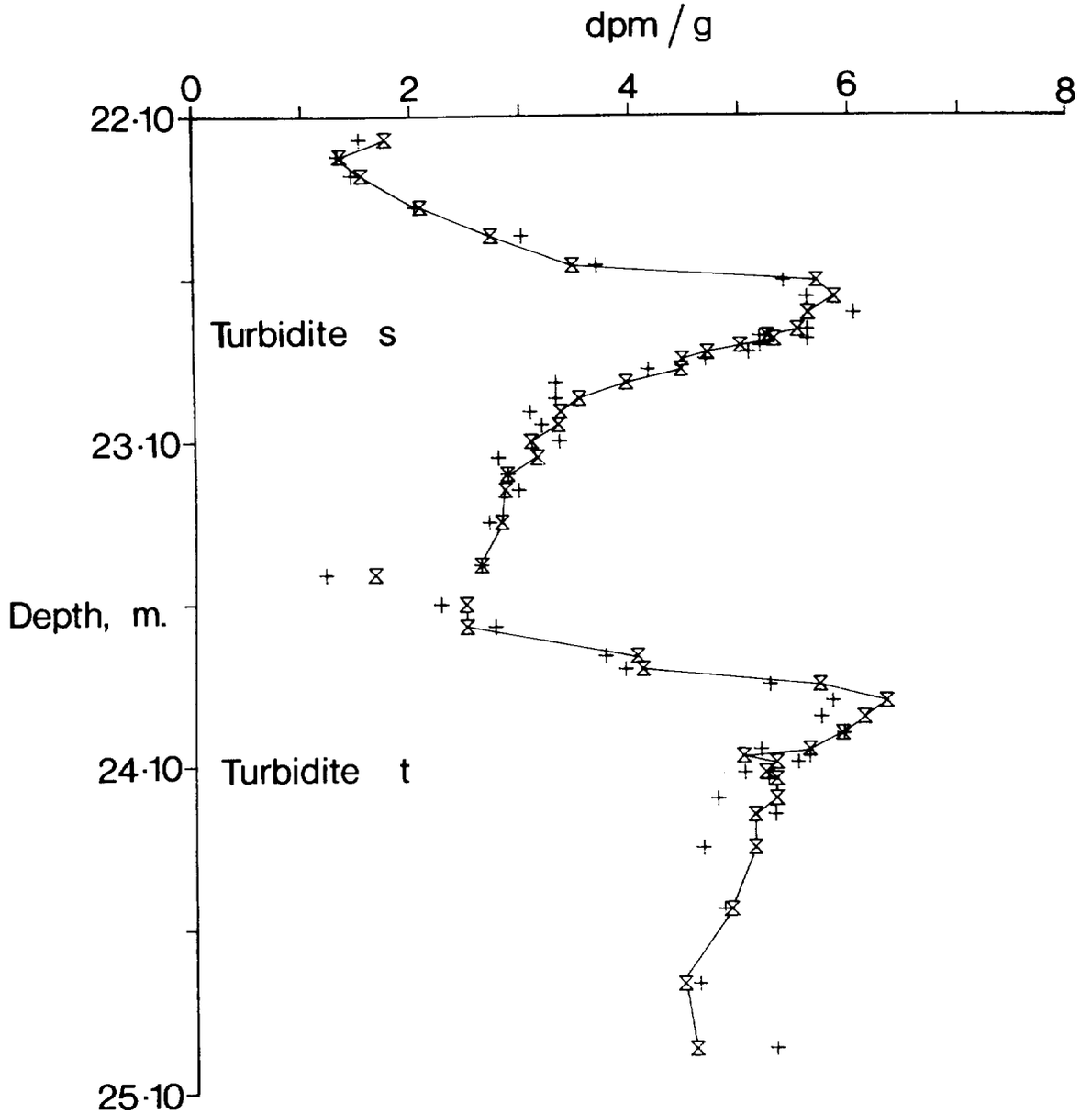

Figure 14 ^{226}Ra (bow-ties) and ^{210}Po (crosses) profiles *versus* depth for turbidites *s* and *t*. The ^{226}Ra data points are joined together within the turbidite units to illustrate the profile shape.

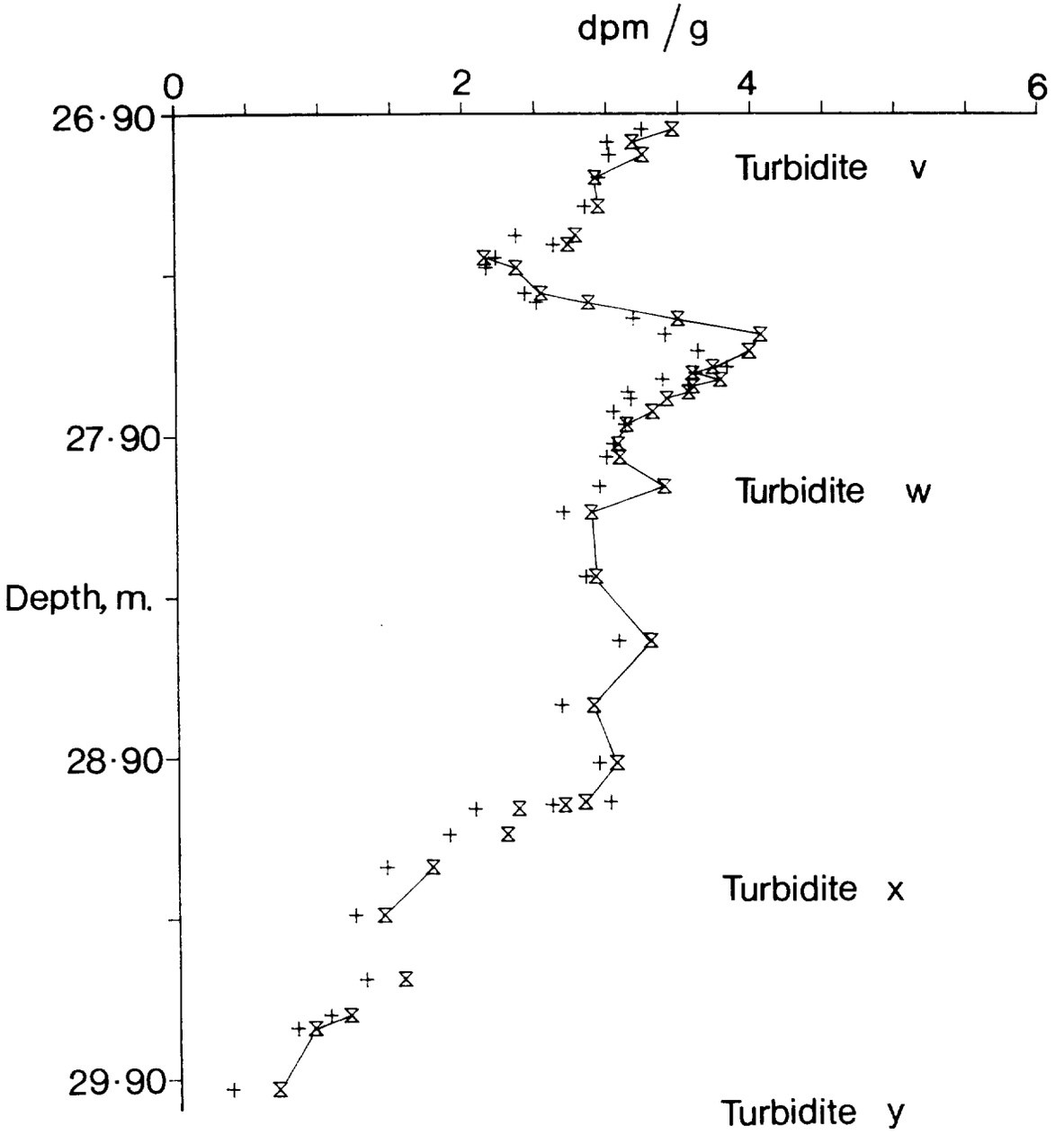

Figure 15 ^{226}Ra (bow-ties) and ^{210}Po (crosses) profiles *versus* depth for the lower part of turbidite *v* and for turbidites *w*, *x* and *y* from core MD24. The ^{226}Ra data points are joined together within the turbidite units to illustrate the profile shape.

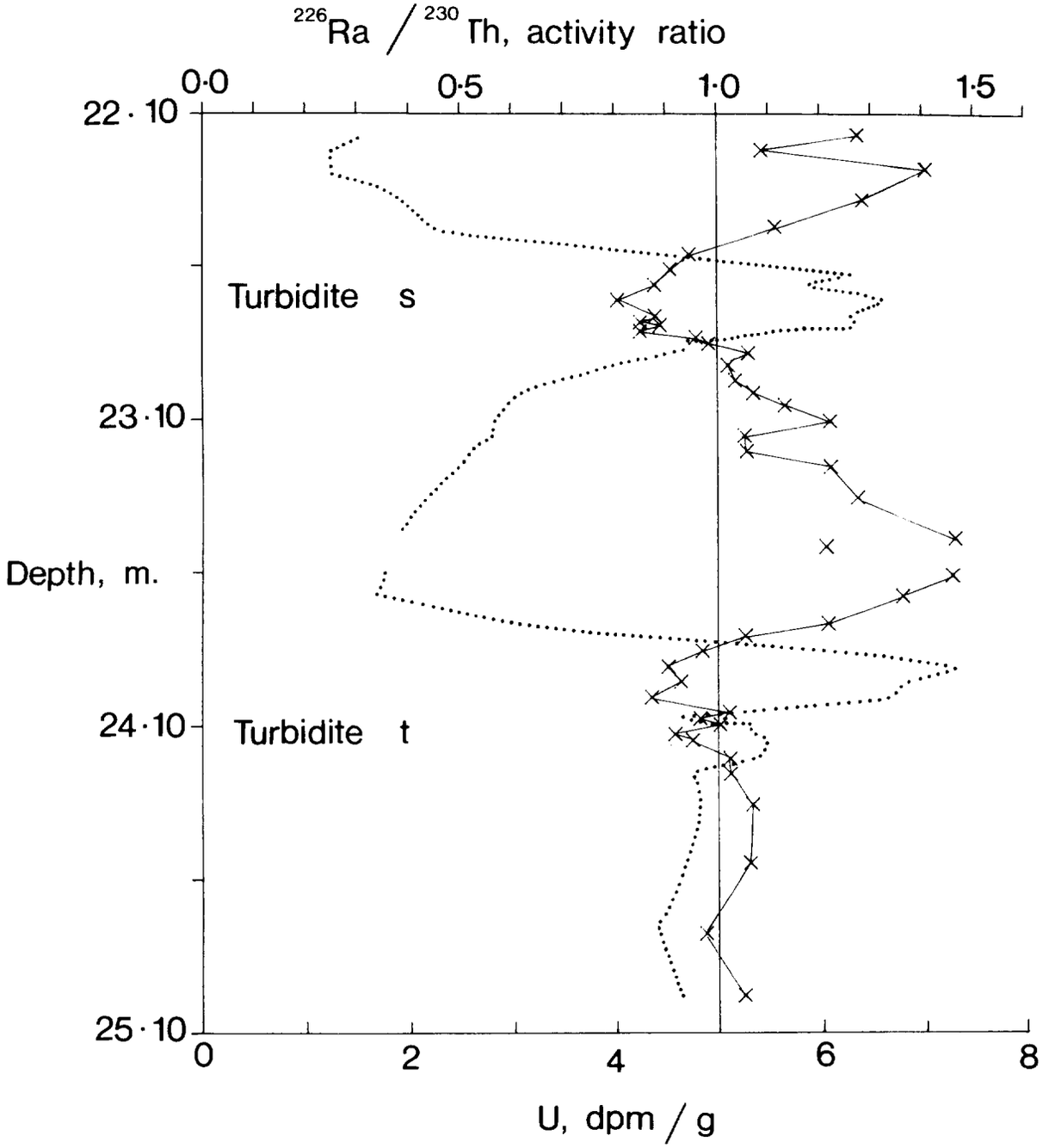

Figure 16 $^{226}Ra/^{230}Th$ activity ratio (crosses) *versus* depth for turbidites *s* and *t* from core MD24. The data points are joined within the turbidite units. The vertical line is the secular equilibrium value of this ratio. The positions of the U peaks are indicated by a dotted trace of the U profile.

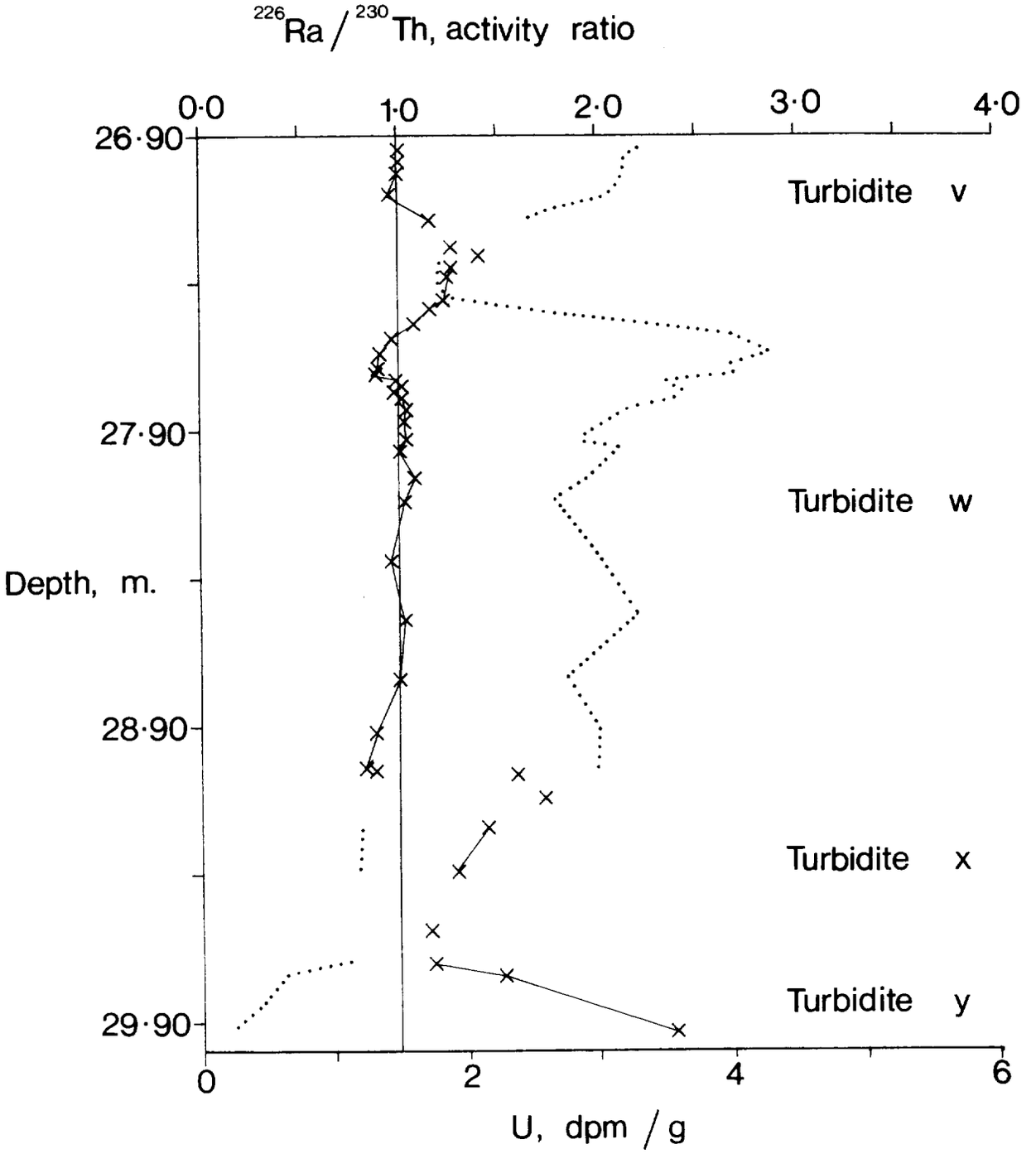

Figure 17 $^{226}Ra/^{230}Th$ activity ratio (crosses) *versus* depth for the lower part of turbidite *v*, and for turbidites *w*, x and y. The data points are joined within the turbidite units. The vertical line is the secular equilibrium value of this ratio. The position of the U peak is indicated by a dotted trace of the U profile.

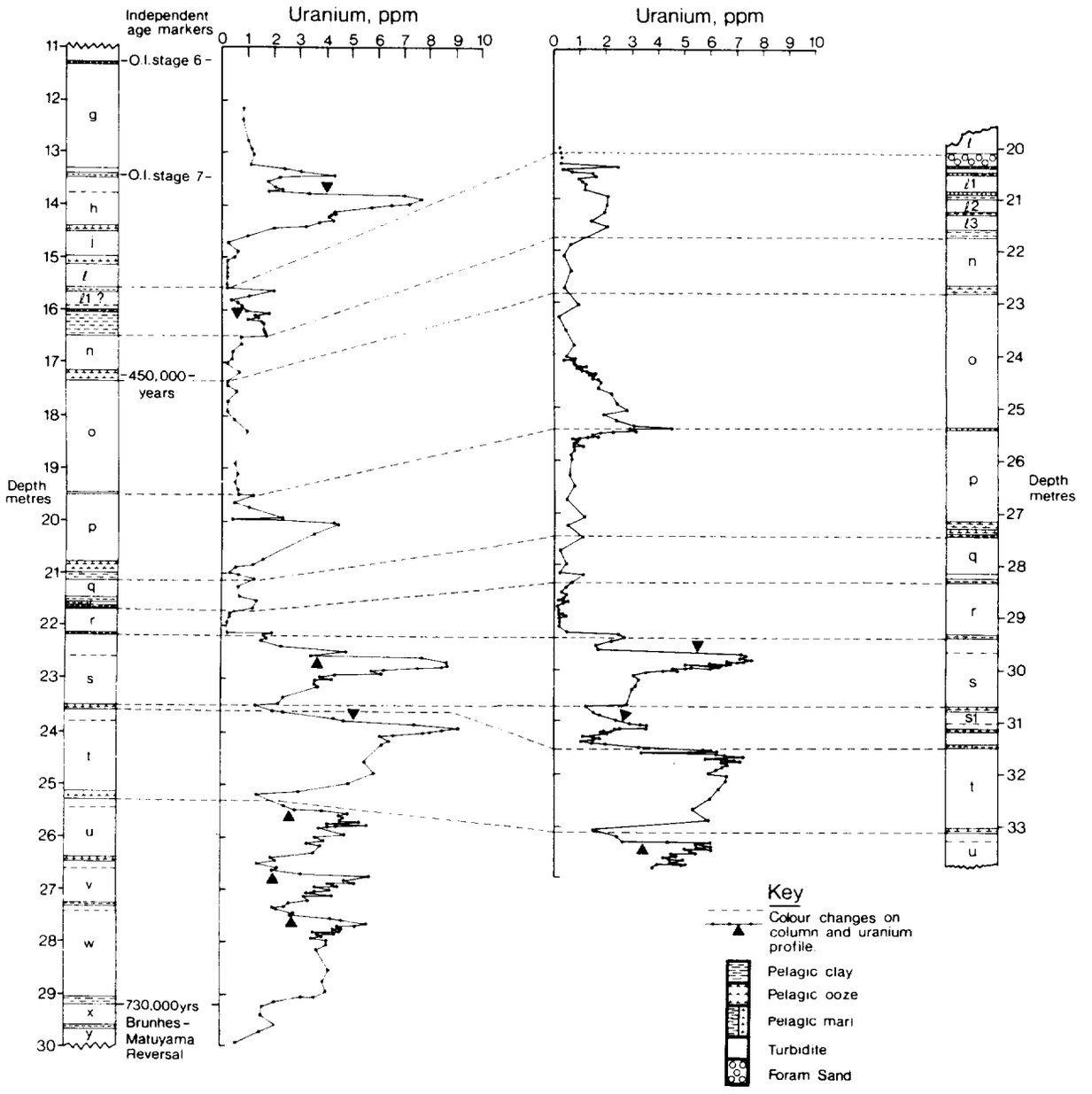

Figure 18 Stratigraphic logs and solid phase U profiles for core MD24 (LHS) and MD10 (RHS). Equivalent units are correlated between cores using dashed lines.

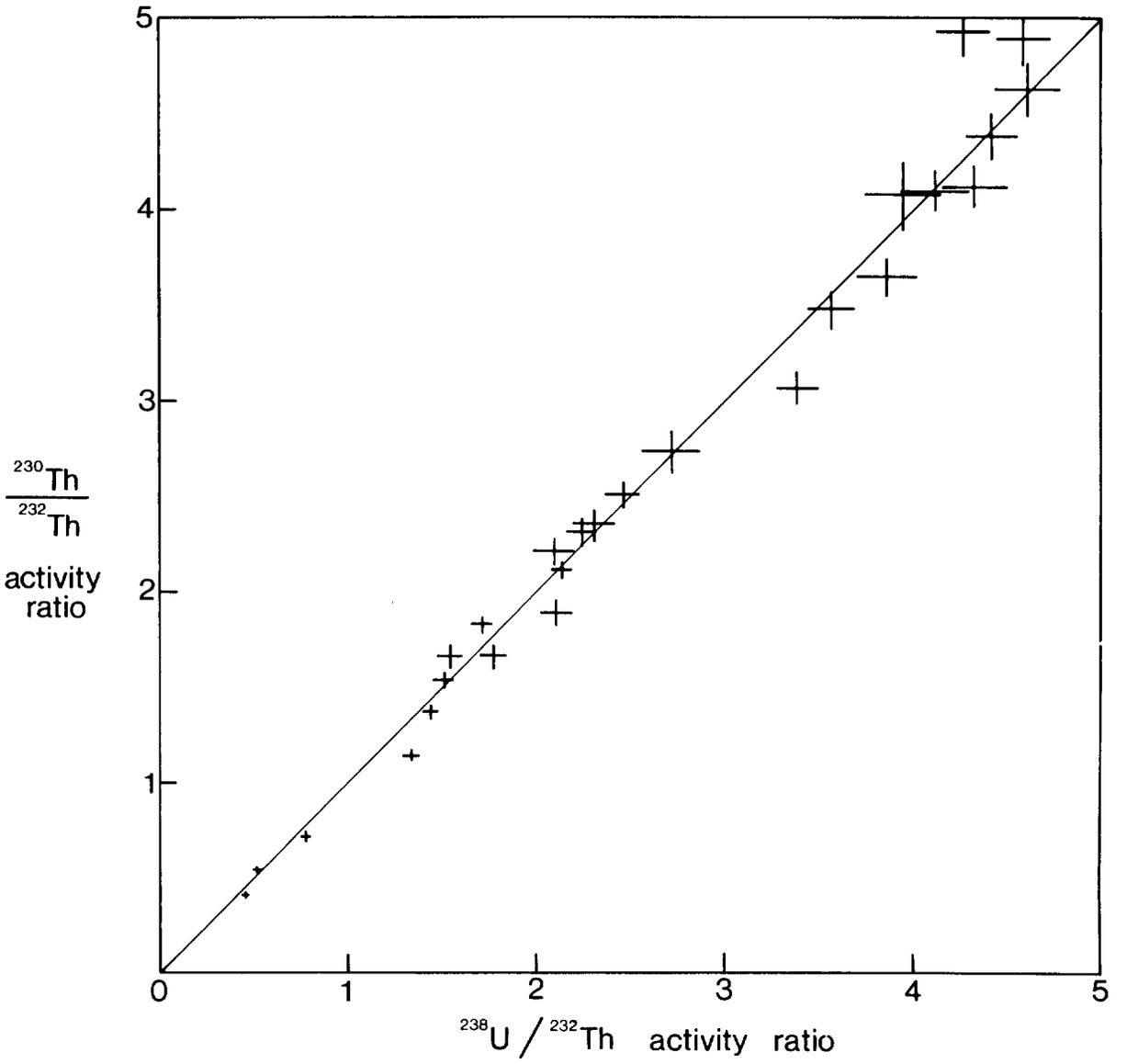

Figure 19 An isochron plot for turbidite *s* from core MD24. The best fit line has a gradient of 45° and corresponds to the equiline.

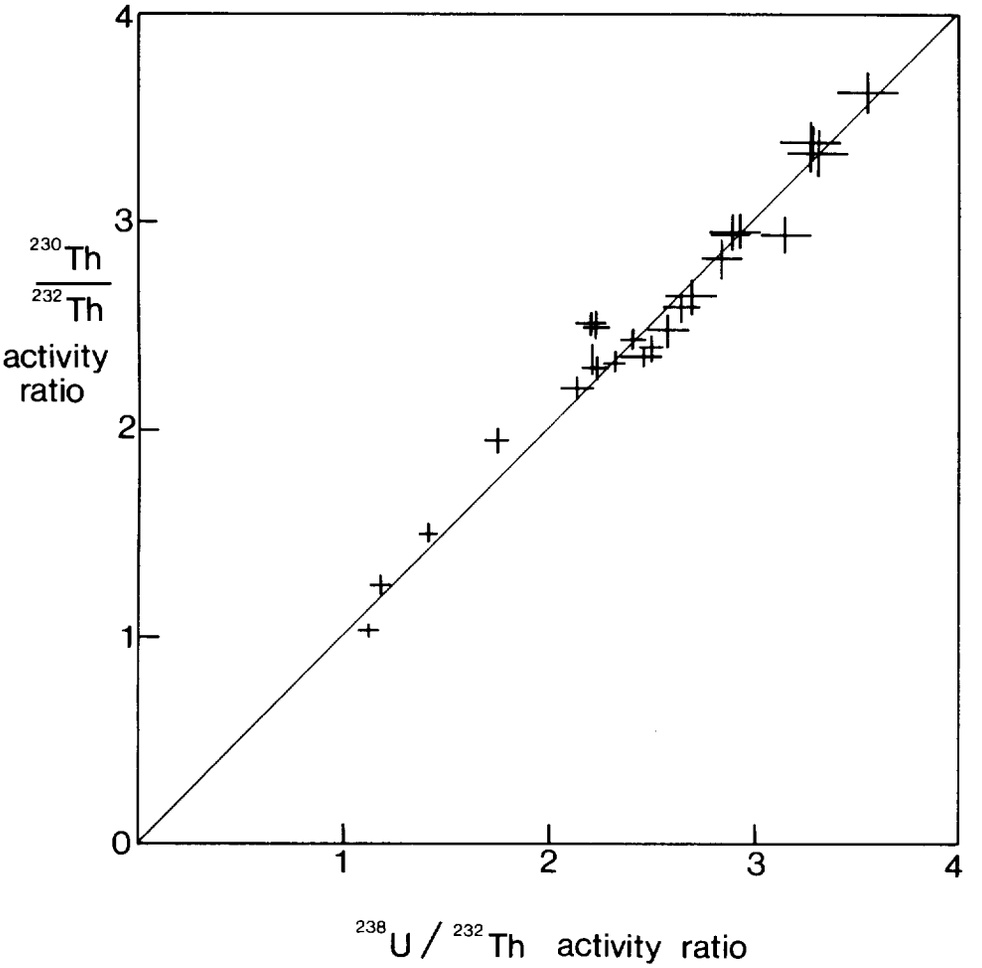

Figure 20 An isochron plot for turbidite *w* from core MD24. The best fit line has a gradient of 45° and corresponds to the equiline.

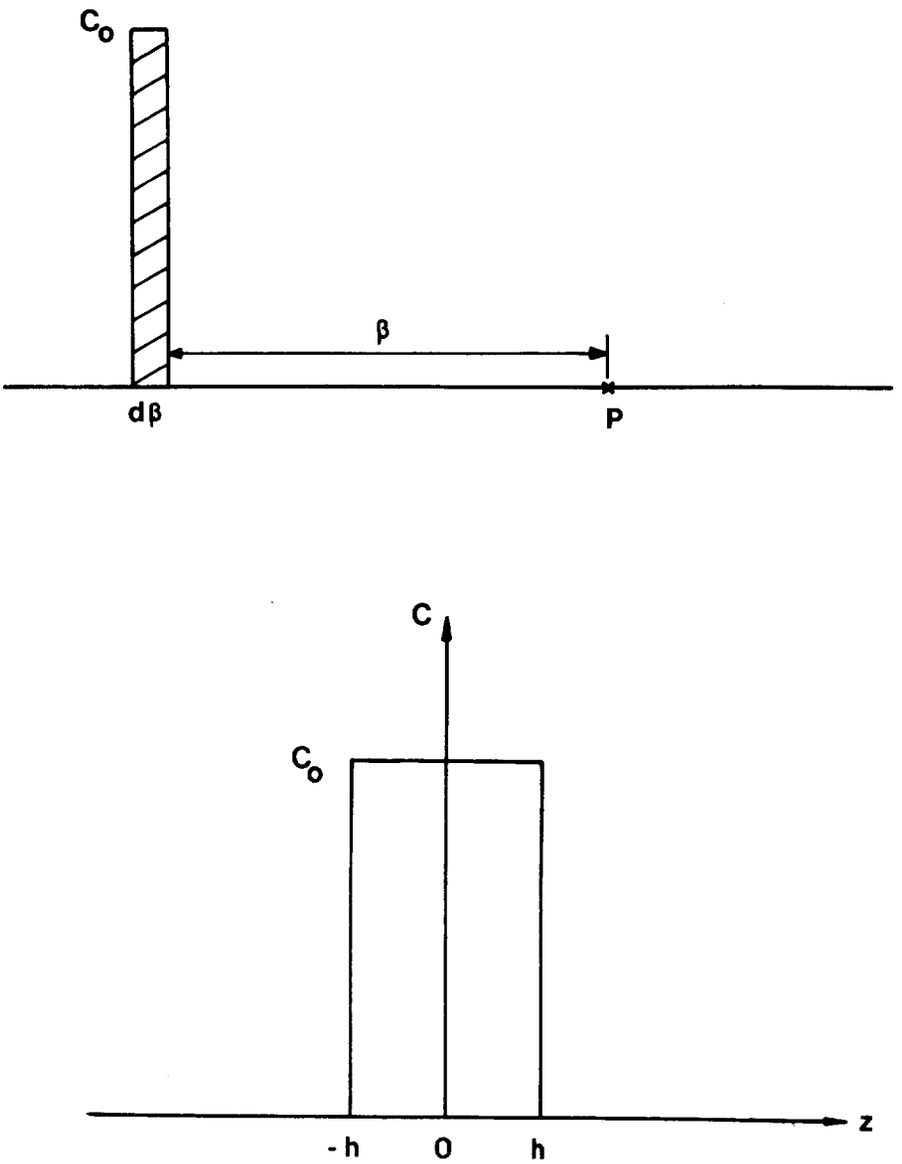

Figure 21 (a) (above) Representation of the diffusing strip used for the diffusion model.
(b) (below) A diffusing strip of width 2h with its centre at the origin.

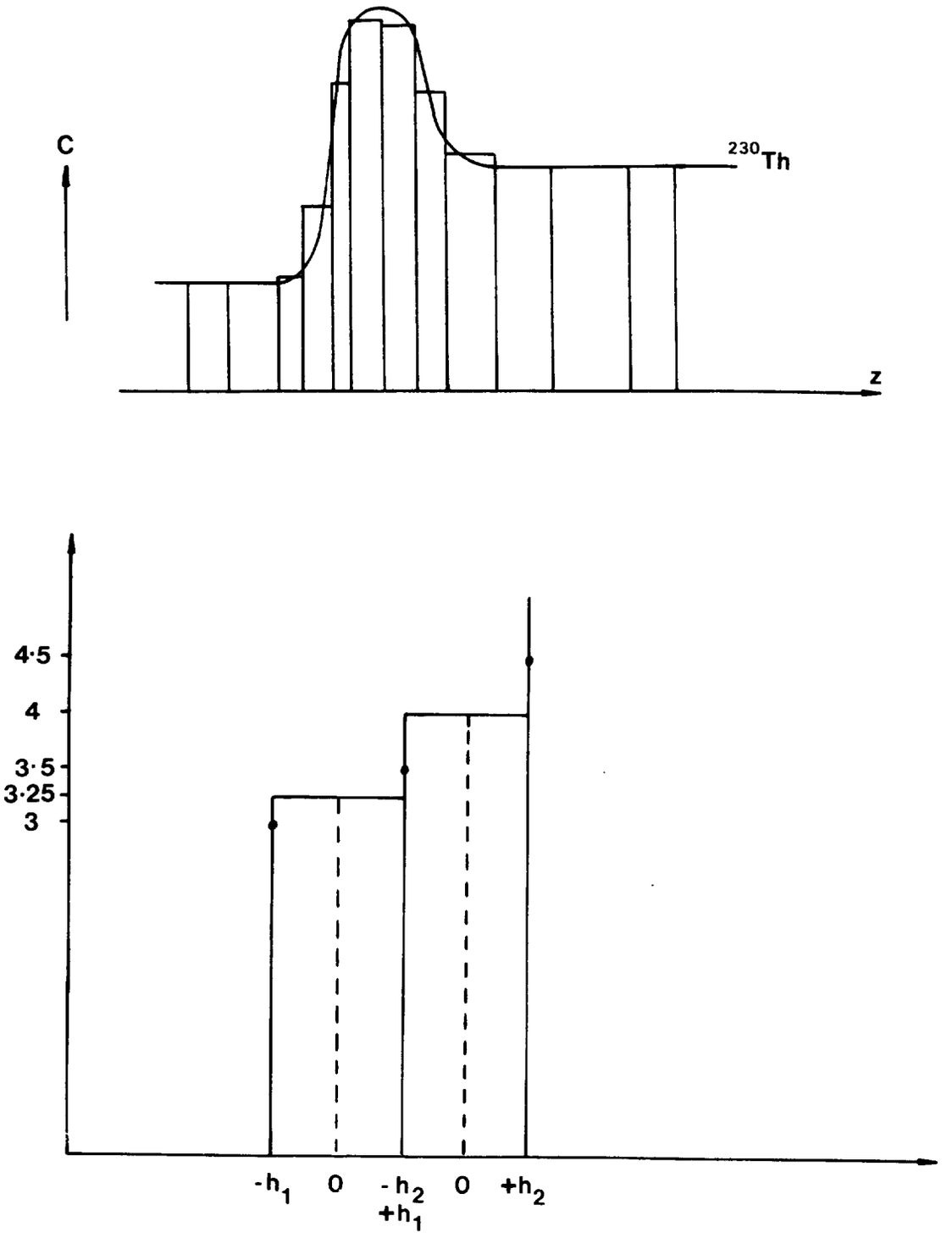

Figure 22 (a) (above) Approximation of the parent ^{230}Th profile as a series of strips.

(b) (below) A source of error in the model: approximation into strips.

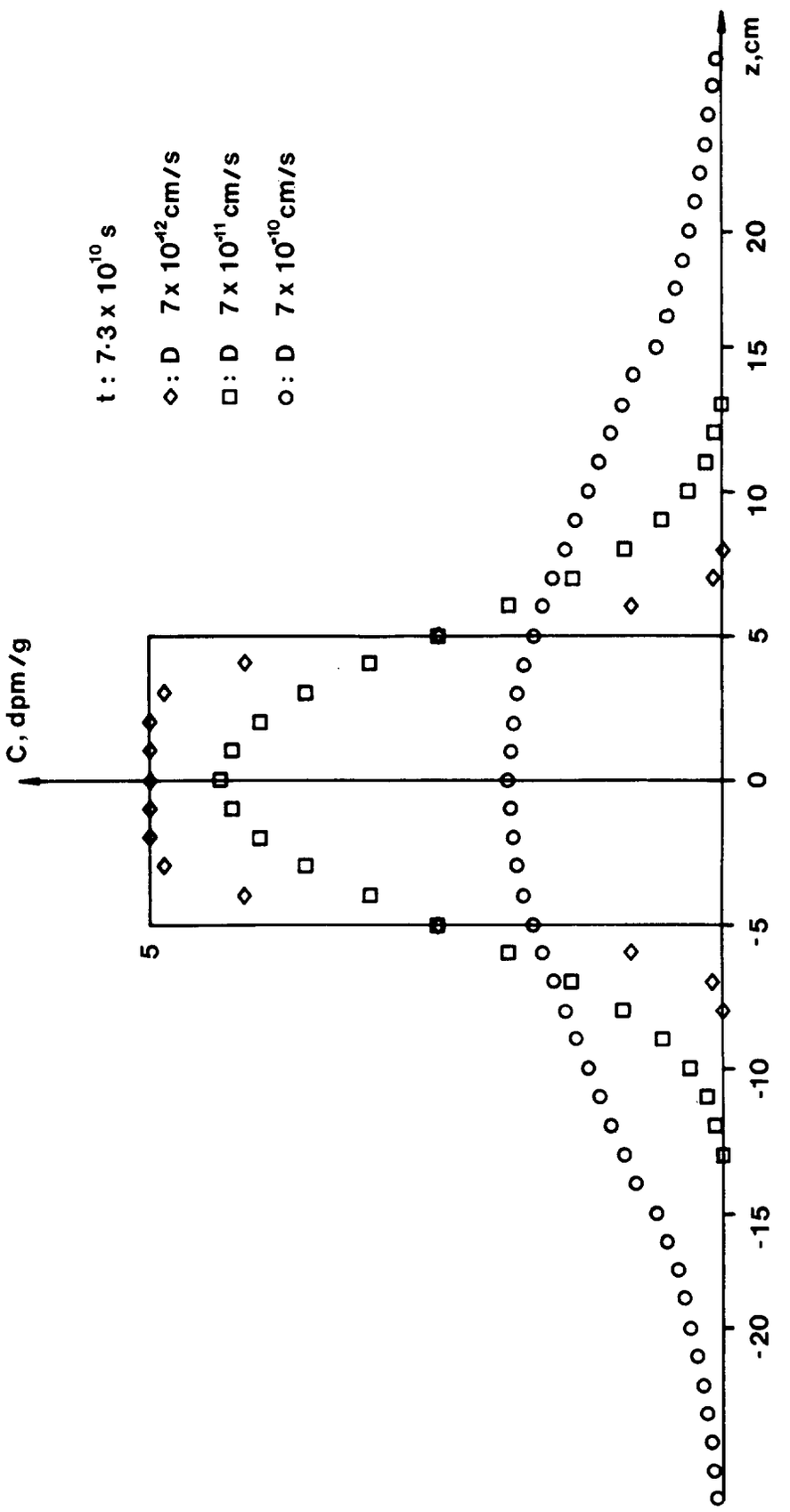

Figure 23 Profiles resulting from allowing a single strip (height 5 dpm/g) to diffuse for the mean life of ^{226}Ra (7.3×10^{10}s) with different values of the effective diffusion coefficient D.

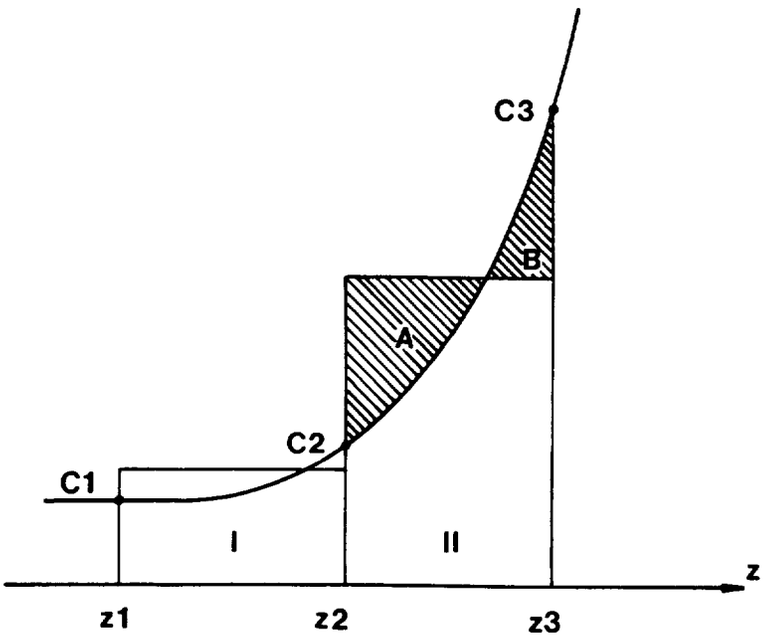

Figure 24 A source of error in the model: area B (omitted from strip II) is smaller than area A, which is included in strip II.

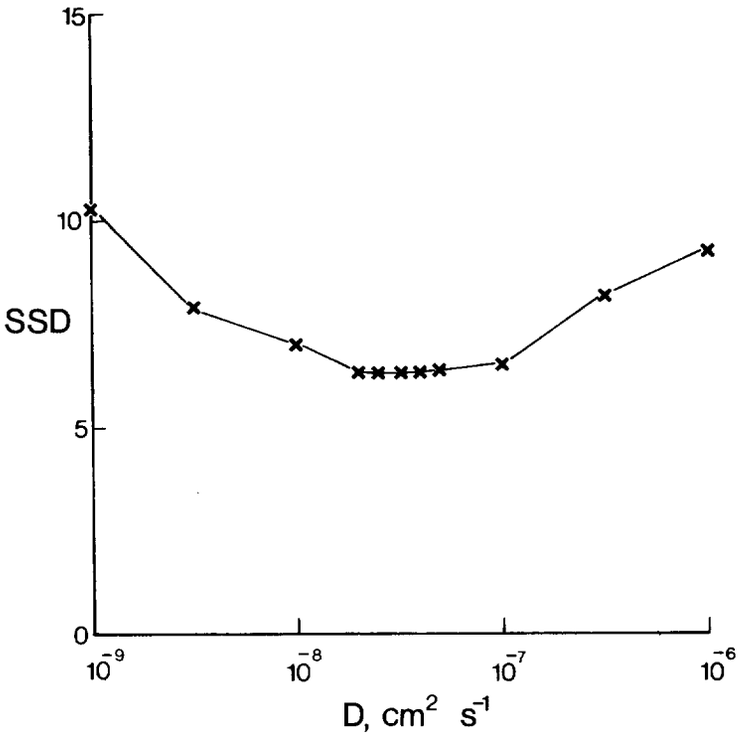

Figure 25 Diagram illustrating how the sums of the squares of the differences between model and experimental data are minimised by varying D. The optimum D in this case is 4×10^{-8} cm^2 s^{-1}.

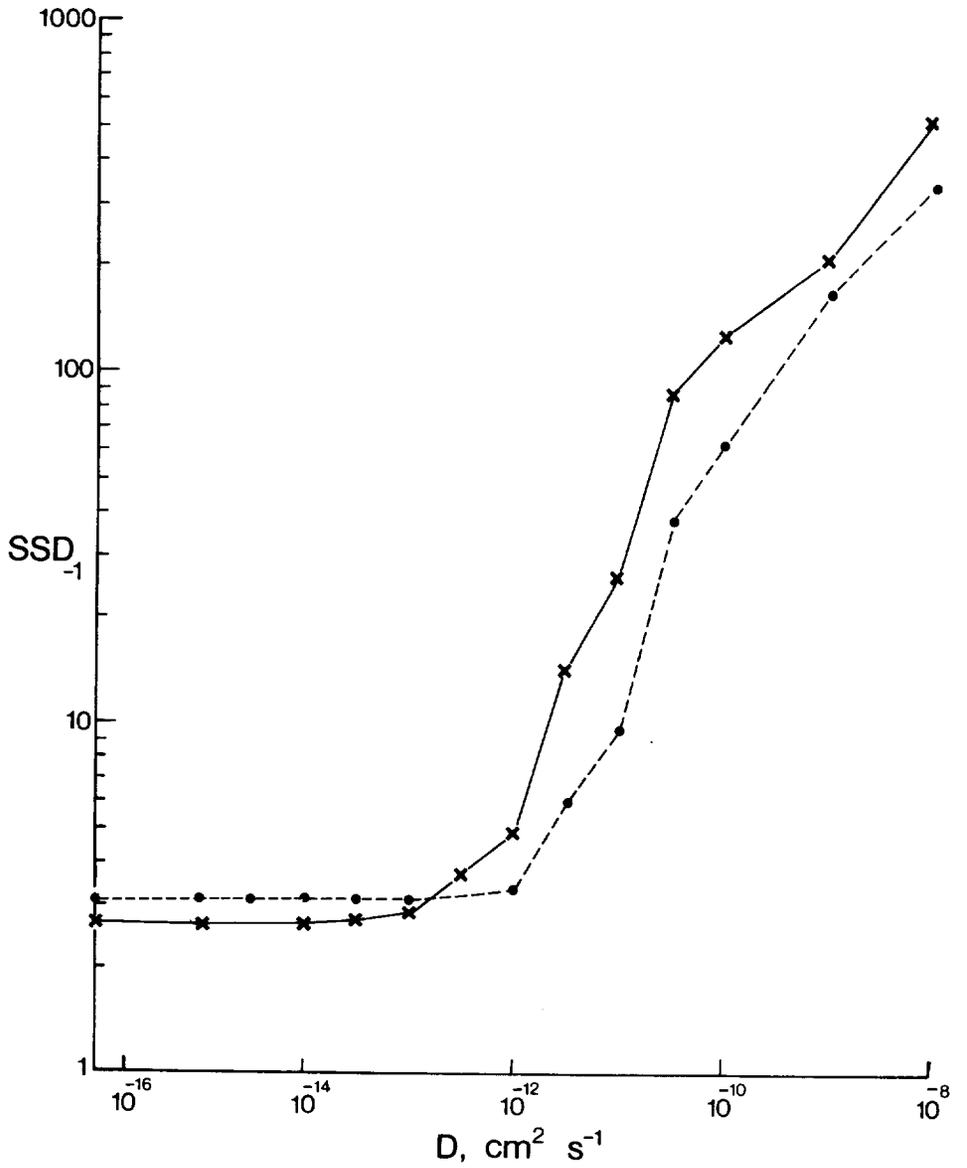

Figure 26 Variation of SSD with D for ^{238}U - ^{234}U (crosses) and ^{234}U - ^{230}Th (dots) for turbidites *s* and *t* from core MD24.

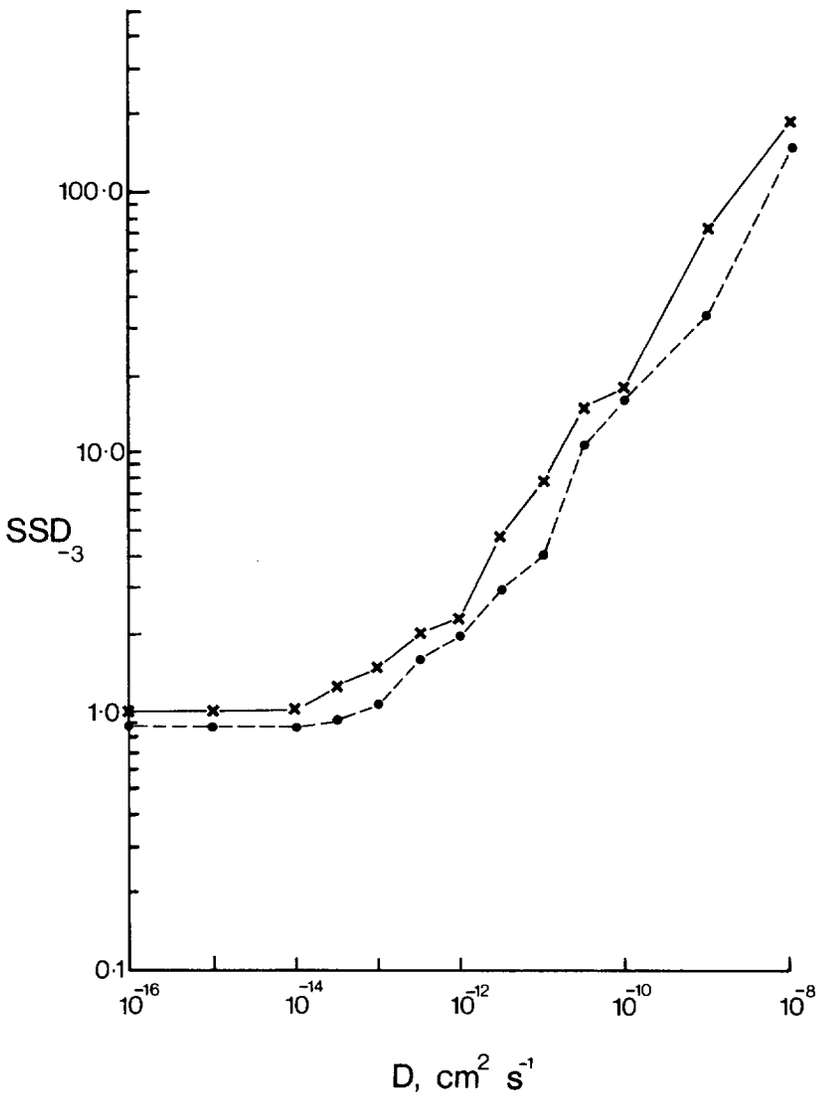

Figure 27 Variation of SSD with D for ^{238}U - ^{234}U (crosses) and ^{234}U - ^{230}Th (dots) for turbidite *w* and surrounding units from core MD24.

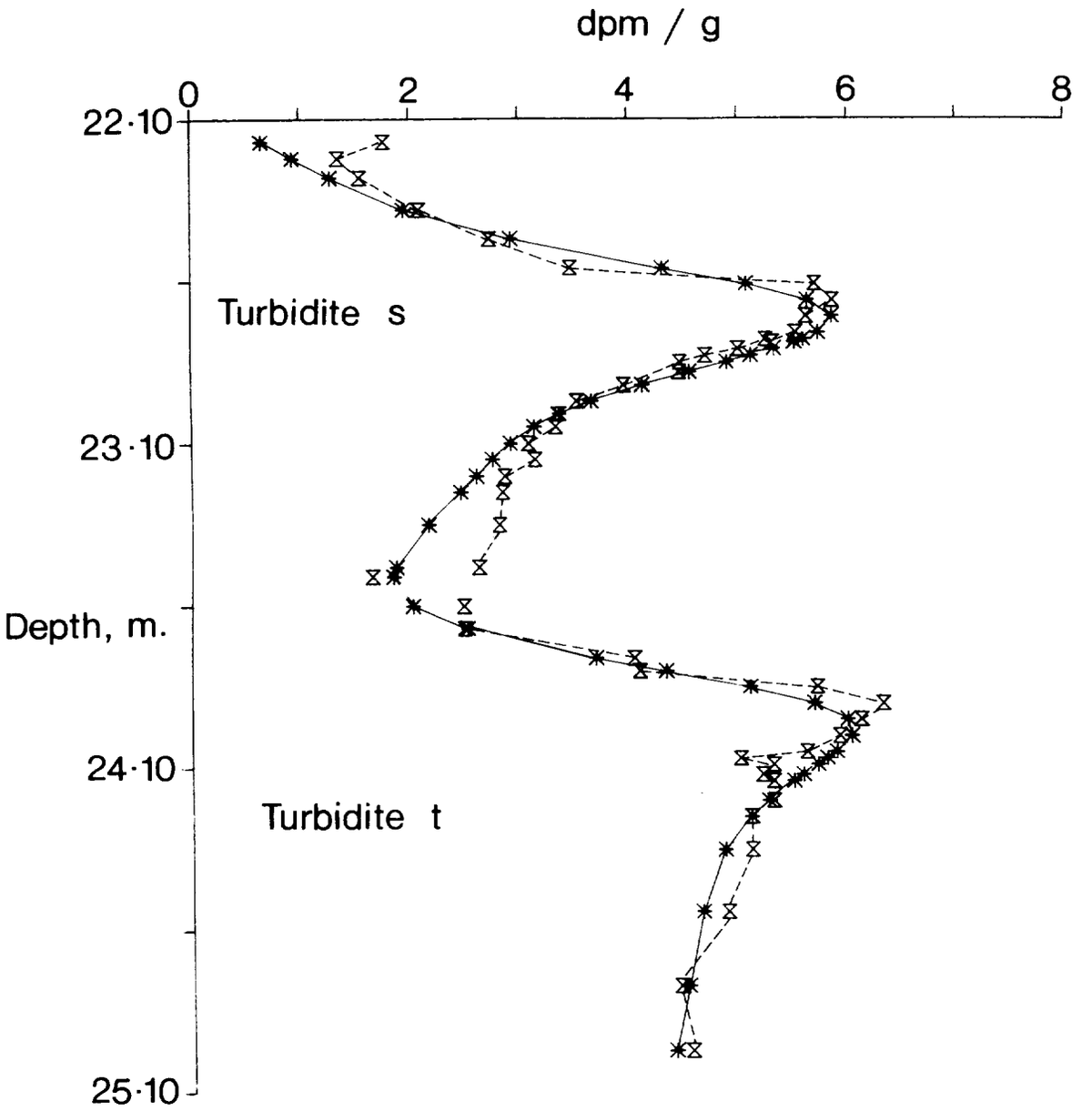

Figure 28 Model ^{226}Ra (stars) and experimental ^{226}Ra (bow-ties) profiles *versus* depth for turbidites *s* and *t* from core MD24. 100% ^{226}Ra mobility is assumed. The optimum D_{eff} (omitting the top sample in the calculation) is 7×10^{-10} cm^2 s^{-1}.

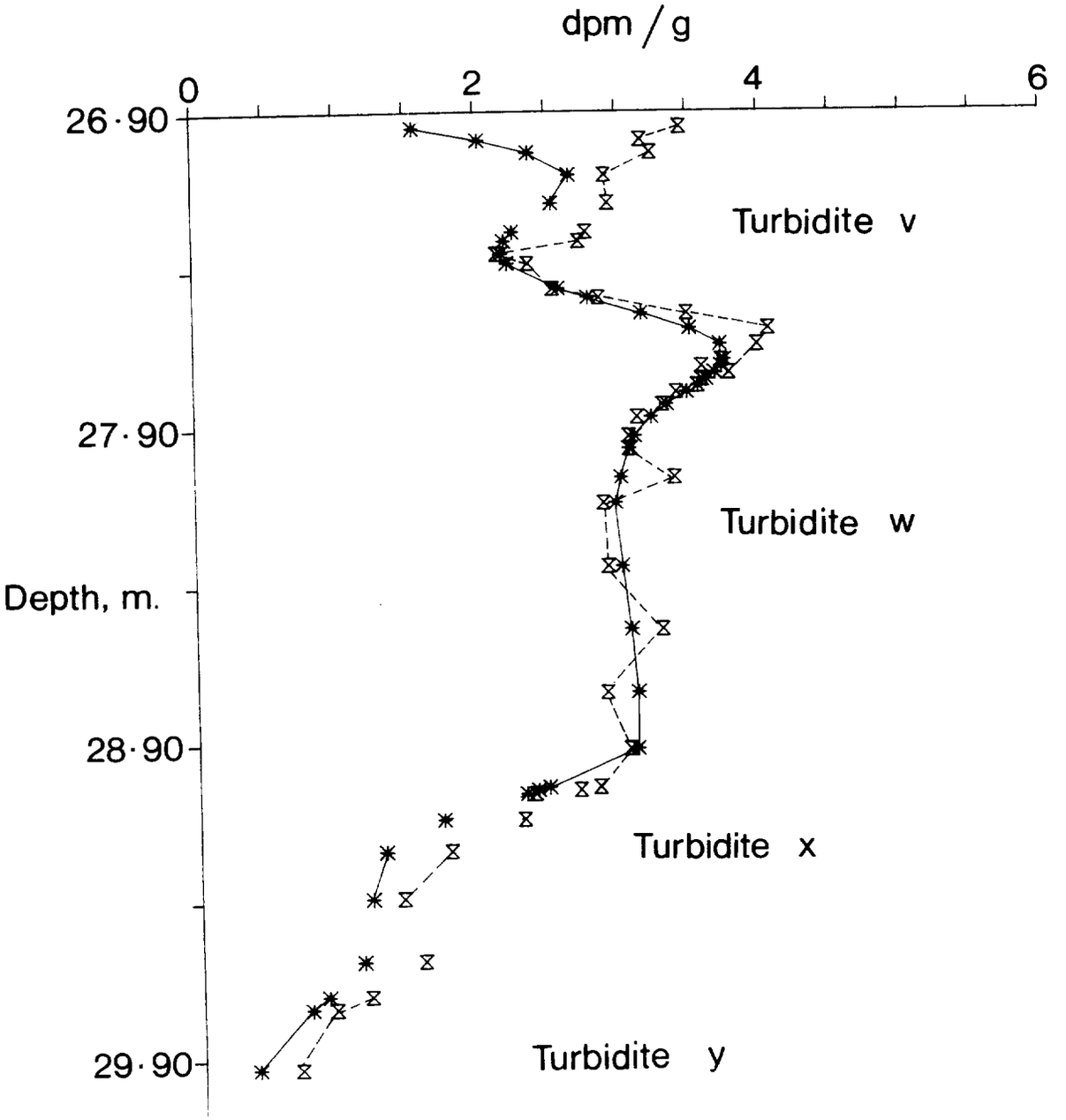

Figure 29 Model ^{226}Ra (stars) and experimental ^{226}Ra (bow-ties) profiles *versus* depth for turbidite *w* and surrounding units from core MD24. 100% ^{226}Ra mobility is assumed. The optimum D_{eff} (omitting the top three samples in the calculation) is 7×10^{-10} cm^2 s^{-1}.

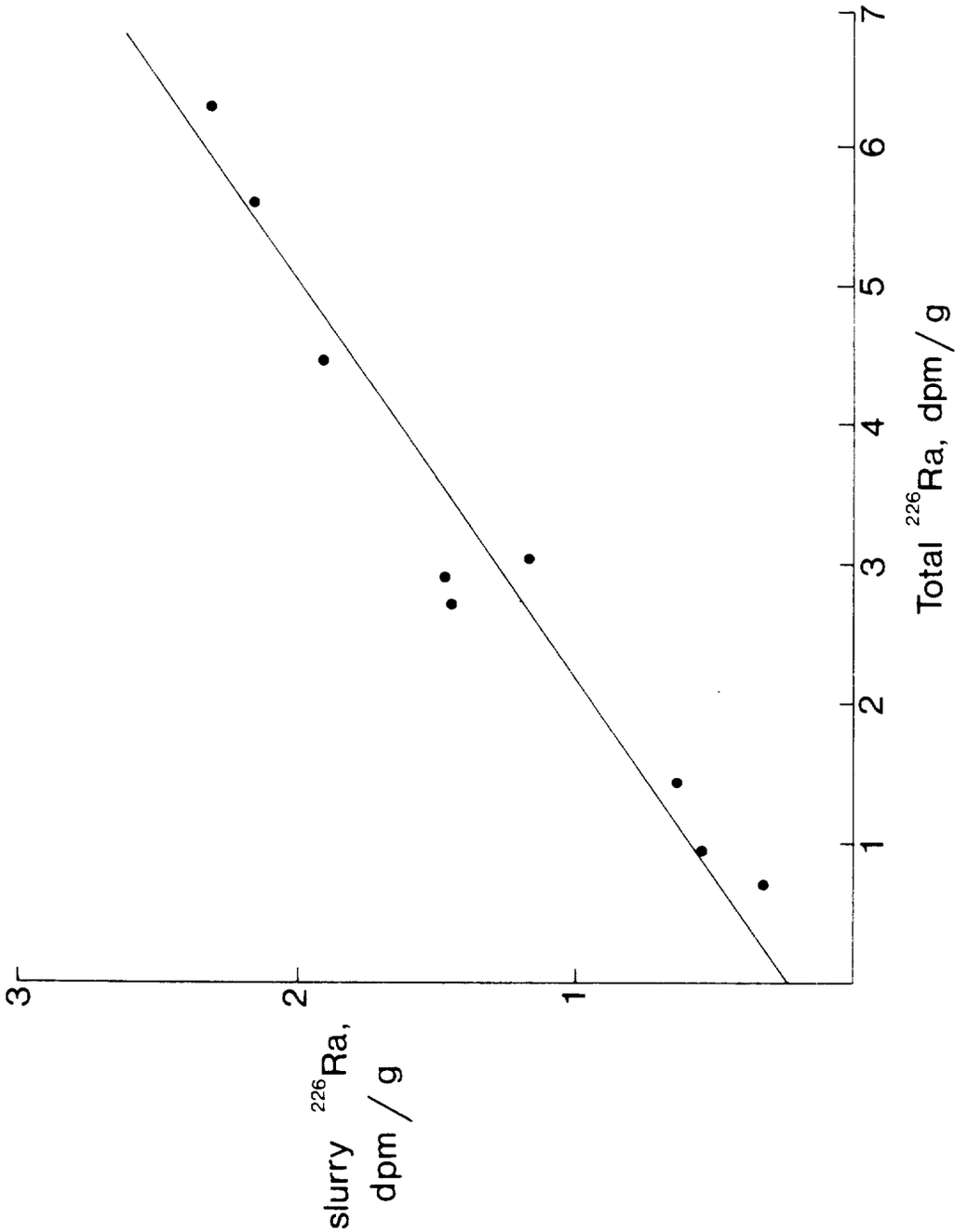

Figure 30 Plot of ^{226}Ra in sediment slurries *versus* total ^{226}Ra for the samples analysed. The gradient of the line is 0.35.

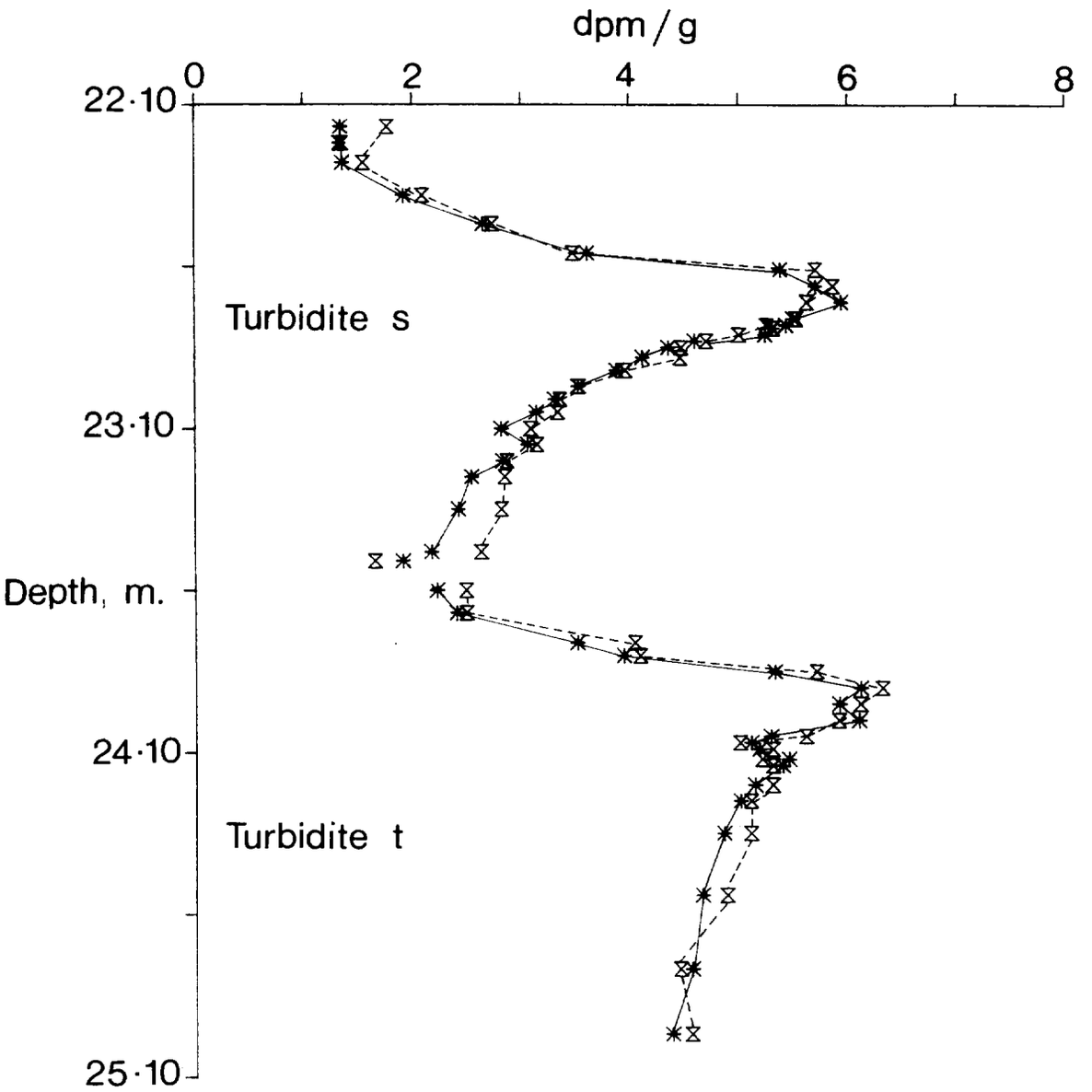

Figure 31 Model ^{226}Ra (stars) and experimental ^{226}Ra (bow-ties) profiles *versus* depth for turbidites *s* and *t* from core MD24, with 35% ^{226}Ra diffusing. The optimum D_{eff} (omitting the top sample in the calculation) is 6×10^{-9} cm^2 s^{-1}.

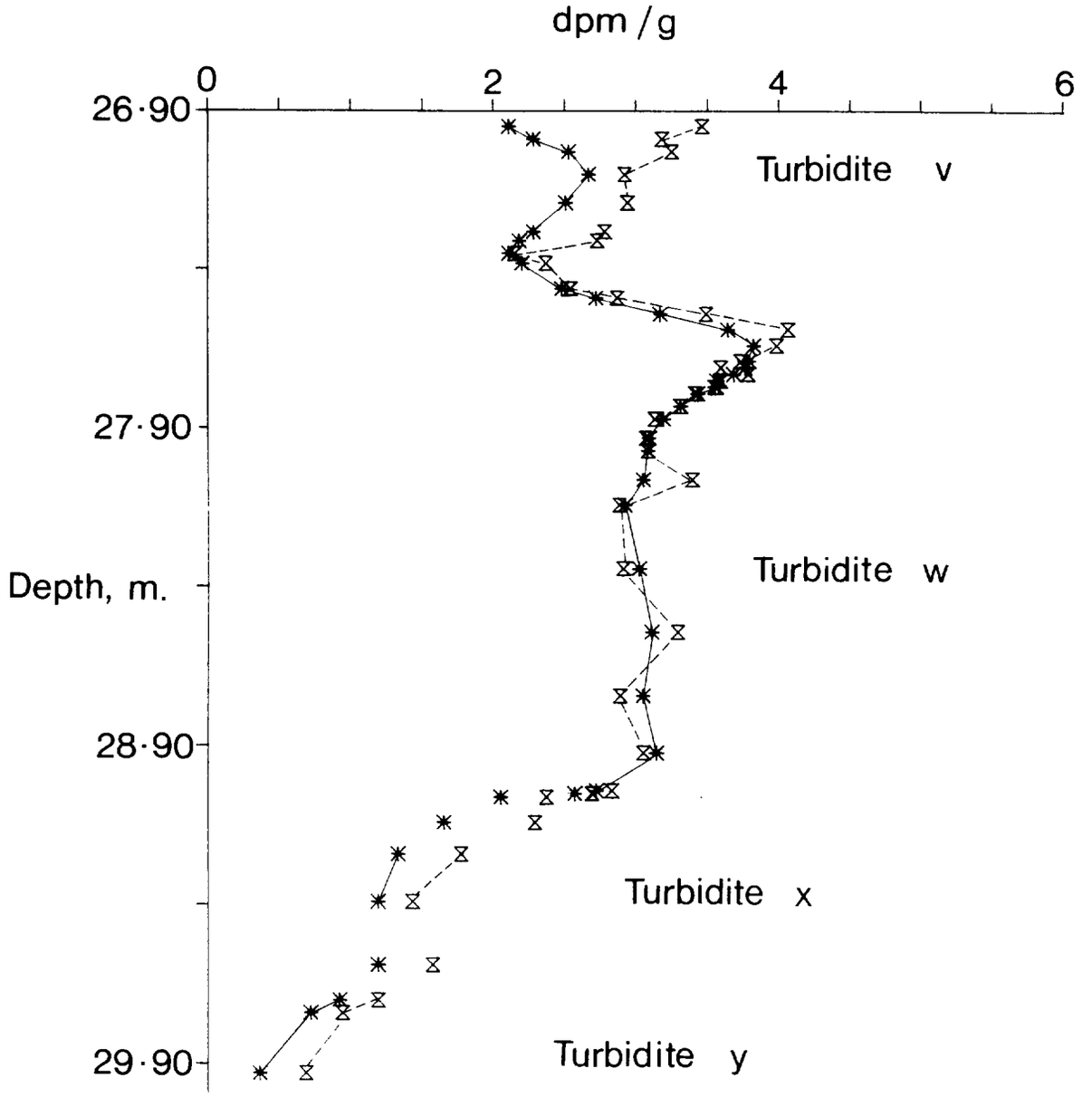

Figure 32 Model ^{226}Ra (stars) and experimental ^{226}Ra (bow-ties) profiles *versus* depth for turbidite ***w*** and surrounding units from core MD24, with 70% ^{226}Ra diffusing. The optimum D_{eff} (omitting the top three samples from the calculation) is 1×10^{-9} cm^2 s^{-1}.

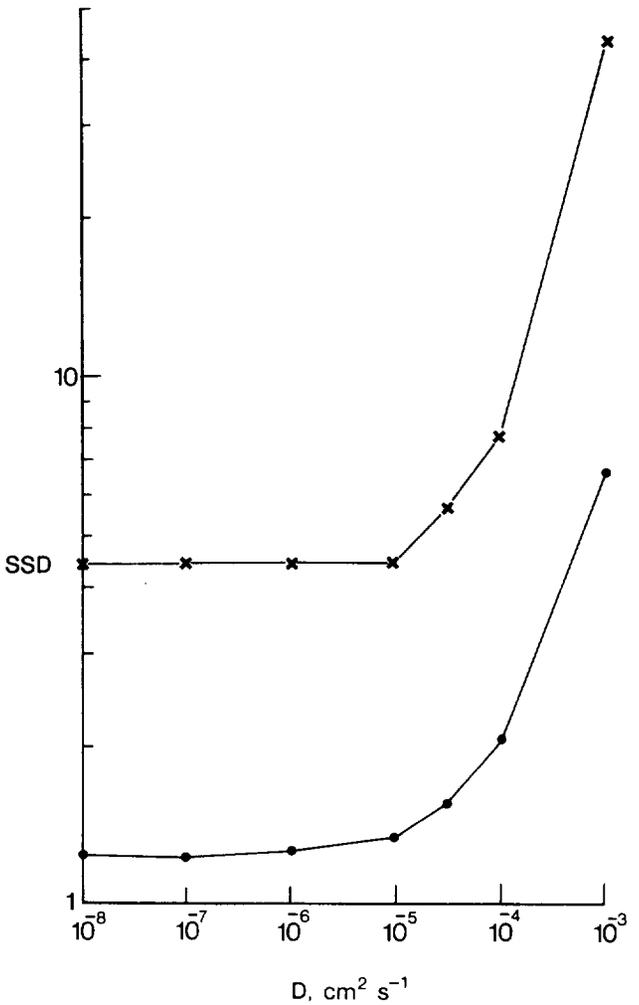

Figure 33 Variation of SSD with D for ^{226}Ra - ^{210}Po for turbidites *s* and *t* (crosses), and turbidite *w* and surrounding units (dots) in core MD24.

Geochimica et Cosmochimica Acta Vol. 53, pp. 1223–1234
0016-7037/89/$3.00 + .00

Uranium relocations and derivation of quasi-isochrons for a turbidite/pelagic sequence in the Northeast Atlantic

S. COLLEY[1], J. THOMSON[1] and J. TOOLE[2]

[1]Institute of Oceanographic Sciences, Brook Road, Wormley, Godalming, Surrey GU8 5UB, England, U.K.
[2]Scottish Universities Research and Reactor Centre, East Kilbride, Glasgow G75 0QU, Scotland, U.K.

(*Received April* 25, 1988; *accepted in revised form March* 27, 1989)

Abstract—The systematics of U relocation in the organic-rich distal turbidite sequence of sediments of the Madeira Abyssal Plain are investigated by examination of solid phase [U]/depth and selected pore water [U] profiles. The characteristic U profile developed in these homogeneous turbidites by oxidation fronts can be recognised in examples emplaced up to 750 ky ago. Profiles in individual turbidites can be correlated in cores over 100 km apart. In the surficial turbidite, where an oxidation front is currently active, the pore water profiles from a box core and an *in situ* sampler show maximum pore water [U] in the vicinity of the front with fluxes both upwards and downwards. The pore water profiles do not, however, support the loss of U to bottom waters implied by solid phase mass balances in this surficial turbidite, and in weakly reducing conditions below the active front, the pore water [U] is as high as that of sea water (3.3 $\mu g \cdot l^{-1}$). Examples from two buried turbidites where the oxidation fronts are extinct show excess U in the peaks over that expected from the relocation process, so that these turbidites appear to have gained U, presumably from bottom water, during the time their fronts were active. In one of these examples, the pore water U content now appears proportional to the authigenic sediment [U], although this may be an oxidation artifact. The immobility of the solid phase profiles in reducing conditions is demonstrated by the construction of "isochrons" based on ^{230}Th ingrowth from ^{238}U, where the data from each turbidite conform to a distinctive line. Values of time calculated from the isochrons have poor chronological significance because of violations of the model requirements when the fronts were active, but a 600-ky-old turbidite conforms to the equiline and confirms good chemical closure in the $^{238}U \rightarrow {}^{230}Th$ decay sequence in the long term.

INTRODUCTION

THE GEOCHEMICAL BEHAVIOUR of U is generally highly predictable in deep-sea sediments: pelagic sediments have low contents of preserved organic carbon and negligible authigenic U, and an oxic redox condition in pore waters to considerable depth. Enhanced sediment U contents are usually found in shallower water sediments in association with higher organic levels and anoxic pore waters (VEEH, 1967; KOLODNY and KAPLAN, 1973; MO *et al.*, 1973; VEEH *et al.*, 1974; DEGENS *et al.*, 1977; YAMADA and TSUNOGAI, 1984; CARPENTER *et al.*, 1984; COCHRAN *et al.*, 1986). High U contents in deep-ocean sediments are therefore sufficiently unusual to warrant further investigation.

A U redistribution phenomenon in organic-rich deep-sea turbidites was reported by COLLEY *et al.* (1984) from a deep site at the foot of the Mid-Atlantic Ridge, and a mechanism was proposed which was subsequently supported by pore water data from an area of the Madeira Abyssal Plain (WILSON *et al.*, 1985, 1986; THOMSON *et al.*, 1987). The sequence of events is that an organic-rich turbidite, with an associated enhanced U content, is emplaced into pelagic conditions. Bottom water oxygen penetrates into the surficial layers of this new sediment, oxidises the labile C_{org} and releases the authigenic U fraction to solution in oxic pore water conditions. A marked redox contrast is set up in the sediment column at the level of zero oxygen, and this contrast progresses downwards as the oxidation front diffuses deeper into the turbidite sediment with time. Uranium is progressively relocated to the weakly reducing conditions immediately below the active front (pore waters with a post-oxic condition *sensu* BERNER, 1981). COLLEY and THOMSON (1985) demonstrated that two types of U were involved, an inert detrital fraction (2.7 ppm U calcium carbonate-free) and a potentially mobile authigenic U fraction. Figure 1 illustrates the development of the resulting U concentration/depth profile characteristic of the process. COLLEY and THOMSON (1985) also found that this profile shape was preserved in buried turbidites where the oxidation fronts responsible were no longer active and that the U peaks were located just below the colour changes in the turbidites, which marked the extents of penetration of the fronts when active. Organic-poor turbidites from the same abyssal plain succession do not contain appreciable authigenic U and do not develop U peaks (COLLEY and THOMSON, 1985).

The above findings are pertinent to the general mechanism of authigenic U uptake by anoxic sediments, which remains uncertain despite recent studies. The work of ANDERSON (1982, 1984, 1986) demonstrates that a water column supply of U by biological or inorganic particulate material is unlikely to be the major factor, suggesting that diffusion of the bottom water U(VI) carbonate complex into sediments with subsequent retention must be involved (ANDERSON, 1986; COCHRAN *et al.*, 1986). Two retention mechanisms have been proposed: reduction of the sea water U(VI) carbonate complex to a less soluble U(IV) compound (BONATTI *et al.*, 1971; YAMADA and TSUNOGAI, 1984; ANDERSON, 1987), or complexation of U(VI) by organic matter in reducing conditions (BATURIN *et al.*, 1971; KOLODNY and KAPLAN, 1973; DEGENS *et al.*, 1977). Examples of coastal pore water U concentration profiles *versus* depth seem somewhat at variance with expectation from both mechanisms (COCHRAN, 1982). Buzzards Bay profiles, for example, exhibit higher U concentrations in anoxic conditions in both pore waters and sediments, when compared with oxic conditions (COCHRAN *et al.*, 1986). Such high solution U concentrations from anoxic

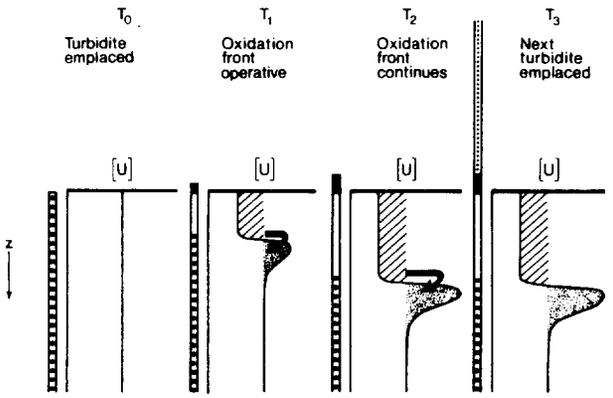

FIG. 1. Representation of the formation of diagenetic U profiles in organic-rich GME distal turbidites. At T_0, the turbidite is newly emplaced with an homogenous U content: both detrital and authigenic U forms are present. At T_1 bottom water oxygen has diffused into the turbidite surface, oxidising organic carbon and mobilising authigenic U only (shaded area). A small quantity of pelagic sediment has accumulated, and a fraction of the remobilised U has formed a peak below the progressive oxidation front (stippled area). At T_2 the progressive oxidation front has moved further into the sediment and the U peak been augmented and has migrated with the front. At T_3 another turbidite has been emplaced, the progressive oxidation front has been terminated because diffusive contact with bottom water has been blocked, and the U peak remains as a relict indication of the process.

conditions may be suspect because of the processing necessary to extract pore waters, as will be discussed later.

The sequence of organic-rich turbidites on the Madeira Abyssal Plain which have been modified by prolonged exposure to bottom water between emplacement events allows investigation of the phenomenon of U relocalisations over a long period by solid phase studies. This paper provides new information on the areal correlation of U peaks and their mass balances in the same turbidites at different locations, on their associated pore water profiles, and on the persistence of the characteristic profile shape in individual turbidites over 750 ky. The U peak immobility following burial is also demonstrated quantitatively for the first time using quasi-isochron plots of $^{230}Th/^{232}Th$ *versus* $^{238}U/^{232}Th$ activity ratios.

SAMPLING AND METHODS

Figure 2 shows the locations of samples investigated in the Great Meteor East (GME) area of the Madeira Abyssal Plain. The materials were collected on RRS *Discovery* Cruises 149 and 160, except for cores 10688 (COLLEY and THOMSON, 1985) and MD24. The latter core was retrieved during the 1985 "Étude des Sédiments Océaniques par Pénétration" (ESOPE) cruise of MS *Marion Dufresne* using the STACOR 30 m piston coring device (SCHUTTENHELM *et al.*, 1989). Pore waters from the uppermost turbidite were obtained by the IOS Mark II *in situ* pore water sampler, from box cores, and from a deeper turbidite in one piston core. Subcores from the box cores were extruded in a glove box and samples transferred to squeezer units for hydraulic squeezing. These operations were carried out under nitrogen and at 4°C. The piston core section containing a buried turbidite was also opened and sampled in a nitrogen atmosphere at 4°C. In this case, the pore waters were extracted by centrifugation, using sealed centrifuge vials filled with nitrogen and a centrifuge cooled to 4°C. A final filtration of *in situ*, squeezer and centrifuged samples was performed in a nitrogen atmosphere using 0.4 μm Nuclepore filters.

All box core sediment samples analysed are from squeezed sediment cakes remaining after shipboard processing for pore water extraction. Additional sediment samples from piston cores were sampled from split sections. All samples were stored at 4°C, dried at 110°C (except for 11143BX: 70°C) and ground in an agate swing mill.

Analyses for the α-emitting isotopes of U and Th were performed by the method of THOMSON (1982), using a $^{232}U/^{228}Th$ spike. Calculation of sample Th isotope concentrations using this spike assume that sample ^{228}Th and ^{232}Th are at equilibrium. Loss of ^{228}Ra has occurred from the top 5 cm of box core samples, and Th analyses from these intervals were corrected for this disequilibrium from unspiked analyses which determined true sample $^{228}Th/^{232}Th$ ratios. Total U analyses were also obtained commercially using a delayed neutron method: these were usually lower than the α-spectrometric analyses by 10%. Pore water U determinations were made by the fission track method (FLEISCHER and DELANEY, 1976) as modified by TOOLE *et al.* (1984). Organic carbon was determined by the method of THOMSON *et al.* (1984).

RESULTS AND DISCUSSION

The record of U peak formation through time

The sediments of the GME area have been studied by comparison of conventional piston cores (10–15 m in length) taken by IOS and Rijks Geologische Dienst (The Netherlands) workers. As a result of the number and spread of piston cores available, the stratigraphy of the area 30 to 33°N, 23 to 26°W is well known, and good stratigraphic correlations over the past 250 ky have been demonstrated by means of coccolith palaeontology (WEAVER and KUIJPERS, 1983; WEAVER *et al.*, 1985; WEAVER and ROTHWELL, 1987). The turbidites of the area are identified by an alphabetical code with the most recent turbidite as *a*.

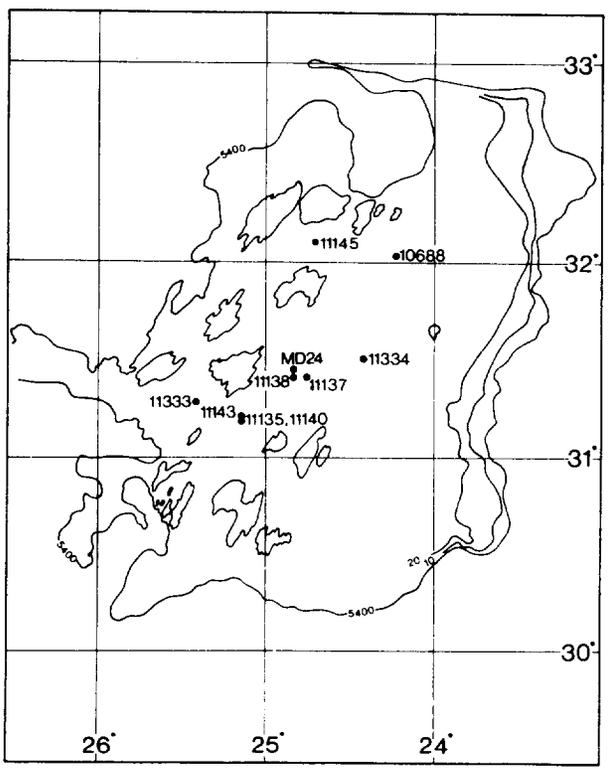

FIG. 2. Locations of cores used in this study on a simplified bathymetric map of the GME area, Madeira Abyssal Plain.

The stratigraphic investigations of WEAVER and KUIJPERS (1983) were limited by the sediment accumulation rate in the GME area and the length of normal piston cores. One such core (10688) was used by COLLEY and THOMSON (1985) to define the U behaviour over this time period. Thirty-meter piston cores collected on the ESOPE cruise have enabled much older, deeper-buried turbidites with associated U peaks and C_{org} steps to be studied (SCHUTTENHELM *et al.*, 1989).

Figure 3 shows the U profile for one of these cores (MD24) together with the provisional stratigraphic log, some independent age estimates and the C_{org}/depth profile (SCHUTTENHELM *et al.*, 1989). The profile commences at a depth of 12 m (within turbidite *g*) and thus overlaps with the profile for core 10688 studied by COLLEY and THOMSON (1985). Authigenic U enrichments are present in turbidites *h, p, s, t, u, v* and *w*, the oldest having persisted for about 750 ky. With

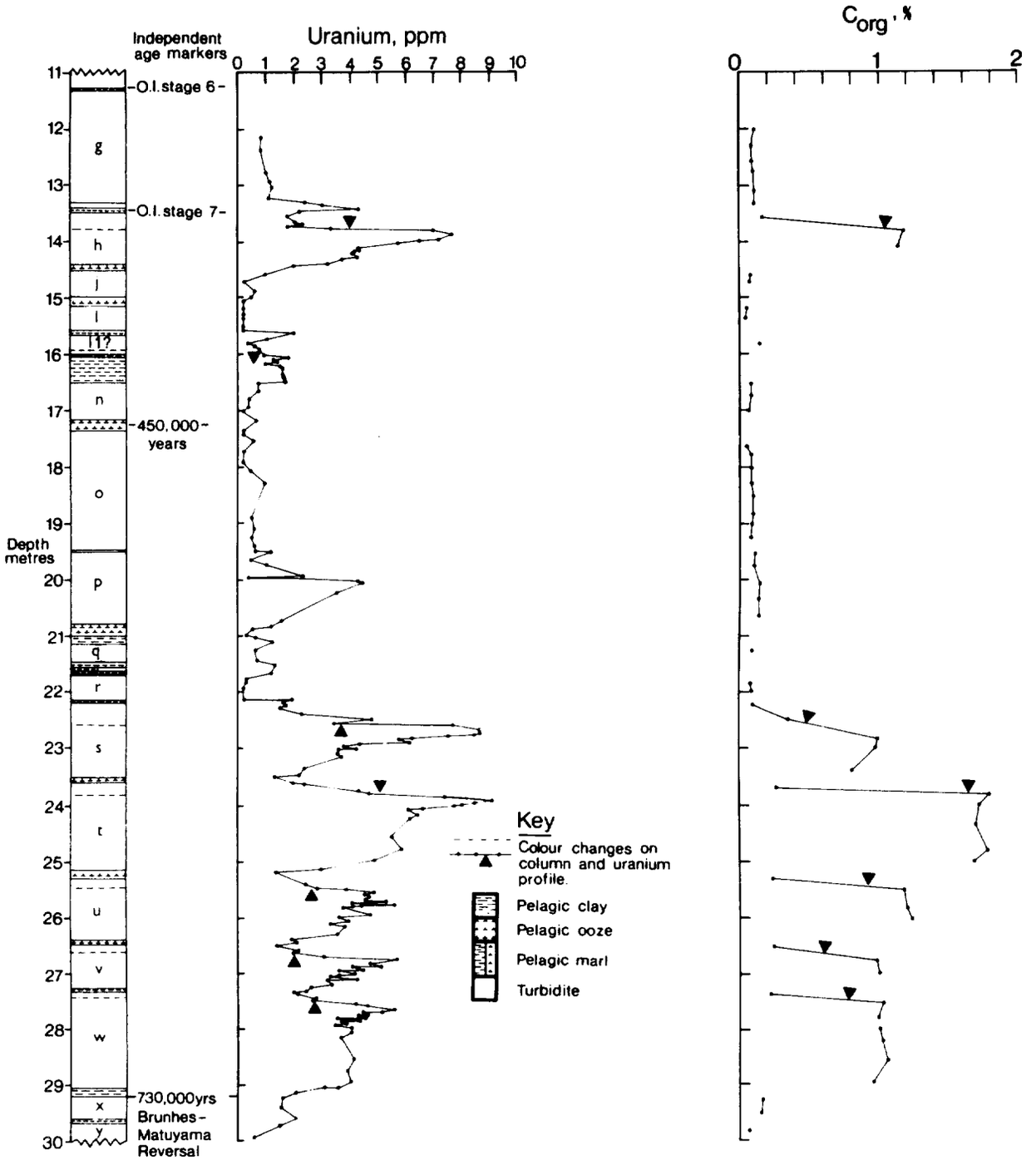

FIG. 3. Stratigraphic log, solid phase U profile and organic C profiles of core MD 24. The organic C data are from the turbidite units only. This core overlaps with core 10688 reported by COLLEY and THOMSON (1985), and has the same alphabetical nomenclature for the turbidite succession. All data from SCHUTTENHELM *et al.* (1989).

the exception of turbidite *p*, the peak concentrations of U are positioned below colour changes within the turbidites, which are coincident with steps in C_{org} content. These colour changes are believed to mark the extent of progressive oxidation fronts when active (THOMSON *et al.*, 1987; JARVIS and HIGGS, 1987). The U enrichments associated with turbidites *u* and *v* show rather less-characteristic shapes: the concentrations of U increase sharply in similar positions relative to the relict colour changes in these turbidites, but the lower sides of the peaks are less well developed, and it is not possible to estimate a reliable baseline emplacement value, such as is illustrated in Fig. 1, for either turbidite. Grain-size variation (grading), within these two turbidites may have produced these irregular profiles. Further work is required to ascertain whether these differences of detail are due to primary sedimentological effects or to U migration following the burial which terminates the oxidation front process.

Stratigraphic correlation of U peaks in individual turbidites

Three individual organic-rich turbidites (*a*, *d* and *e*) were sampled from a suite of box and piston cores from the GME area to ascertain the reproducibility of the U peak in a particular unit. Uranium relocation and peak formation were found previously in turbidites *a* and *e* (COLLEY and THOMSON, 1985), but it is now known that turbidite *d* was thin and completely oxidised in the piston core described in that work (JARVIS and HIGGS, 1987). Other piston cores from the GME area contain thicker examples of *d* which preserve colour changes and U peaks, and such examples are considered here. Composite U and C_{org} concentration/depth profiles are presented for these turbidite units in Figs. 4, 5 and 6. The colour changes in the turbidites, interpreted as the maximum penetration levels achieved by the oxidation fronts when active, are chosen as the zero depth references in all three cases.

The U peak shapes and positions, together with the steps in C_{org} concentrations in buried turbidites, show remarkable consistency between the piston cores sampled (Figs. 5 and 6), despite the fact that the cores are up to 110 km distant from each other (Fig. 2) and that the zero reference levels are at variable depths in the different cores (6–7 m for turbidite *d*, 7.5–9.5 m for *e*). The greatest peak enrichments of U in buried turbidites are localised in 20 to 30 cm-thick zones starting about 5 cm below the colour fronts, although the lower sides of the peaks may show much more gradual decreases to the unaltered turbidite baseline U values. This is especially noticeable for turbidite *e*.

There is a similar coincidence in the C_{org} step and change in U concentration in equally widely spaced cores where a progressive oxidation front is active (Fig. 4). The enrichments seen in turbidite *a* are less well developed than in the older, preserved examples, and are seen nearer to the colour change (Fig. 4, especially 11135), rather than 5 to 10 cm below, as in the older examples (Figs. 5 and 6).

In order to evaluate a mass balance for U in individual turbidite units, a comparison is required between the quantity mobilised by the oxidation front when active and the quantity immobilised in the peak. These two quantities correspond

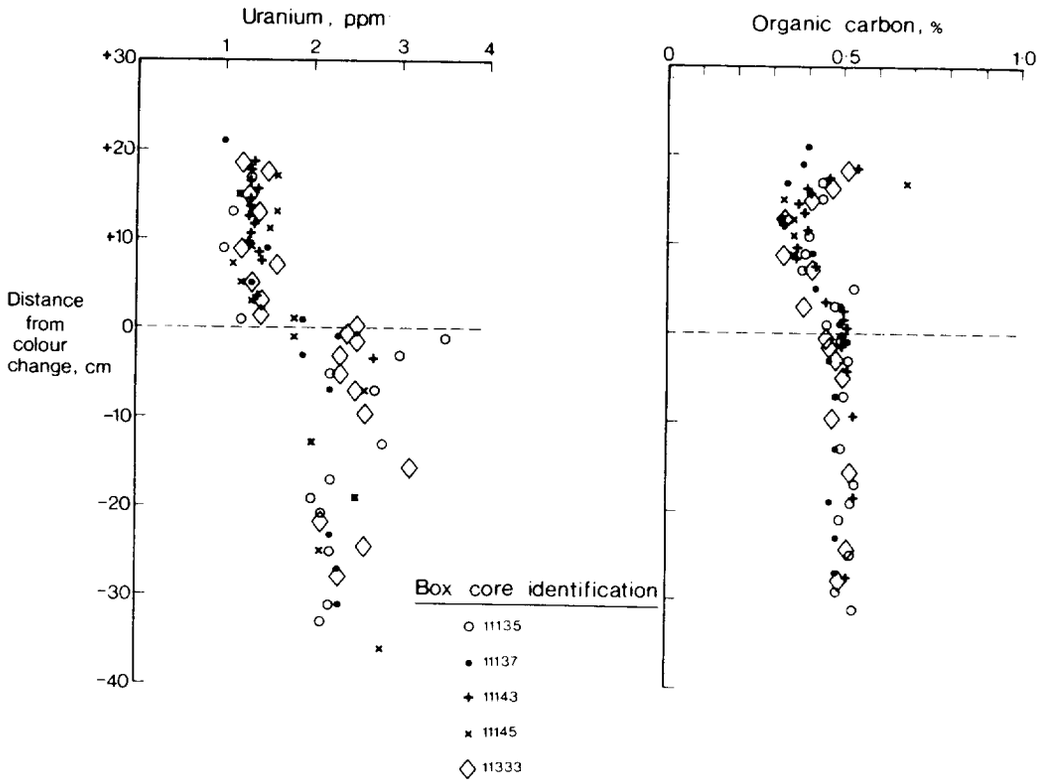

FIG. 4. Composite U and organic C profiles *versus* depth in five box cores sampling turbidite *a* only. The zero reference depth is the colour change related to the active progressive front in each case.

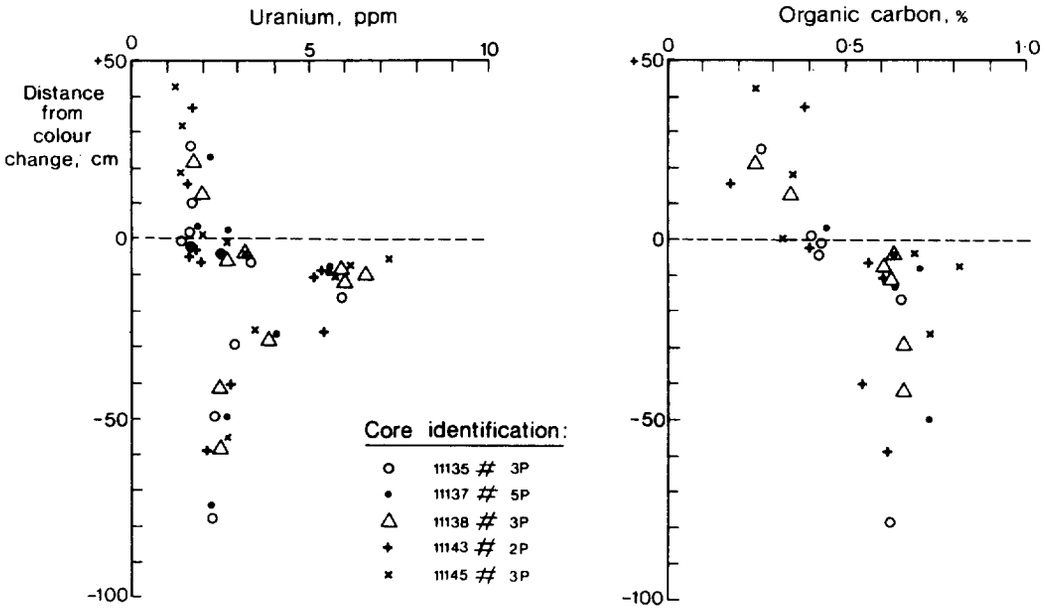

FIG. 5. Composite U and organic C profiles *versus* depth in five piston cores sampling turbidite *d*. The zero reference depth is the colour change marking the fossil oxidation front in each case. From THOMSON *et al.* (1987).

to the shaded and stippled areas of Fig. 1, respectively. The emplacement U content of the turbidite is assumed to be given by the average of the deepest points below the U peaks. For each core, the calculations are then

$$\text{U mobilised } (\mu g/cm^2) = (\text{Emplacement U content} \cdot \text{density} \cdot \text{depth to colour change}) - (\text{Average U content above colour change} \cdot \text{density} \cdot \text{depth to colour change})$$

and, for n sections in the peak,

$$\text{U immobilised } (\mu g/cm^2) = \sum_{1}^{n} [(\text{Section U content} \cdot \text{density} \cdot \text{section thickness}) - (\text{Emplacement U content} \cdot \text{density} \cdot \text{section thickness})].$$

In all cases, the density used is the bulk sediment dry density. The U mass balance so defined is given for the box cores sampling only turbidite *a* in Table 1, and for the piston cores sampling turbidites *d* and *e* in Table 2. Varying proportions of the U mobilised from the oxic section of turbidite *a* are immobilised below the colour changes (Table 1); but there is always <100% conservation, and a loss of U, presumably to bottom water, is required in all cases. There is no problem in identifying the oxic length in these cores, and the major element homogeneity of these same cores has been demonstrated (THOMSON *et al.*, 1988).

In the case of the buried turbidites, on the other hand (Table 2), U immobilised in the peaks is >100% of U mobilised from above the colour front, with one exception (97% in turbidite *d*, core 11145). The percentage surpluses vary between cores, possibly due to poor definition of some peaks by few data points and also to the problem of estimating oxidised turbidite thicknesses where bioturbation has obscured upper boundaries of the units. The fact that the amounts of U present in the peaks are substantially greater than the deficits in the formerly oxidised sections of these turbidites implies that, in addition to U relocalisation within the turbidite during the progression of the front, peak U concentrations must have been enhanced by U scavenging from sea water. It might be expected that the cores showing the shortest oxidised tops should have the largest U peak excess, because the zone where the redox environment was favourable to U scavenging would have remained at a shallower depth within the sediment for a longer time, allowing greater incorporation of U from sea water. No clear relationship appears to exist, however, suggesting that the incorporation process is more complex or that estimation of the former oxidised top lengths is more uncertain than it appears, because of bioturbation or piston coring distortion.

The dissimilarities between the surficial (turbidite *a*) and buried (turbidites *d* and *e*) cases are not well understood. The most notable differences between turbidite *a* and buried examples where the oxidation fronts are inactive are that *a* had a slightly lower initial C_{org} content when emplaced, and a lower proportion of this C_{org} has been oxidised compared with older turbidites (Table 3). An obvious possibility is that the different turbidites contain C_{org} of different reactivities. The colour change between the oxidised and unaltered section in turbidite *a* is buff/grey compared with apple green/olive green in the deeper, more organic-rich examples. In addition, the oxidation process has only been active in turbidite *a* for about 500 y (THOMSON *et al.*, 1988), whereas the fronts preserved in older turbidites would have been active for tens of thousands of years before burial by an overlying unit halted their progress.

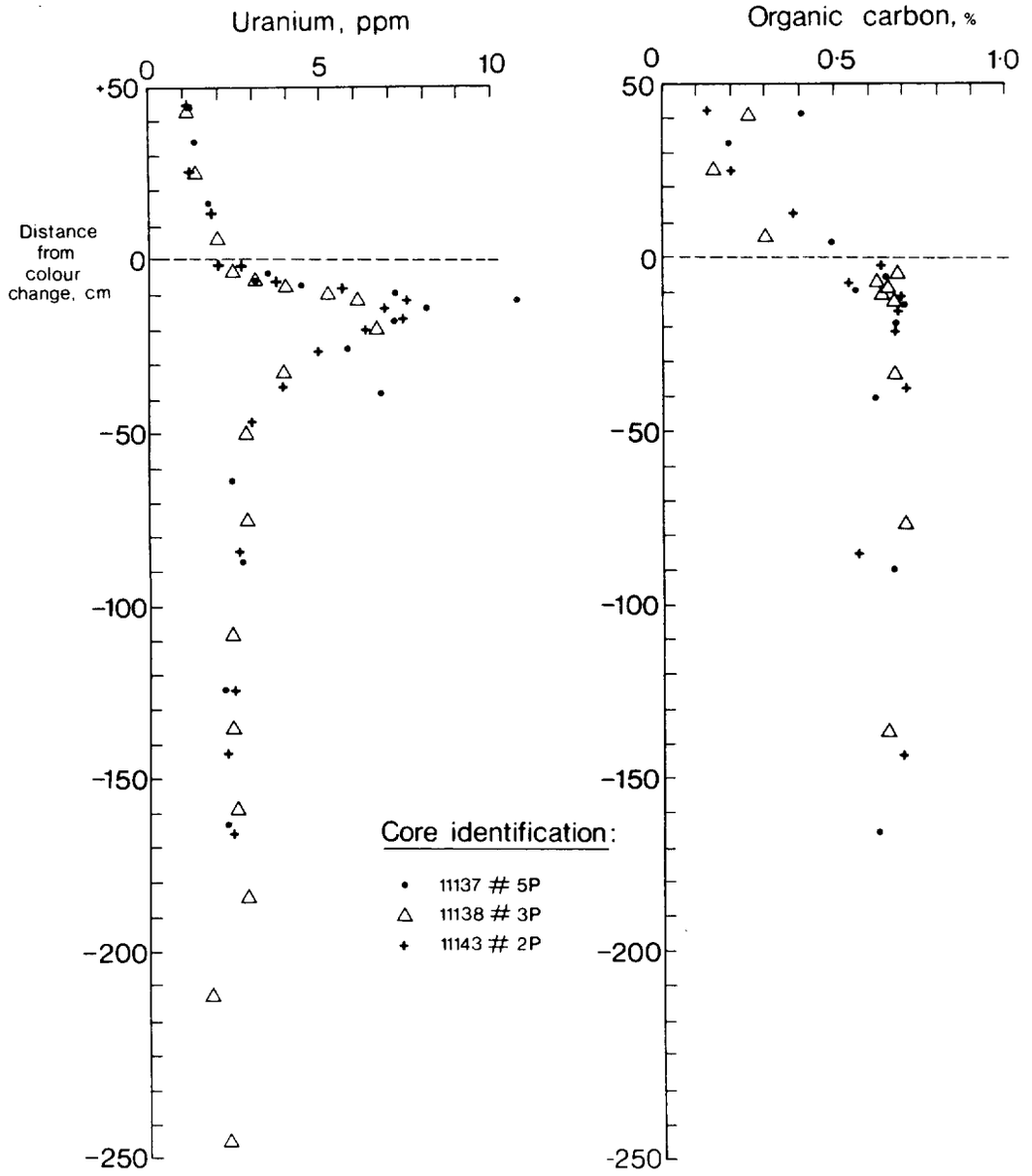

FIG. 6. Composite U and organic C profiles *versus* depth in three piston cores sampling turbidite *e*. The zero reference depth is the colour change in each case.

The mechanism of U fixation

Previous work on the redistribution of metals in GME turbidites has provided three distinct lines of evidence from solid phase data for a redox mechanism of U fixation (*i.e.* U[VI] → U[IV]):

1. Where the turbidites are thin, U peaks are displaced out of the turbidite units into the immediately underlying pelagic units which have low C_{org} contents. Such offsets of U peaks from high C_{org} levels favour the redox mechanism over the formation of organo-uranyl complexes (COLLEY and THOMSON, 1985).

2. Other elements (notably Cu and V) are also found to have concentration peaks at slightly shallower depths than U (JARVIS and HIGGS, 1987). The U/Cu/V association, with U located deeper (*i.e.* in more reducing conditions) than Cu and V is reminiscent of the relative locations of these elements in roll-front U deposits, which are believed to form by a redox mechanism (HARSHMAN, 1974; MAYNARD, 1983, and references therein).

3. In an example where the progressive oxidation front has been continuously active for 330 ky, a differential behaviour of ^{234}U and ^{238}U was observed (COLLEY *et al.*, 1984). This isotopic disequilibrium is generally ascribed to a production of ^{234}U in the (VI) oxidation state from ^{238}U in the (IV) state through radioactive decay (KU, 1965; KOLODNY and KAPLAN, 1970; MANGINI and DOMINIK, 1979).

Such interpretations are based on extrapolations from thermodynamic data, which suggest that U is present in sea

TABLE 1 - URANIUM PEAK ENRICHMENTS IN TURBIDITE a

Box core	Average U above colour change μg/g	Depth to colour change cm	U deficit above colour change μg/cm²	Excess U below colour change μg/cm²	Excess U / U deficit %
11135	1.18	18	8.96	4.8	54
11137	1.38	22	8.75	1.0	11
11143	1.33	19	8.03	ND	ND
11145	1.40	18	6.98	2.9	41
11333	1.46	19	6.79	5.2	76

Note: Average emplacement U for turbidite a in all cores is 2.175 μg/g.
Dry bulk density used is 0.5 g/cm³ (Includes salt).
ND - No data for lower part of unaltered turbidite.

water as the soluble U(VI) carbonyl complex $UO_2(CO_3)_3^{4-}$, and that U(IV) minerals or complexes have very low solubility products. Alternative hypotheses also exist: KRYLOV *et al.* (1985), for example, suggest that U(VI) is present in sea water as the species $UO_2(OH)_4^{2-}$, and KNIEWALD and BRANICA (1988) suggest that U(V) may be a significant species in the environment, especially at the boundary between oxic and anoxic conditions.

A different approach to elucidating geochemical behaviour is to investigate pore water U profiles, on the basis that such data may reveal where mobilisation or immobilisation reactions are active in the sediment column, and indicate the directions and magnitude of pore water fluxes of U. The difficulty with such investigations is that pore water U levels measured appear to be particularly susceptible to artifacts which can occur. Brief exposure of anoxic sediments to air during processing can produce elevated solution U values (ANDERSON, 1984; J. K. COCHRAN, pers. commun., 1988), and TOOLE *et al.* (1984) have suggested that U may be precipitated along with pore water carbonate by the pressure release experienced during core retrieval from the sea floor. Pore water profiles from an active and a relict oxidation front will now be considered.

Uranium in the pore waters of an active progressive oxidation front

Turbidite *a* forms the upper unit of the sedimentary succession in the GME area, which allows a comparison between pore waters extracted from box core sediment and extracted *in situ* by the IOS Mark II pore water sampler. The demonstrated horizontal and vertical solid phase compositional homogeneity of turbidite *a* at the sites sampled (THOMSON *et al.*, 1988) allows a valid comparison between the pore waters collected by the two methods, despite the fact that the box corer and *in situ* device deployments were not made at exactly the same place. Other data (THOMSON *et al.*, 1987) also demonstrate the similarities in box core pore water profiles of redox-sensitive species (O_2, NO_3^-, Mn^{2+} and Fe^{2+}), which reveal that an active progressive oxidation front is located at 20 ± 2 cm below the sediment/water interface in turbidite *a*.

TABLE 2 - URANIUM PEAK ENRICHMENTS IN TURBIDITES d AND e

TURBIDITE d - Calculated using average detrital and emplacement U values for each individual turbidite example (Assumed dry density = 0.65 g/cm³)

Core	Depth to colour change cm	U deficit above colour change ug/cm²	Excess U in peak ug/cm²	Peak / Deficit %
11135	42	19	33	175
11137	48	16	39	238
11138	36	19	46	248
11143	50	14	44	305
11145	47	42	40	97

TURBIDITE e - Calculated using average detrital and emplacement U values for each individual turbidite example (Assumed dry density = 0.65 g/cm³)

Core	Depth to colour change cm	U deficit above colour change ug/cm²	Excess U in peak ug/cm²	Peak / Deficit %
11137	67	37	137	369
11138	55	48	85	183
11143	74	45	85	191

TABLE 3 - COMPARISON OF RELATIVE AMOUNTS OF ORGANIC CARBON OXIDISED IN DIFFERENT TURBIDITES

Turbidite	Average C_{org} in oxidised section %	Average C_{org} in unaltered turbidite %	Percentage of C_{org} destroyed in oxidised section
a	0.35	0.50	30
d	0.26	0.65	60
e	0.20	0.66	69

Figure 7 illustrates the solid phase and pore water U profiles in a box core at site 11135, and two *in situ* sampler profiles. The *in situ* sampler site 11140 is near-coincident with site 11135, while site 11137 is to the northeast (Fig. 2). All three pore water profiles (Fig. 7) exhibit maxima in the region of the active oxidation front located at around 20 cm in turbidite *a*, although the two *in situ* values are greater than that of the box core. Maxima are expected around this depth from the solid phase U profiles of turbidite *a* (Fig. 4) because U is required to be continuously mobilised at the active front and immobilised below it (Fig. 1). The gradients from these maxima imply fluxes of U in solution upwards and downwards from the active front. In the more detailed box core profile (Fig. 7, center) the downwards flux is greater (sharper gradient) over a distance of 8 cm. While consistent with both remobilisation of U from the front downwards to form a U peak and a loss upwards, however, the pore water data do not suggest a loss to sea water as required by the solid phase mass baiance (Table 1). Most values above the active front in the core and *in situ* sampler profiles are less than the sea water value, so that a flux out of the sediments to bottom water is not indicated. All pore water data deeper than 25 cm indicate pore water U contents similar to that of sea water within the measurement uncertainties.

Overall, it is difficult to reconcile these pore water data with the solid phase U evidence elsewhere in this study. While the box core and *in situ* data are similar in this case, they give no evidence of a loss to bottom water (Table 1), and it is unexpected to find that the sea water U value is maintained below the depth where uptake is occurring in post-oxic conditions and where authigenic U exists. The analytical technique employed in this study to determine solution U concentrations measures total U, and it has been tacitly assumed that the same U species is always present in pore water solution. It may be that U speciation changes in response to changes in the redox environment with depth. A clear example of such changes is provided by the behaviour of I at progressive oxidation fronts, where complex pore water I profiles comprise both I^- and IO_3^- components (KENNEDY and ELDERFIELD, 1987). A change in solution speciation would not, however, change the conclusion that the pore waters indicate no loss to bottom water.

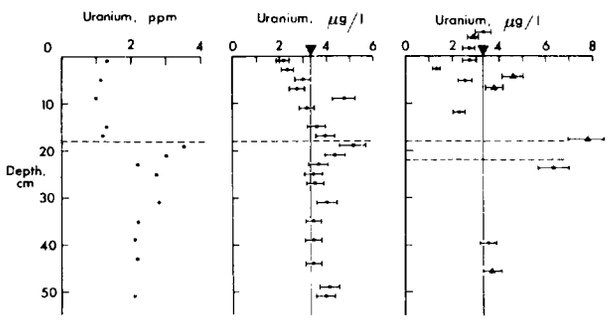

FIG. 7. Solid phase U *versus* depth profile from box core 11135 (left), pore water U *versus* depth profile in box core 11135 (center) and *in situ* pore water U *versus* depth profiles from IOS Mark-II sampler stations 11137 (dots) and 11140 (triangles) (right). The colour change associated with the active progressive oxidation front in turbidite *a* is shown as the dashed line (box core 11135), and the two dashed lines (right) show the overall range of depths at which this change is observed in box cores sampling turbidite *a*. The compositional homogeneity of turbidite *a* is demonstrated by THOMSON *et al.* (1988). The vertical lines mark the sea water U concentration.

Uranium in the pore waters of a fossil progressive oxidation front

The purpose of a further pore water experiment was to examine the pore water U profile associated with a solid phase U peak buried in reducing (post-oxic) conditions as fossil evidence of a former oxidation front. A section of piston core 11143 which contained the upper section of turbidite *e* was introduced to a nitrogen atmosphere and split, opened and sampled. Samples were taken relative to the preserved colour change of the unit which was at 887 cm depth. Turbidite *e* was emplaced at the end of oxygen isotope stage 5 (WEAVER and KUIJPERS, 1983) 73 ky ago (KOMINZ *et al.*, 1979) and was isolated from bottom water around the end of stage 4 (61 ky ago).

Figure 8 illustrates the data obtained for the corresponding solid phase and pore water [U]. Values for the detrital and emplacement solid phase levels (Fig. 1) can be estimated from the solid phase profile shape as follows. The average emplacement value of turbidite *e* is 2.46 ppm (Fig. 6). The detrital level is taken as the lowest value in the formerly oxic section, 1.4 ppm: this may be compared with an estimate of 1.24 ppm derived from the $CaCO_3$ content of turbidite *e* (53%, JARVIS and HIGGS, 1987) and the relationship between detrital U and $CaCO_3$ in North Atlantic pelagic sediments found by COLLEY and THOMSON (1985). Figure 9 illustrates

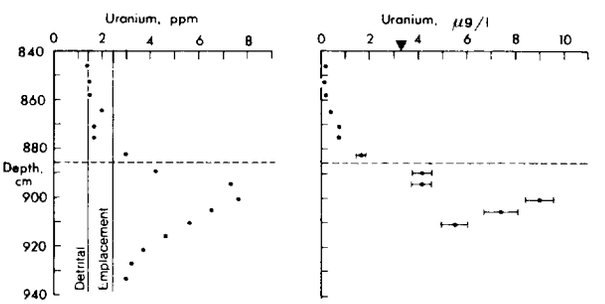

FIG. 8. Corresponding U *versus* depth profiles of solid phase (left) and pore water (right) in turbidite *e* in piston core 11143. The dashed lines indicate the colour change which marks the penetration of the fossil oxidation front. Estimated emplacement and detrital U levels are shown on the solid phase profile. The sea water U concentration is indicated.

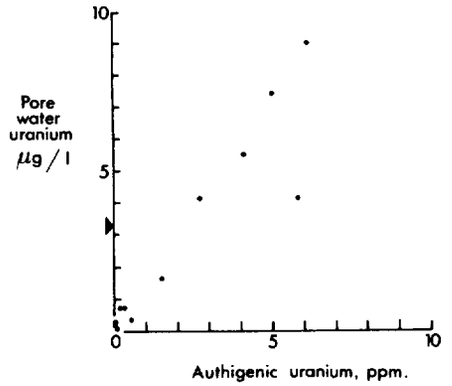

FIG. 9. Plot of pore water U *versus* authigenic solid phase U from Fig. 8. The sea water U concentration is indicated.

the relationship between authigenic solid phase [U] (defined as measured content—1.4 ppm) and the pore water [U]. This presentation suggests a linear relationship between the authigenic and pore water U levels, with a small intercept (0.13 $\mu g.l^{-1}$).

The data of Figs. 8 and 9 may be compared with those of SANTSCHI *et al.* (1988) who investigated GME core MD 24. Pore water U levels between 0.05 and 2.12 $\mu g.l^{-1}$ were found in that core, and these were correlated with measured redox potential (SANTSCHI *et al.*, 1988). Despite the generally low pore water U levels, SANTSCHI *et al.* (1988) believed that certain of their data had been enhanced by air oxidation during pore water separation. The samples which they analysed, however, were composites of several small aliquots from 1 m core sections. Sampling was performed without benefit of the solid phase U profile of core MD 24 subsequently obtained (Fig. 2), so it is uncertain what contribution samples with high authigenic U content may have made to their data.

It may be, therefore, that the pore water data of Figs. 8 and 9 are high because of inadvertent oxidation by air contamination during pore water extraction, in which case Fig. 9 illustrates that the authigenic U fraction is preferentially affected. All samples with little or no authigenic U (from the upper, formerly oxic, section of Fig. 8) exhibit low pore water U levels, less than one-third the sea water U value, and are similar to those observed by SANTSCHI *et al.* (1988).

Alternatively, if the data of Figs. 8 and 9 are not affected by oxidation, then they suggest that the authigenic U supports a high level of U in solution. This relationship can be characterised by the distribution ratio R_D, where

$$R_D = \frac{\mu g \text{ authigenic U}}{g_{solid}} \div \frac{\mu g \text{ solution U}}{g_{solution}}.$$

The mean R_D implied by Fig. 9 is $8 \cdot 10^2$, which is a low R_D value for an element which appears to have limited mobility from the other evidence presented in this paper (*cf.* I.A.E.A., 1985). High solution U contents might be expected to cause extensive migration of U along pore water concentration gradients. For migration in solution in sediments, factors besides tortuosity can act so as to reduce the solution diffusion coefficient (D_{soln}) to a much lower effective diffusion coefficient (D_{eff}). Various scenarios can be invoked which would limit the migration in the present case:

1. Colloidal particles containing U would pass with the solution phase through the 0.45 μ filters used here, in which case D_{eff} would be expected to be lower than for a species in solution. There was, however, no evidence of track clustering in the U fission track analysis.
2. ELDERFIELD (1981) has argued by reference to the Stokes Einstein relationship that low D_{eff} values may be expected if large molecular weight metal/organic complexes are involved.
3. BERNER (1976) has illustrated that adsorptive or ion exchange equilibrium between solution and solid phase will also act so as to make D_{eff} much smaller than D_{soln}.

Speciation information on the form of U in solution would be required to decide between these possible alternatives. Such possibilities are, however, also consistent with both high pore water U contents and long-term solid phase profile stability, as an alternative to the oxidation artifact explanation.

A quasi-isochron model for ^{230}Th ingrowth

So far the immobility of the U concentration/depth profile characteristic of the oxidation front process has been argued qualitatively by comparison of profile shapes, and the discussion has been in terms of U only. By consideration of the ingrowth of the U daughter ^{230}Th towards secular equilibrium with ^{234}U, however, the discussion can be taken further. Thorium is an element with very little mobility in a sedimentary environment, a fact which is the basis of $^{230}Th_{excess}$ methods of determining sediment accumulation rates (KU, 1976).

ALLÈGRE (1968) showed that isochrons could be constructed in an analogous fashion to the Rb-Sr method of age determination for rocks, using instead U and Th isotopic ratios. The disequilibrium relationship used for ^{230}Th is (ALLÈGRE, 1968)

$$\left(\frac{^{230}Th}{^{232}Th}\right) = \left(\frac{^{238}U}{^{232}Th}\right) \cdot (1 - e^{-\lambda t}) + \left(\frac{^{230}Th}{^{232}Th}\right)_0 \cdot e^{-\lambda t}$$

where activity ratios are used throughout and are indicated by the parenthesis convention, λ is the decay constant for ^{230}Th and t is the time since formation. Assuming that (i) the (^{230}Th/^{232}Th) was homogeneous at a unique time of formation of the system, (ii) (^{234}U/^{238}U) = 1.00 and (iii) a chemically closed situation obtains, then a plot of (^{230}Th/^{232}Th) *versus* (^{238}U/^{232}Th) will yield a slope of $(1 - e^{-\lambda t})$ and an intercept which is a function of time t and the initial (^{230}Th/^{232}Th). With progressive ^{230}Th ingrowth, the line will rotate counterclockwise from the horizontal with a decreasing intercept, until six ^{230}Th half-lives (450,000 years) have elapsed, when the points will closely approximate a straight line of slope 1 and zero intercept (the equiline).

ALLÈGRE (1968) used data from TADDEUCCI *et al.* (1967) to demonstrate that an estimate of age could be found from separate isotope determinations of mineral types in a single volcanic rock unit. In that case, the minerals had the same initial (^{230}Th/^{232}Th) ratio, but varying U contents which gave a spread of points on the x axis. This approach has been further applied to mineral separates from Pacific pelagic sed-

iments (BERNAT and ALLÈGRE, 1974) and to phosphorite deposits (ROE *et al.*, 1983) to estimate times of formation.

In the present case, the assumption is made that for each turbidite the homogeneity of the unit on emplacement provides a constant ($^{230}Th/^{232}Th$) and ($^{238}U/^{232}Th$) throughout the turbidite thickness. Variation in ($^{238}U/^{232}Th$) from a constant input value is provided as a result of the downward relocation of the authigenic U component. This violates the closed system formality of the isochron model, because the U redistribution takes place over some tens of thousands of years, and homogeneity of ($^{238}U/^{232}Th$) since emplacement has therefore not been conserved. A precise chronological significance is not, therefore, expected from the slope of the line constructed for each turbidite, and we term the lines "quasi-isochrons".

Figure 10 shows a ($^{230}Th/^{232}Th$) *versus* ($^{238}U/^{232}Th$) plot for the most recently deposited turbidite *a* using data collected from two cores. It can be deduced from the water column supply of ^{230}Th and the inventory of near-surface $^{230}Th_{excess}$ over the background turbidite ^{230}Th that this turbidite was deposited about 500 years ago (THOMSON *et al.*, 1988). Since then, bottom water O_2 has diffused into the sediment and authigenic U has been remobilised. Two domains of ($^{238}U/^{232}Th$) have thus developed, the lower values (0.75–0.95) corresponding with points above the oxidation front where authigenic U has been removed, and the values >1.5 representing unoxidised turbidite sediment from below the front. The best-fit line through these two domains, using the unweighted method for cases where both *x* and *y* axis variables are subject to uncertainty (KERMACK and HALDANE, 1950), is approximately horizontal and represents $t \doteqdot 0$, because only a short time relative to the ^{230}Th half-life (75 ky) has elapsed since emplacement. The points lying in the lower domain of ($^{238}U/^{232}Th$) values, but away from the horizontal trend, separated by the dashed line in Fig. 10, have not been included in the isochron construction. They are samples from the top 7 cm of the sediment, where extra $^{230}Th_{excess}$ supplied from the water column since emplacement has been bioturbated into the turbidite (THOMSON *et al.*, 1988). When choosing samples from older turbidites, it is therefore necessary to avoid areas of bioturbation near the summits of the units. Samples selected from the U peak as well as from altered sections above and unaltered turbidite below will also provide a greater spread of ($^{238}U/^{232}Th$) when compared with turbidite *a* where a U peak is not well developed.

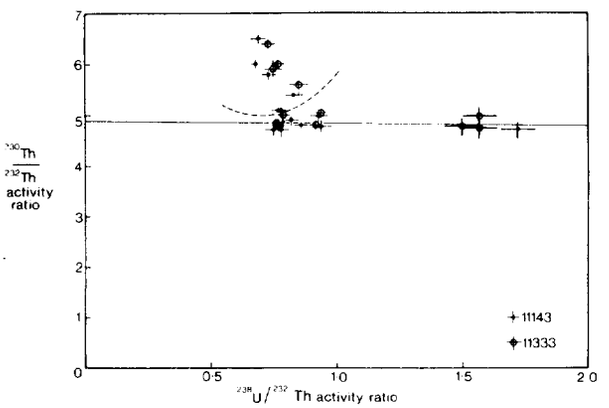

FIG. 10. Isochron plot for samples from two box cores sampling turbidite *a*. Near-surface samples are separated from the remainder of the data by the broken line and have been omitted in calculation of the continuous best-fit line (KERMACK and HALDANE, 1950).

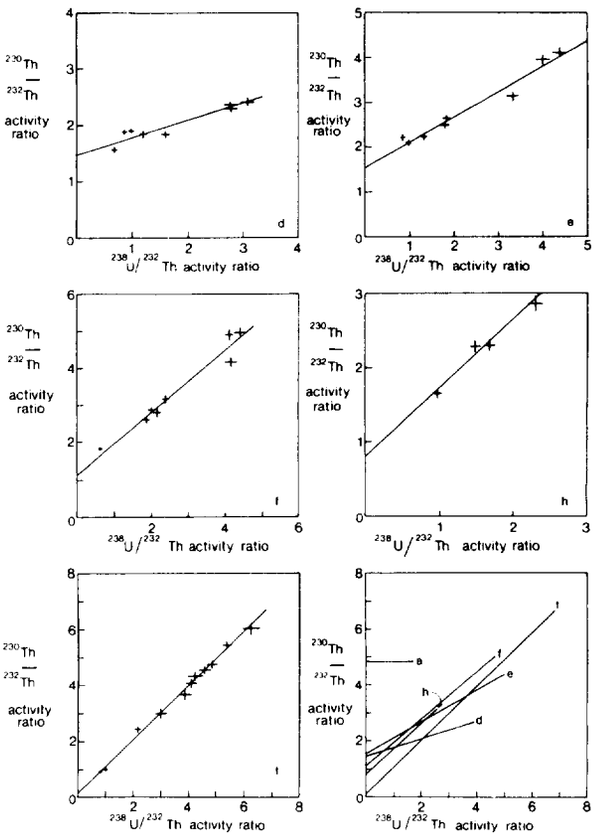

FIG. 11. Isochron plots for individual turbidites: top left, turbidite *d*, core 11145; top right, turbidite *e*, core 11137; middle left, turbidite *f*; middle right, turbidite *h*, both from core 10688 (COLLEY and THOMSON, 1985); bottom left, turbidite *t*, core MD24; bottom right, composite diagram of best-fit lines from all turbidites including turbidite *a* (Fig. 10).

Figure 11 shows quasi-isochron plots for five progressively older turbidites, together with a composite diagram showing all six isochrons (including *a*) superimposed. The fit lines were again constructed using the KERMACK and HALDANE (1950) method. It is evident that the points chosen for each "isochron" show clear linear relationships despite the initial violation of the model due to post-deposition U migration, and that the "isochrons" rotate as would be expected from the horizontal towards the line for turbidite *t*, which is indistinguishable from the equiline. The remarkable linearity of the plots for turbidites ranging from active surface examples to one from a depth of 24 m is a strong indication that very little movement of U away from the peaks has occurred since the oxidation fronts became inactive after burial. The U profiles are therefore set up over thousands of years while the turbidite is at the surface and then preserved without further alteration after burial. The data from turbidite *t* are particularly noteworthy, since the equiline can only be maintained in a situation where the system is chemically closed between ^{238}U and ^{230}Th; *i.e.*, no migration can be occurring. In general, the intercepts on the ($^{230}Th/^{232}Th$) axis rotate towards the origin with increasing age complying with the model. Turbidite *d* is the exception, having a lower intercept than *e*

despite its younger age. This suggests that the initial ($^{230}Th/^{232}Th$) varies between turbidites, which would not be unexpected.

The sedimentological record of the pelagic sections between turbidites indicates that turbidites are usually deposited between oxygen isotope stages (WEAVER and KUIJPERS, 1983). Table 4 is a comparison of ages calculated from the gradients of the quasi-isochrons with those derived from the oxygen isotope record, and shows that the ages only agree loosely between the different methods. This is most likely a function of the violations of the model boundary conditions.

Closed system behaviour can only occur if uranium peaks become isolated from bottom water influence and downward relocation of U is halted. This is illustrated in Fig. 12 by the ($^{230}Th/^{232}Th$) *versus* ($^{238}U/^{232}Th$) plot of data from the single turbidite in core 10311 (colour change at 127 cm) examined by COLLEY *et al.* (1984). The oxidation front in this core is inferred to have been active for 330,000 years, so that U isotopes are still relocating very slowly, and the ingrown ^{230}Th peak is not coincident with the ^{238}U peak but rather is located at a slightly shallower depth. Marked $^{234}U/^{238}U$ disequilibrium also exists in the peak region. The failure of the plot here illustrates the reason for the chronological uncertainty of the quasi-isochron model: points above the peak (132 cm) and on the upper arm will have had higher U contents in the past so that more ^{230}Th than expected will be present, while the reverse is true for points from the lower arm of the peak which will have less ^{230}Th than expected from their current ^{238}U content.

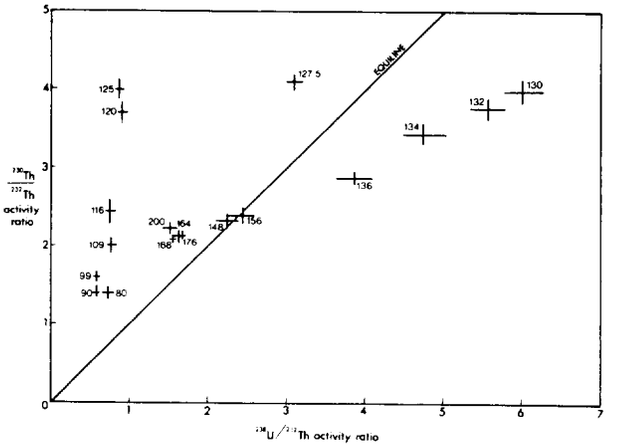

FIG. 12. Isochron plot for core 10311 (COLLEY *et al.*, 1984). The progressive oxidation front in this core is believed to have been continuously active for around 330 ky, so that ^{230}Th ingrowth towards equilibrium with ^{238}U is disrupted by U remobilization. Each datum is labelled with the sample depth in cm: the colour change is at 127 cm and the U peak maximum at 132 cm.

CONCLUSIONS

This investigation of U geochemistry and U-series decay systematics in the deep-water distal turbidite sequence of the GME area has shown that:

1. The characteristic U redistribution patterns caused by progressive oxidation fronts in individual turbidites are recognisable in units up to 750 ky old in a 30 m piston core.

2. The solid phase U profiles are laterally consistent relative to the associated colour change in three different turbidites in transects up to 110 km long. Mass balance considerations, however, show a consistent loss of U from the example where an oxidation front is currently active, while both fossil examples show consistent overall gains. The reasons for this difference are not understood, but bottom waters are considered to be the likely sink or source of the U content disparities in both cases.

3. Pore water profiles in the case where the oxidation front is active reveal gradients consistent with both diffusion upwards and downwards from the front with immobilisation below the front. The pore water profiles do not, however, support the loss of U to bottom waters indicated by the solid phase data. Both box core and *in situ* sampler pore waters in post-oxic conditions have U concentrations similar to that of sea water. In a fossil example at 8 m depth there are uncertainties due to possible air oxidation, but the pore water contents are roughly proportional to the authigenic solid phase U content and are low where no authigenic U is present.

4. Quasi-isochrons can be constructed from ($^{230}Th/^{232}Th$) *versus* ($^{238}U/^{232}Th$) plots for individual turbidites. The best-fit lines rotate from the horizontal towards the equiline (45° gradient and zero intercept) with increasing turbidite age as expected from the isochron model, but the gradients have a poor chronological precision because of violation of model boundary conditions. Data from a 600-ky-old turbidite, however, conform to the equiline, illustrating that good chemical closure must exist in the $^{238}U \rightarrow ^{230}Th$ decay sequence in the long term.

TABLE 4 - COMPARISON OF INTERPRETED STRATIGRAPHIC AGES AND QUASI-ISOCHRON AGES

Turbidite	Oxygen isotope stage boundaries and ages nearest summits and bases of turbidites		Quasi-isochron age
	summit	base	
d	3/2, 29 ky	4/3, 61 ky	40 ky
e	4/3, 61 ky	5/4, 73 ky	91 ky
f	5/4, 73 ky	6/5, 127 ky	197 ky
h	6/7, 190 ky	8/7, 247 ky	256 ky
t	Estimated age	600 ky	Equiline attained (> 450 ky)

Acknowledgements—The authors would like to thank Dr. T. R. S. Wilson for supplying pore water samples from the Mark II *in situ* pore water sampler for uranium analysis and Drs. R. Carpenter, J. K. Cochran and E. R. Sholkovitz for helpful review comments. They are grateful for the assistance given by the scientific and ship's staff of RRS *Discovery* and the members of the ESOPE cruise of the MS *Marion Dufresne*. This research has been carried out under contract to the Department of the Environment, U.K., as part of the radioactive waste management research program, and to the CEC (cost-sharing contract No. FI1W/0146 in the framework of its R and D Program on management and storage of radioactive waste). The results of this work will be used in the formulation of government policy, but the views expressed in this document do not necessarily represent that policy.

Editorial handling: E. R. Sholkovitz

REFERENCES

ALLÈGRE C. J. (1968) ^{230}Th dating of volcanic rocks: A comment. *Earth Planet. Sci. Lett.* **5**, 209–210.

ANDERSON R. F. (1982) Concentration, vertical flux, and remineralization of particulate uranium in seawater. *Geochim. Cosmochim. Acta* **46**, 1293–1299.

ANDERSON R. F. (1984) A method for determining the oxidation state of uranium in natural waters. *Nucl. Instrum. Methods Phys. Res.* **223,** 213–217.

ANDERSON R. F. (1986) Uranium geochemistry in the Black Sea. *Eos* **67,** 1069.

ANDERSON R. F. (1987) Redox behaviour of uranium in an anoxic marine basin. In *Concentration Mechanisms of Uranium in Geological Environments—A Conference Report* (eds. B. POTY and M. PAGEL); *Uranium* **3,** 145–164.

BATURIN G. N., KOCHENOV A. V. and SENIN Y. M. (1971) Uranium concentration in recent ocean sediments in zones of rising currents. *Geochem. Intl.* **8,** 281–286.

BERNAT M. and ALLEGRE C. J. (1974) Systematics in uranium-ionium dating of sediments. *Earth Planet. Sci. Lett.* **21,** 310–314.

BERNER R. A. (1976) Inclusion of adsorption in the modelling of early diagenesis. *Earth Planet. Sci. Lett.* **29,** 333–340.

BERNER R. A. (1981) A new geochemical classification of sedimentary environments. *J. Sediment. Petrol.* **51,** 359–365.

BONATTI E., FISHER D. E., JOENSUU O. and RYDELL H. S. (1971) Post-depositional mobility of some transition elements, phosphorus, uranium and thorium in deep sea sediments. *Geochim. Cosmochim. Acta* **35,** 189–201.

CARPENTER R., PETERSON M. L., BENNETT J. T. and SOMAYAJULU B. L. K. (1984) Mixing and cycling of uranium, thorium and ^{210}Pb in Puget Sound sediments. *Geochim. Cosmochim. Acta* **48,** 1949–1963.

COCHRAN J. K. (1982) The oceanic chemistry of the U- and Th-series nuclides. In *Uranium Series Disequilibrium: Applications to Environmental Problems* (eds. M. IVANOVICH and R. S. HARMON), pp. 384–430. Clarendon Press, Oxford.

COCHRAN J. K., CAREY A. E., SHOLKOVITZ E. R. and SUPRENANT L. D. (1986) The geochemistry of uranium and thorium in coastal marine sediments and sediment pore waters. *Geochim. Cosmochim. Acta* **50,** 663–680.

COLLEY S. and THOMSON J. (1985) Recurrent uranium relocations in distal turbidites emplaced in pelagic conditions. *Geochim. Cosmochim. Acta* **49,** 2339–2348.

COLLEY S., THOMSON J., WILSON T. R. S. and HIGGS N. C. (1984) Post-depositional migration of elements during diagenesis in brown clay and turbidite sequences in the North East Atlantic. *Geochim. Cosmochim. Acta* **48,** 1223–1235.

DEGENS E. T., KHOO F. and MICHAELIS W. (1977) Uranium anomaly in Black Sea sediments. *Nature* **269,** 566–569.

ELDERFIELD H. (1981) Metal-organic associations in interstitial waters of Narragansett Bay sediments. *Amer. J. Sci.* **281,** 1184–1196.

FLEISCHER R. L. and DELANEY A. C. (1976) Determination of suspended and dissolved uranium in water. *Anal. Chem.* **48,** 642–645.

HARSHMAN E. N. (1974) Distribution of elements in some roll-type uranium deposits. In *Formation of Uranium Ore Deposits,* pp. 169–184, I.A.E.A.-SM-183/4, Vienna.

I.A.E.A. (1985) Sediment K_ds and concentration factors for radionuclides in the marine environment. *Tech. Rept. Ser. 247,* 73p.

JARVIS I. and HIGGS N. C. (1987) Trace element mobility during early diagenesis in distal turbidites: Late Quaternary of the Madeira Abyssal Plain, North Atlantic. In *Geology and Geochemistry of Abyssal Plains* (eds P. P. E. WEAVER and J. THOMSON); *Geol. Soc. London Spec. Publ. 31,* 179–213.

KENNEDY H. A. and ELDERFIELD H. (1987) Iodine diagenesis in non-pelagic deep-sea sediments. *Geochim. Cosmochim. Acta* **51,** 2505–2514.

KERMACK K. A. and HALDANE J. B. S. (1950) Organic correlation and allometry. *Biometrika* **37,** 30–41.

KNIEWALD G. and BRANICA M. (1988) Role of uranium (V) in marine sedimentary environments: A geochemical possibility. *Mar. Chem.* **24,** 1–12.

KOLODNY Y. and KAPLAN I. R. (1970) Uranium isotopes in seafloor phosphorites. *Geochim. Cosmochim. Acta* **34,** 3–24.

KOLODNY Y. and KAPLAN I. R. (1973) Deposition of uranium in the sediment and interstitial water of an anoxic fjord. In *Proceedings of Symposium on Hydrochemistry and Biogeochemistry* (ed. E. INGERSON), Vol. 1, pp. 418–442, The Clarke Co., Washington D.C.

KOMINZ M. A., HEATH G. R., KU T-L. and PISIAS N. G. (1979) Brunhes time scale and the interpretation of climatic change. *Earth Planet. Sci. Lett.* **45,** 394–410.

KRYLOV O. T., NOVIKOV P. D. and NESTEROVA M. P. (1985) Calculation of relative amounts of uranium forms in sea water. *Oceanology* **25,** 185–187.

KU T-L. (1965) An evaluation of the ^{234}U/^{238}U method as a tool for dating pelagic sediments. *J. Geophys. Res.* **70,** 3457–3474.

KU T-L. (1976) The uranium-series methods of age determination. *Ann. Rev. Earth Planet. Sci.* **4,** 347–379.

MANGINI A. and DOMINIK J. (1979) Late Quaternary sapropel on the Mediterranean Ridge: U-budget and evidence for low sedimentation rates. *Sediment. Geol.* **23,** 113–125.

MAYNARD J. B. (1983) *Geochemistry of Sedimentary Ore Deposits.* Springer-Verlag, 305p.

MO T., SUTTLE A. D. and SACKETT W. M. (1973) Uranium concentrations in marine sediments. *Geochim. Cosmochim. Acta* **37,** 35–51.

ROE K. K., BURNETT W. C. and LEE A. I. N. (1983) Uranium disequilibrium dating of phosphate deposits from the Lau Group, Fiji. *Nature* **302,** 603–606.

SANTSCHI P. H., BAJO C., MANTOVANI M., ORCIUOLO D., CRANSTON R. E. and BRUNO J. (1988) Uranium in pore waters from North Atlantic (GME and Southern Nares Abyssal Plain) sediments. *Nature* **331,** 155–157.

SCHUTTENHELM R. E. *et al.* (1989) *Geoscience Investigations of Two North Atlantic Abyssal Plains.* CEC-Joint Research Centre, J.R.C. Report, EUR.

TADDEUCCI A., BROECKER W. S. and THURBER D. L. (1967) ^{230}Th dating of volcanic rocks. *Earth Planet. Sci. Lett.* **3,** 338–342.

THOMSON J. (1982) A total dissolution method for determining of the α-emitting isotopes of uranium and thorium in deep sea sediments. *Anal. Chim. Acta* **142,** 259–268.

THOMSON J., WILSON T. R. S., CULKIN F. and HYDES D. J. (1984) Non-steady state diagenetic record in eastern equatorial Atlantic sediments. *Earth Planet. Sci. Lett.* **71,** 23–30.

THOMSON J., COLLEY S., HIGGS N. C., HYDES D. J., WILSON T. R. S. and SØRENSEN J. (1987) Geochemical oxidation fronts in North East Atlantic distal turbidites and their effects in the sedimentary records. In *Geology and Geochemistry of Abyssal Plains* (eds. P. P. E. WEAVER and J. THOMSON); *Geol. Soc. London Spec. Publ. 31,* 179–213.

THOMSON J., COLLEY S. and WEAVER P. P. E. (1988) Bioturbation into a recently emplaced deep sea turbidite surface as revealed by ^{210}Pb$_{excess}$, ^{230}Th$_{excess}$ and planktonic foraminifera distributions. *Earth Planet. Sci. Lett.* **90,** 157–173.

TOOLE J., THOMSON J., WILSON T. R. S. and BAXTER M. S. (1984) A sampling artefact affecting the uranium content of deep sea pore waters obtained from cores. *Nature* **308,** 263–266.

VEEH H. H. (1967) Deposition of uranium from the ocean. *Earth Planet. Sci. Lett.* **3,** 145–150.

VEEH H. H., CALVERT S. E. and PRICE N. B. (1974) Accumulation of uranium in sediments and phosphorites on the South West African Shelf. *Mar. Chem.* **2,** 189–202.

WEAVER P. P. E. and KUIJPERS A. (1983) Climatic control of turbidite deposition on the Madeira Abyssal Plain. *Nature* **306,** 360–363.

WEAVER P. P. E. and ROTHWELL R. G. (1987) Sedimentation on the Madeira Abyssal Plain over the last 300,000 years. In *Geology and Geochemistry of Abyssal Plains* (eds. P. P. E. WEAVER and J. THOMSON); *Geol. Soc. Spec. Publ. 31,* 71–86.

WEAVER P. P. E., SEARLE R. C. and KUIJPERS A. (1985) Turbidite deposition and the origin of the Madeira Abyssal Plain. In *North Atlantic Palaeoceanography* (eds. C. P. SUMMERHAYES and N. J. SHACKLETON); *Geol. Soc. Spec. Publ. 21,* 131–143.

WILSON T. R. S., THOMSON J., COLLEY S., HYDES D. J., HIGGS N. C. and SØRENSEN J. (1985) Early organic diagenesis: The significance of progressive subsurface oxidation fronts in pelagic sediments. *Geochim. Cosmochim. Acta* **49,** 811–822.

WILSON T. R. S., THOMSON J., HYDES D. J., COLLEY S., CULKIN F. and SØRENSEN J. (1986) Oxidation fronts in pelagic sediments: Diagenetic formation of metal-rich layers. *Science* **232,** 972–975.

YAMADA M. and TSUNOGAI S. (1984) Post-depositional enrichment of uranium in sediment from the Bering Sea. *Mar. Geol.* **54,** 263–276.